Nucleotide Binding and Conformational Switching
in the Hexameric Ring of a AAA+ Machine

by

Benjamin M. Stinson

B.A., University of Pennsylvania (2009)
M.S., University of Pennsylvania (2009)

Submitted to the Department of Biology
in Partial Fulfillment of the Requirements for the Degree of

Doctor of Philosophy

at the

MASSACHUSETTS INSTITUTE OF TECHNOLOGY

February 2015

Signature of Author……………………………………………………………………….
January 15, 2014
Department of Biology

Certified by…………………………………………………………………………………...
Robert T. Sauer
Salvador E. Luria Professor of Biology
Thesis Supervisor

Certified by…………………………………………………………………………………...
Tania A. Baker
E.C. Whitehead Professor of Biology
Thesis Co-supervisor

Accepted by……………………………………………………………………………….
Amy E. Keating
Co-chair, Biology Graduate Committee

Nucleotide Binding and Conformational Switching
in the Hexameric Ring of a AAA+ Machine

by

Benjamin M. Stinson

Submitted to the Department of Biology on January 15, 2014
in Partial Fulfillment of the Requirements for the Degree of Doctor of Philosophy

ABSTRACT

ATP-powered proteases enforce protein quality-control and regulation in all domains of life. ClpX, a AAA+ ring homohexamer, uses the energy of ATP binding and hydrolysis to power conformational changes that unfold and translocate target proteins into the ClpP peptidase for degradation. X-ray crystal structures show that some ClpX subunits occupy nucleotide-loadable conformations and others occupy unloadable conformations. Furthermore, biochemical evidence suggests that multiple classes of nucleotide-loadable subunits exist. How asymmetry among subunits is coordinated to achieve mechanical function has remained unlear.

Using a combination of mutagenesis, disulfide crosslinking, and fluorescence methods to assay the conformations and nucleotide-binding properties of individual subunits, we demonstrate dynamic interconversion of loadable and unloadable subunits. Such interconversion is required to couple ATP hydrolysis by ClpX to mechanical work, plays a role in substrate binding and ClpP interaction, and is not strictly coupled to the ATP hydrolysis cycle. ATP binding to different classes of subunits drives allosteric changes in ring conformation to allow hydrolysis and coupled machine function, and we present a subunit-specific single molecule nucleotide occupancy assay to elucidate details of this process.

Thesis Supervisor: Robert T. Sauer
Title: Salvador E. Luria Professor of Biology

Thesis Co-supervisor: Tania A. Baker
Title: E.C. Whitehead Professor of Biology

TABLE OF CONTENTS

ACKNOWLEDGMENT

CHAPTER 1

Introduction to AAA+ proteases

AAA+ machines and intracellular protein degradation

AAA+ machines (ATPases associated with various cellular activities) are an important family of enzymes found in all domains of life (Neuwald et al., 1999). They drive myriad cellular processes, including protein unfolding and degradation, DNA and RNA unwinding, protein disaggregation, mictrotubular transport and severing, and transcriptional activation (Ogura and Wilkinson, 2001). AAA+ enzymes are related by conserved ATP-binding domains, which generally assemble into hexameric ring structures. Multiple cycles of ATP binding and hydrolysis drive conformational changes that allow the AAA+ ring to perform mechanical work on macromolecular substrates (Hanson and Whiteheart, 2005; White and Lauring, 2007). The work presented here focuses on the mechanism of *Escherichia coli* ClpX, a model AAA+ machine involved in protein degradation (Gottesman et al., 1993; Baker and Sauer, 2011)

Intracellular proteolysis is an essential process for cellular viability, allowing cells to respond to environmental stresses and/or developmental cues. Misfolded or damaged proteins are degraded to prevent toxic aggregation in the crowded cellular environment and recycle amino acids, and functional proteins are degraded for regulatory purposes. Intracellular proteolysis occurs through multiple pathways. In the lysosomes of eukaryotic cells, protein degradation is catalyzed by relatively non-specific ATP-independent proteases. In bacteria, archaea, and the cytoplasm, nucleus, and organelles of eukaryotic cells, proteolysis of specific target proteins is carried out by proteases that recognize only a limited number of peptide sequences or by ATP-dependent AAA+ proteases.

Because protein degradation is an irreversible process, non-apoptotic intracellular proteolysis must be tightly regulated, as non-specific degradation of essential proteins would be catastrophic. Regulation in the autophagy-lysosomal pathway is achieved by encapsulation of proteolytic enzymes within a membrane organelle, precluding nonspecific degradation of cytosolic proteins. Furthermore, the acidic environment (~pH 5) of the lysosome helps unfold protein substrates and activates lysosomal hydrolases, which would have minimal activity in the neutral cytosol (Mellman et al., 1986).

ATP-independent proteolysis outside the lysosome is regulated through a combination of specific substrate recognition motifs, post-translational modification, and regulatory proteins that may associate with either a protease or substrate to prevent degradation. For example, the separase protease, responsible for cleaving cohesin and allowing sister chromatids to separate during anaphase of mitosis, is inactivated upon association with the securin regulator (Ciosk et al., 1998; Uhlmann et al., 1999). Another example is the *Escherichia coli* periplasmic protease DegS, which cleaves the transmembrane protein RseA in response to outer-membrane stress, initiating a proteolytic cascade that releases cytosolic σ^E to activate a transcriptional response (Alba and Gross, 2004). Not only must DegS be activated by binding peptides derived from outer-membrane proteins (Walsh et al., 2003), but RseA protection by RseB must be relieved by lipopolysaccharides, which bind to RseB and release it from RseA (Lima et al., 2013). In both of these examples, the active proteases also recognize specific motifs within their substrates, providing another layer of regulation (Uhlmann et al.,

1999; Walsh et al., 2003).

AAA+ proteases

Architectural features ensure the substrate specificity of AAA+ proteases, which carry out ATP-dependent proteolysis in all domains of life. In these enzymes, the proteolytic active sites are sequestered within a barrel-like chamber, which has narrow axial pores that prevent entry of folded proteins. However, a AAA+ ring hexamer can recognize substrates, mechanically unfold them, and translocate the denatured polypeptide into the degradation chamber (Figure 1). This common architecture and mechanism of action is shared among AAA+ proteases from archaea, bacteria, and eukaryotes (for review, see (Sauer and Baker, 2011)).
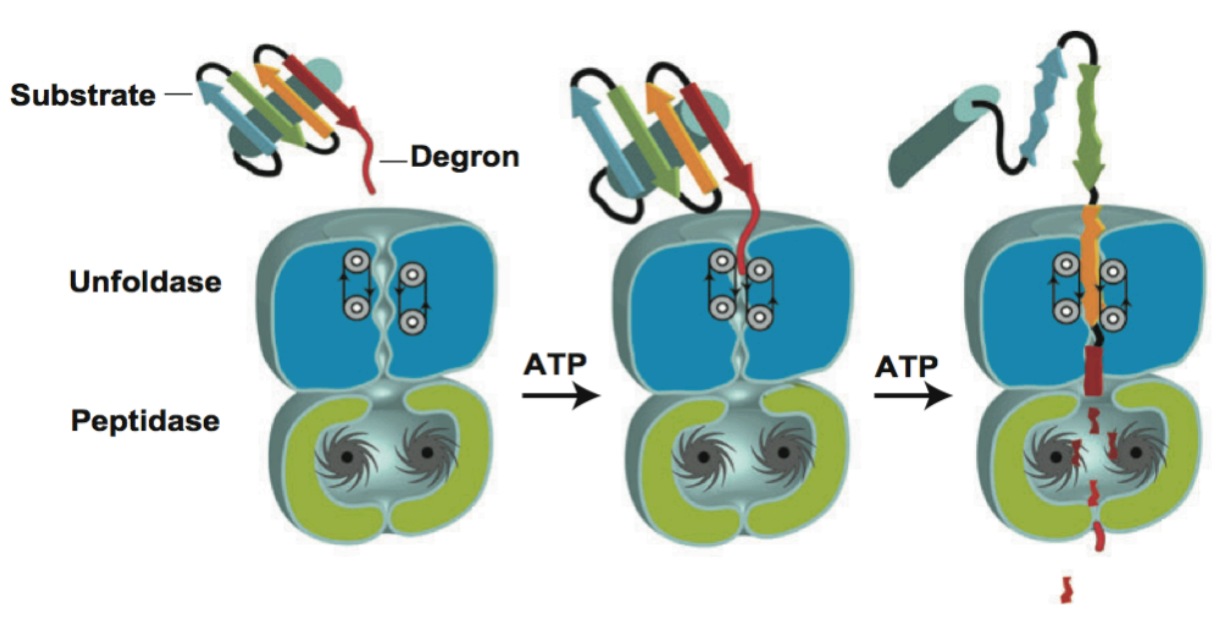
Figure 1. Architecture of AAA+ proteases. A degron on a protein substrate is recognized by the AAA+ unfolding ring. Through multiple cycles of ATP binding and hydrolysis, the substrate is unfolded and then translocated into the peptidase for degradation. Figure from Sauer and Baker, 2011.

Subunit and domain architectures vary among AAA+ proteases. Some of these enzymes contain both AAA+ domains and the protease domain in a single polypeptide chain (e.g. bacterial Lon and FtsH), whereas others consist of separate AAA+ and peptidase partners (e.g., the AAA+ ClpX unfoldase and the ClpP peptidase). In bacteria (Lon, FtsH, HslU, ClpX, and ClpA/ClpC) and archaea (PAN and Cdc48), the AAA+ ring is homo-hexameric, whereas the Rpt_{1-6} AAA+ ring of the eukaryotic 26S proteasome contains six different proteins. The bacterial ClpP and HslV peptidases are homo-oligomers consisting of two stacked heptameric or hexameric rings, respectively. The 20S archaeal and eukaryotic peptidases contain two types of subunits arranged in an $\alpha_7\beta_7\beta_7\alpha_7$ pattern. Nonetheless, all of these ATP-dependent proteases share the basic features of a AAA+ unfolding ring and a self-compartmentalized peptidase.

How do AAA+ proteases recognize specific protein substrates? In eukaryotes, substrates are marked for proteasomal degradation by poly-ubiquitination. Covalent attachment of ubiquitin is performed by coordinated reactions of three enzymes: a ubiquitin-activating enzyme (E1), a ubiquitin-conjugating enzyme (E2), and a ubiquitin ligase (E3). E1 adenylates ubiquitin, activating it for transfer to an active-site E1 cysteine. E1 then passes the ubiquitin to an active-site cysteine of E2. One of hundreds of different E3 enzymes then recognizes a specific protein substrate and catalyzes transfer of ubiquitin from E2 to this target to mark it for degradation (Hershko and Ciechanover, 1998). At least four ubiquitin monomers must be appended to the target substrate for efficient recognition by the 26S proteasome (Thrower et al., 2000). Importantly, proteasomal substrates must also contain an unstructured region for initial

engagement by the Rpt$_{1-6}$ ring (Prakash et al., 2004).

In bacteria, the substrates of AAA+ protease are generally recognized by unstructured N- or C-terminal peptide motifs, termed degrons. Degrons may be recognized directly by the protease, either by the AAA+ pore or an auxiliary domain, or by an adaptor protein that is then recognized by the protease (Sauer et al., 2004; Sauer and Baker, 2011). A well-characterized example is recognition of ssrA-tagged substrates by ClpXP and the SspB adaptor (Levchenko et al., 2000). The 11-residue ssrA tag is appended to the C-terminus of nascent polypeptides by the tmRNA system when normal translation stalls (e.g., when an mRNA lacks a stop codon) (Tu et al., 1995). The tmRNA molecule encoded by the *ssrA* gene possesses dual tRNA- and mRNA-like properties (Komine et al., 1994). tmRNA, charged with alanine, enters the A site of the ribosome, and alanine is appended to the nascent polypeptide. The template switches from the 3′ end of the original mRNA template to the open-reading frame of the tmRNA molecule, which encodes the ANDENYALAA degron (Keiler et al., 1996).

The ssrA tag can be recognized directly by the axial pore of the AAA+ ClpX ring, primarily through the two C-terminal alanine residues and α-carboxylate of the degron (Kim et al., 2000; Flynn et al., 2001). Additionally, delivery of ssrA-tagged substrates can be mediated by the SspB adaptor (Levchenko et al., 2000; Flynn et al., 2001) (Figure 2). A groove in the SspB core binds the N-terminal portion of the ssrA tag upstream of the residues recognized by ClpX (Levchenko et al., 2003), and C-terminal SspB tails bind the auxiliary N-domain of ClpX (Park et al., 2007). Thus, SspB tethers

the substrate to ClpX, increasing the local concentration of the substrate degron near the ClpX pore.
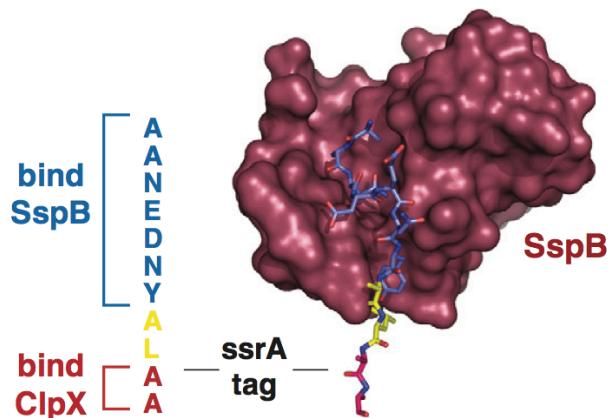
Figure 2. The ssrA degron and SspB adaptor. The C-terminal alanines and α-carboxylate of the ssrA tag are recognized by the ClpX pore, whereas the N-terminal portion of the ssrA tag binds a grove in the body of the SspB adaptor, which has a tail that binds the N-terminal domain of ClpX. Thus, the SspB adaptor helps deliver ssrA-tagged substrates to ClpX. Figure from Baker and Sauer, 2011.

Protein unfolding by AAA+ machines

AAA+ unfoldases apply mechanical force to denature stably folded substrates. In the axial pore of the hexameric AAA+ ring, conserved loops containing an aromatic-hydrophobic dipeptide grip the unstructured degron of a substrate. Conformational changes within the ring drive movement of these pore loops, pulling the folded substrate against the narrow axial pore, resulting in an unfolding force. Upon unfolding, the same pore loops drive translocation of the denatured polypeptide.

Recent optical-trap studies provide a detailed view of protein unfolding and translocation by the ClpXP and ClpAP proteases (Aubin-Tam et al., 2011; Maillard et al., 2011; Sen et al., 2013; Cordova et al., 2014; Olivares et al., 2014). In these single-molecule experiments, a multi-domain substrate is attached to a bead via a flexible DNA linker

and the AAA+ protease is attached to a second bead via a biotin-streptavidin linkage (Figure 3A). After trapping each bead in a separate infrared laser beam, the protease is allowed to engage the substrate and unfolding and translocation are monitored by recording changes in bead-to-bead distance. Unfolding events are marked by sharp increases in bead-to-bead distance, as folded domains are denatured and stretched between the beads. Subsequent translocation results in a gradual decrease in bead-to-bead distance (Figure 3B). Close inspection of translocation traces reveals discrete stepping of the AAA+ machine along its polypeptide track. The smallest discernible ClpXP and ClpAP steps are ~1 nm in length, corresponding to 5-8 amino acid residues and ~5 kT (~$4×10^{-21}$ J) of mechanical work against a force of 20 pN (Aubin-Tam et al., 2011). The distribution of physical step sizes varies between ClpX and ClpA. ClpA usually takes ~1 nm steps, whereas ClpX takes steps ranging from 1-4 nm, with the longer steps probably resulting from kinetic bursts of a 1 nM fundamental step (Cordova et al., 2014; Olivares et al., 2014). These differences may reflect specialization of particular AAA+ unfoldases for particular substrates.

Another prominent feature of these single-molecule traces is pre-unfolding dwells, in which the bead-to-bead distance remains constant (Figure 3B). During these periods, the AAA+ machine has completed translocation of the previous domain and is working to unfold the next domain. Indeed, bulk assays show that substrate unfolding is a slow step in degradation and the ClpX hexamer hydrolyzes hundreds of ATP molecules, on average, before successful unfolding of stable protein substrates occurs (Kenniston et al., 2003).
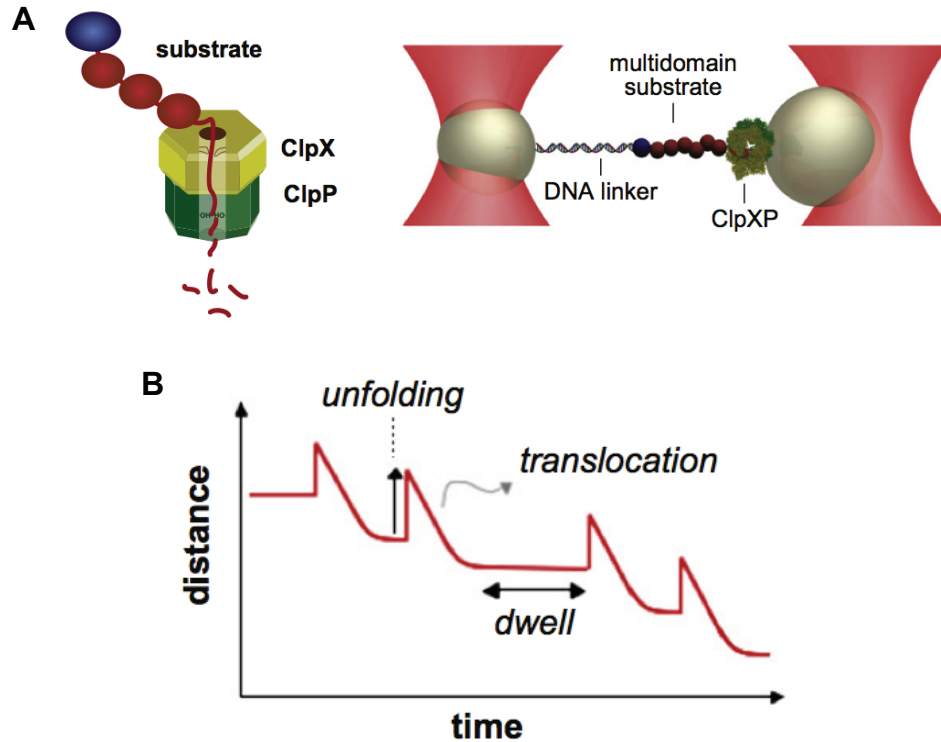
Figure 3. Optical trapping assays. **(A)** Cartoon of the experimental setup, as described in the text. ClpXP is attached to the right bead via a streptavidin linkage to biotinylated ClpX, whereas ClpAP is attached via biotinylated ClpP. **(B)** Representation of major events observed in single molecule traces. Sharp upward transitions in bead-to-bead distance are unfolding, downward slopes are translocation, and flat regions are pre-unfolding dwells. Figure adapted from Aubin-Tam et al., 2011.

How does substrate stability affect unfolding by AAA+ machines? From studies of ClpAP degradation of circular permutants of *E. coli* dihydrofolate reductase (DHFR), Matouschek and colleagues first proposed a model in which local substrate stability proximal to the degradation tag dictates resistance to AAA+ unfolding (Lee et al., 2001). Studies of ClpXP degradation also provide support for this model. For example, introducing mutations that disrupt secondary structure next to the degradation tag of a model substrate (titin^{I27}-ssrA) results in increased degradation rates both in bulk assays and in single-molecule experiments (Kenniston et al., 2003). Notably, however, degradation rates need not be correlated with global thermodynamic or kinetic stability.

Kenniston *et al*. generated variants of *T. thermophilus* ribonuclease-H containing at various locations a single surface-exposed cysteine, to which an ssrA tag was attached by disulfide crosslinking (Kenniston et al., 2004). These variants have similar thermodynamic stabilities but are degraded by ClpXP at rates differing by more than 10-fold, consistent with the hypothesis that substrate stability proximal to the degron, rather than global stability, largely dictates ease of unfolding. In other studies, Nager *et al*. generated ssrA-tagged circular permutants of GFP and found that global thermodynamic or kinetic stability is not a good predictor of resistance to ClpXP degradation (Nager et al., 2011). The relationship between global thermodynamic or kinetic stability and rates of ClpXP degradation of variants of different ssrA-tagged substrates is shown in Figure 4.
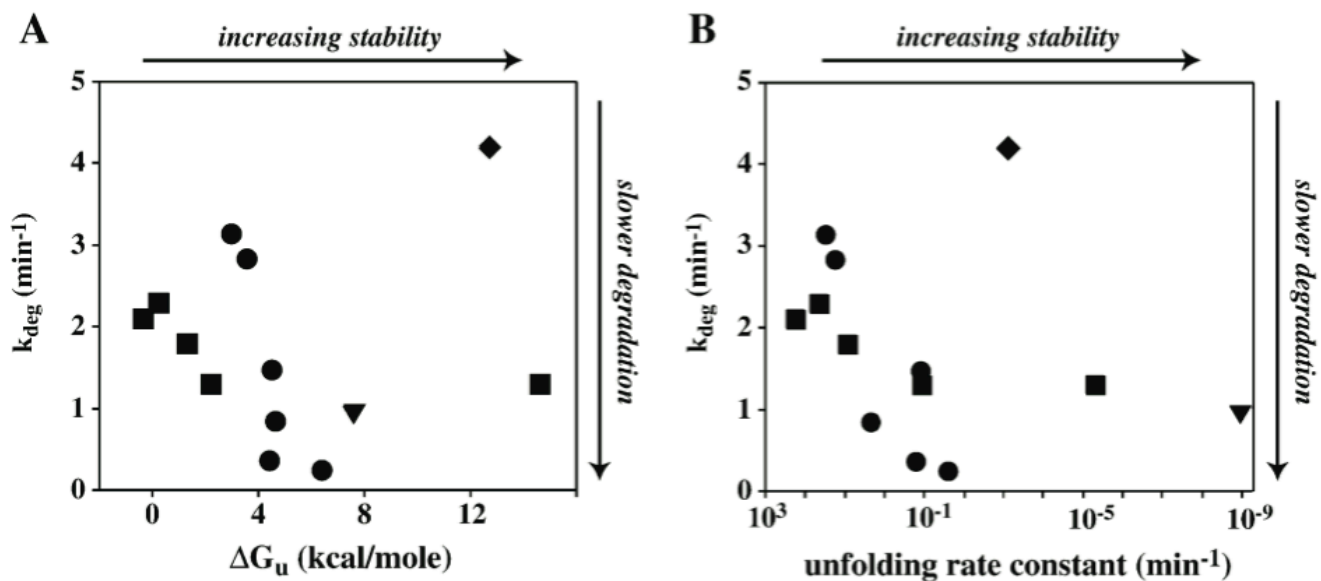
Figure 4. Correlation between ClpXP degradation rates and global thermodynamic stability. **(A)** or kinetic stability **(B)**. In both panels, titin[I27]-ssrA variants are shown as circles, Arc-ssrA variants are shown as squares, GFP-ssrA is shown as a triangle, and ribonuclease-H-ssrA is shown as a diamond. Figure from Kenniston et al., 2003.

Nucleotide interactions

ATP and ATPγS but not ADP support strong interactions between ClpX and ssrA-tagged substrates as well as between ClpX and ClpP (Wah et al., 2002; Bolon et al., 2004; Joshi et al., 2004; Lee et al., 2010). Studies using a ClpX mutation that uncouples ATP binding from conformational changes required for ssrA and ClpP recognition suggest that at least three ClpX subunits must bind ATP/ATPγS to support both interactions (Martin et al., 2005), and strong positive cooperativity in the ATP dependence of ssrA-tag binding also suggests multiple ATP-bound subunits are required for ssrA recognition (Hersch et al., 2005).

In solution, different subunits in the ClpX hexamer display asymmetric interactions with nucleotide. Isothermal-calorimetry experiments reveal a binding stoichiometry of 3-4 ATPs bound per ClpX ring, and nucleotide-dissociation experiments indicate the presence of at least two classes of nucleotide-bound subunits (Hersch et al., 2005). Similar results have been obtained for the related HslU unfoldase (Yakamavich et al., 2008). Nucleotide binding to tight and weak sites of ClpX and the conformational changes that result are a major focus of Chapter 2.

Structures of AAA+ machines

A mechanistic understanding of ClpX and related AAA+ machines requires information about conformational states involved in coupling ATP binding and hydrolysis to mechanical work. Numerous crystal structures of hexameric ClpX rings have been reported and provide glimpses of accessible conformational states (Glynn et al., 2009;

Stinson et al., 2013).

Each *E. coli* ClpX subunit consists of an N-domain (residues 1-62) and the AAA+ module, which consists of large (residues 63-314) and small (residues 320-424) domains separated by a flexible hinge region (residues 315-319). The family-specific N-domain is involved in recognition of some substrates and adaptor molecules (Wojtyra et al., 2003), but is dispensable for unfolding and degradation of ssrA-tagged substrates (Martin et al., 2005). The N-domain forms a stable dimer in solution and in structures of the isolated domain (Donaldson et al., 2003) but is absent in the ClpX variants that have yielded crystal structures of hexameric rings.

The ClpX AAA+ module (residues 63-424) consists of a large domain and a small domain connected by a flexible hinge. Rigid-body interactions between the small domain of one subunit and the large domain of the adjacent subunit bring six subunits together in a topologically-closed hexamer. This major interface between subunits is largely invariable in crystal structures (Glynn et al., 2009) (Figure 5A). Moreover, ClpX hexamers containing subunits "stapled" together at this interface with two disulfide bonds between each subunit are active in protein degradation, indicating that the hexamer in solution functions as a topologically-closed ring in which rigid-body interactions between adjacent subunits remain relatively intact (Glynn et al., 2012).

Although the rigid-body interface between ClpX subunits is largely invariant, individual subunits show highly variable orientations of the large and small domains with respect

to each other (Figure 5B). Two basic classes of subunit conformations, termed loadable (L) and unloadable (U), can be defined based on their interactions with nucleotide. L subunits contain a nucleotide-binding pocket in the cleft between the large and small domains, whereas a reorientation of the large and small domain about the hinge in U subunits sterically occludes the nucleotide-binding pocket (Figure 5C). Insertion of a single additional residue in the hinge region results in major degradation defects, suggesting that the hinge plays a critical role in mechanical unfolding and/or translocation (Glynn et al., 2012).
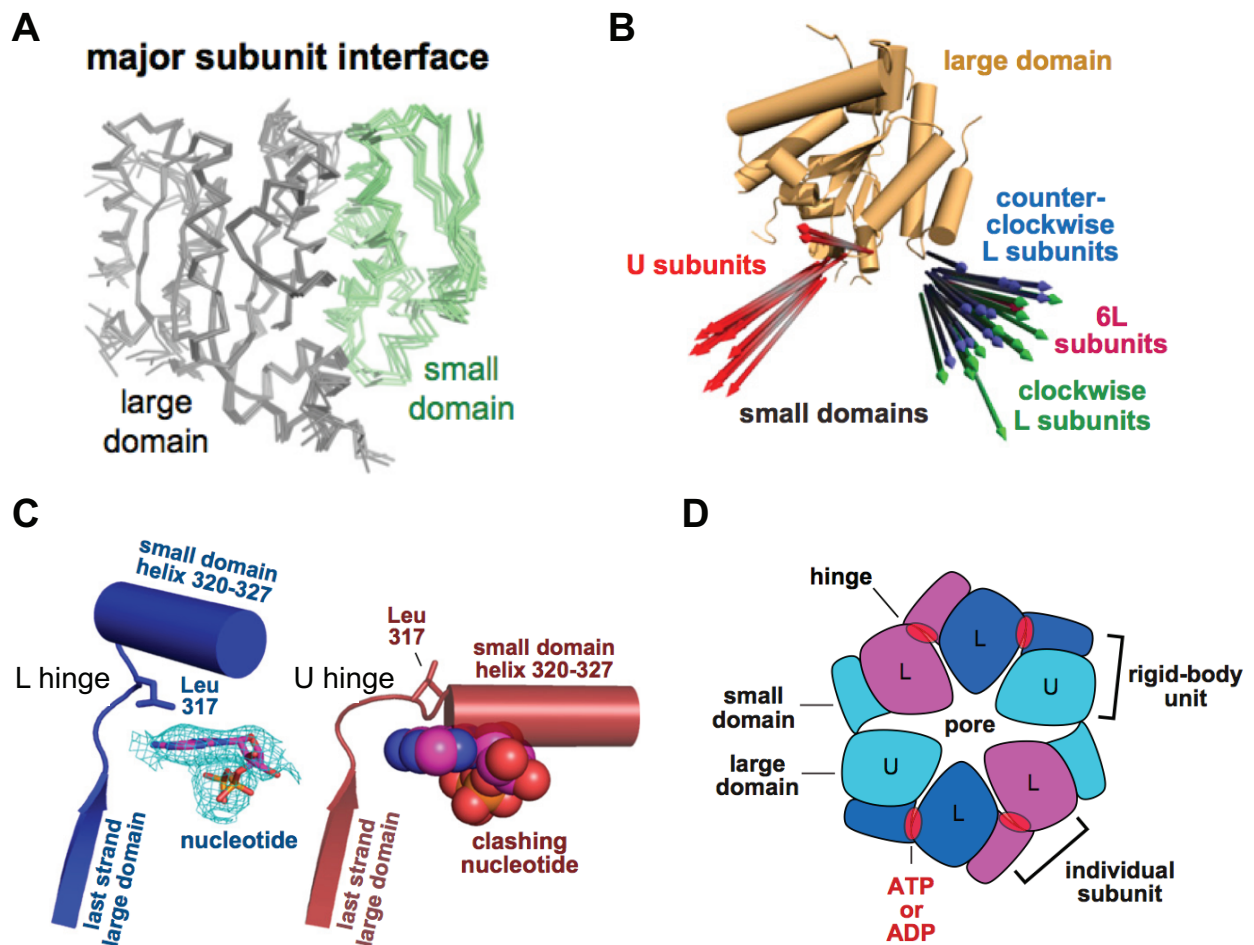
Figure 5. Structures of hexameric ClpX. **(A)** The large AAA+ domains from the 3HWS structure were superimposed, showing the largely invariant position of the adjacent small AAA+ domain (green). Similar results are seen for other crystal structures. **(B)** The large AAA+ domains of all available ClpX hexameric crystal structures were superimposed (tan) and the first helix of the associated small AAA+ domains are represented as arrows, highlighting a large domain rotation between L and U subunits and the variability within L and U classes. **(C)** The nucleotide-binding pocket of L (blue) and U (red) subunits. The domain reorientation in U subunits places the first helix of the small AAA+ domain in the nucleotide pocket, sterically blocking binding. **(D)** Cartoon representation of the 4L:2U subunit arrangement seen in most crystal structures. Nucleotide binds at the hinge region in the cleft between large and small AAA+ domains. (A) and (C) are from Glynn et al., 2009; (B) and (D) are from Stinson et al., 2013.

Most ClpX crystal structures contain a hexamer with four L subunits and two U subunits arranged in an L/L/U/L/L/U pattern with pseudo two-fold symmetry (Figure 5D). Soaking or cocrystallization with ADP, ATP, or ATPγS produces nucleotide density in the four L subunits, although the degree of occupancy is variable. However, one crystal structure contains six L subunits. In Chapters 2 and 3, evidence is presented supporting a functional role for a ClpX hexamer containing five L subunits and one U subunit. Although no crystal structure shows this arrangement of subunits, it is possible to model a 5L:1U hexamer using subunits from available crystal structures, as discussed in Chapter 2.

Three sets of axial pore loops in ClpX are important for recognition of ssrA-tagged substrates (Figure 6). Basic RKH loops, which surround the axial pore on the face of ClpX opposite the ClpP-binding surface, are thought to interact electrostatically with the C-terminal α-carboxylate of the ssrA tag, perhaps guiding subsequent engagement within the pore (Farrell et al., 2007; Martin et al., 2008a). GYVG (pore-1) loops contact the ssrA tag and play a critical role in gripping substrates to drive translocation and unfolding (Martin et al., 2008b; 2008a). In addition, cross-linking studies show that pore-

2 loops also contact the ssrA tag before substantial translocation has occurred and also contact ClpP (Martin et al., 2007). Crystal structures show that asymmetry among ClpX subunits produces a staggering of GYVG and pore-2 loops along the pore axis (Glynn et al., 2009; Figure 6), which is likely to allow the pore-2 loops to contact both ClpP and initially bound ssrA-tagged substrate. Comparison of nucleotide-bound and nucleotide-free structures of ClpX shows that some GYVG loops move toward ClpP upon nucleotide binding, providing a potential mechanism for GYVG loops pushing or pulling substrate through the pore.
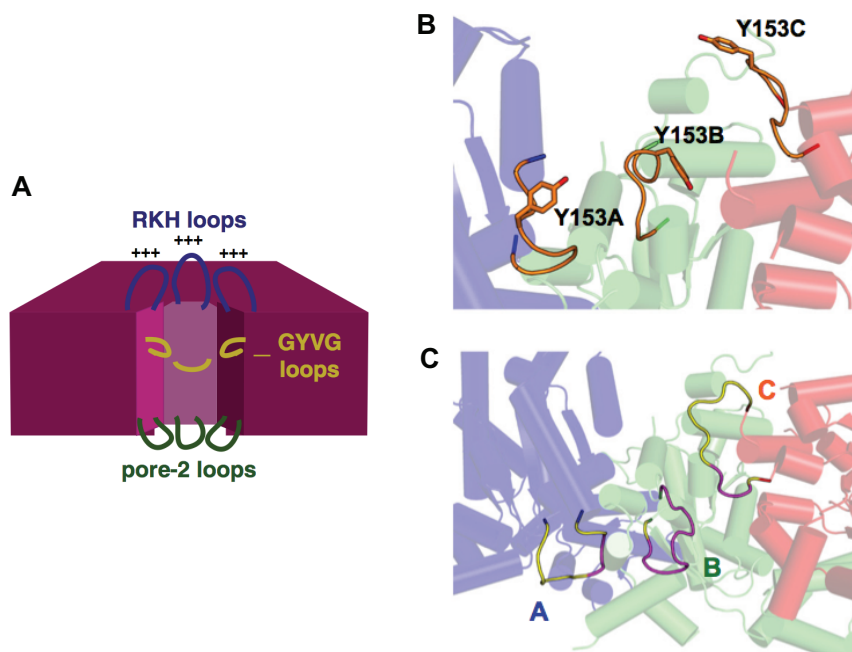
Figure 6. Axial pore loops of ClpX. **(A)** Cartoon of pore loops. All three loops are implicated in substrate binding, and the pore-2 loops are implicated in ClpP interactions (see text). Figure from Baker and Sauer, 2011. Staggering of GYVG **(B)** and pore-2 **(C)** loops along the pore axis. Letters refer to subunits in the 3HWS structure. Panels (B)-(C) are from Glynn et al., 2009.

How do crystal structures of ClpX compare with structures of related single-ring AAA+ enzymes? Structures of the HslU unfoldase have been solved with three, four, or six bound nucleotides, although in structures with fewer than six nucleotides only slight

differences among subunits are apparent, unlike the drastic domain reorientation observed for ClpX (Bochtler et al., 2000; Sousa et al., 2000; Wang et al., 2001; Sousa et al., 2002; Kwon et al., 2003). Similarly, structures of FtsH and *Ton*Lon show six ADP-bound subunits without major differences among subunits (Bieniossek et al., 2006; Cha et al., 2010), and a crystal structure of ClpC, which contains two stacked AAA+ rings, reveals one symmetric ring and one slightly asymmetric ring (Wang et al., 2011).

Spiral "staircase" arrangements of AAA+ modules are observed in a crystal structure of the papillomavirus E1 helicase as well as an EM reconstruction of the Rpt_{1-6} ring of the 26S proteasome (Enemark and Joshua-Tor, 2006; Lander et al., 2012). The two hexamers present in the asymmetric unit of the E1 helicase structure contain 4-5 subunits in ATP/ADP configurations and 1-2 subunits in an "apo" configuration lacking many of the nucleotide contacts present in the ATP/ADP configurations. The Rpt_{1-6} ring reconstruction contains five AAA+ large domains arranged in a spiral with the sixth AAA+ occupying a tilted orientation to close the ring. Furthermore, a crystal structure of the AAA+ dynein ring reveals four nucleotide-binding sites, although the remaining sites of the pseudo hexamer lack consensus motifs for ATP binding (Bhabha et al., 2014).

Crystal and EM structures of AAA+ machines show considerable variability. The asymmetric crystal structures of ClpX are consistent with numerous biochemical observations, including sub-stoichiometric ATP binding and pore-loop crosslinking studies. Structures of the E1 helicase and proteasomal Rpt_{1-6} ring show similar asymmetry and raise the possibility of a ClpX structure containing five L subunits and

one U subunit, which is discussed in subsequent chapters. Symmetric structures observed for other AAA+ enzymes may reflect fundamental mechanistic differences among AAA+ machines, or they may simply represent conformational energy minima in the crystal context that are not functionally significant. Detailed biochemical analyses will be required to distinguish between these possibilities.

Models of subunit coordination

How do AAA+ hexamers coordinate different conformations and nucleotide states among subunits to generate mechanical force? Three models—concerted, sequential, and probabilistic—have been proposed (Figure 7).
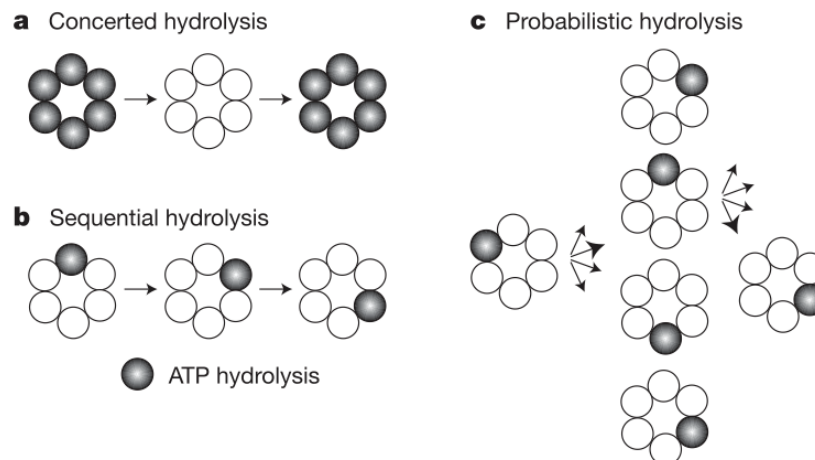
Figure 7. Models of intersubunit coordination. In the concerted model **(A)**, six subunits (or a subset thereof) undergo simultaneous ATP binding, hydrolysis, ADP release, and associated conformational changes. In the sequential model **(B)**, nucleotide and conformational states proceed around the ring in a geometric progression. A clockwise mechanism is shown here for simplicity, but counterclockwise and other models are possible. In the probabilistic model **(C)**, nucleotide and conformational states are not predetermined and do not occur with a strict geometric progression. Not all arrows shown need be equally probable (see text). Figure from Martin et al., 2005.

A concerted mechanism in which ATP binding, hydrolysis, and ADP/P_i release occur

simultaneously in all six subunits has been proposed for the SV40 helicase. Gai *et al.* solved a series of crystal structures of this DNA helicase in various nucleotide states (Gai et al., 2004). They found that ADP, ADP•BeF$_3^-$ (a transition-state analog), and ATP bind the SV40 helicase in an all-or-none manner. Moreover, they note that critical catalytic residues in the nucleotide-binding pocket are positioned for efficient hydrolysis in all six subunits of the ADP-BeF$_3^-$ structure. Thus, they propose that ATP hydrolysis and accompanying conformational changes occur in a concerted fashion among all six subunits.

A sequential model has been proposed for the papillomavirus E1 DNA helicase as well as the archaeal PAN unfoldase (Enemark and Joshua-Tor, 2006; Smith et al., 2011). Enemark and Joshua-Tor solved a crystal structure of the E1 helicase with single-stranded DNA bound in the central pore and bound nucleotide. In this structure, the DNA-binding hairpin of each subunit makes discrete contacts with successive nucleotides of the DNA substrate, with the hairpins arranged in a spiral "staircase". They assigned each subunit to an ATP, ADP, or apo state, with the ATP subunits at the top of the staircase, apo subunits at the bottom, and ADP subunits in between. Thus, they propose a sequential model in which each hairpin makes continuous contact with a base of the DNA and "escorts" the base through the hexamer as the subunit sequentially passes from the ATP state to the ADP and apo states. These events permute sequentially around the ring to allow processive translocation.

In another variation of a sequential model, Smith *et al*. proposed that the PAN unfoldase

assumes an ATP/empty/ADP/ATP/empty/ADP configuration of subunits that then rotates sequentially around the hexameric ring during machine function (Smith et al., 2011). Their model assumes that the PAN hexamer is maximally active with two ATPs and two ADPs bound, with ATP binding inducing an empty state in the clockwise subunit and an ADP state in the counter-clockwise subunit.

Martin *et al.* proposed a probabilistic model of subunit coordination for the ClpX hexamer (Martin et al., 2005). A critical part of this study was the use of covalently linked ClpX variants expressed from genes containing two, three, or six ClpX$^{\Delta N}$ subunits connected by flexible peptide tethers. These linked subunits formed pseudo hexamers consisting of a trimer of dimers, a dimer of trimers, or a single covalent chain. Importantly, this strategy allows ATPase or other mutations to be introduced into specific subunits of ClpX pseudo hexamers. Notably, Martin *et al.* found that a variety of pseudo hexamers with different numbers and geometries of active and inactive subunits supported machine function. Indeed, a ClpX hexamer containing only one ATPase-active subunit was marginally functional. These results were inconsistent with concerted and sequential models of ClpX function. Thus, Martin *et al.* proposed a model in which ATP hydrolysis is probabilistic rather than pre-determined. This probabilistic model does not rule out some degree of inter-subunit coordination, as the probability of certain transitions in the chemo-mechanical cycle may depend on particular contacts with substrate, ClpP, nucleotide state of neighboring subunits, *etc*.

The question of whether other AAA+ machines operate by a probabilistic mechanism

remains unresolved and will require more detailed experiments in these systems. Moreover, how ClpX functions within a probabilistic framework is unclear. The following chapters of this thesis probe the nucleotide interactions and conformational dynamics of individual subunits in the ClpX hexamer in bulk-ensemble and single-molecule experiments.

REFERENCES

Alba, B.M., and Gross, C.A. (2004). Regulation of the Escherichia coli sigma-dependent envelope stress response. Mol Microbiol *52*, 613–619.

Aubin-Tam, M.-E., Olivares, A.O., Sauer, R.T., Baker, T.A., and Lang, M.J. (2011). Single-molecule protein unfolding and translocation by an ATP-fueled proteolytic machine. Cell *145*, 257–267.

Baker, T.A., and Sauer, R.T. (2011). ClpXP, an ATP-powered unfolding and protein-degradation machine. Biochimica Et Biophysica Acta (BBA) - Molecular Cell Research.

Bhabha, G., Cheng, H.-C., Zhang, N., Moeller, A., Liao, M., Speir, J.A., Cheng, Y., and Vale, R.D. (2014). Allosteric Communication in the Dynein Motor Domain. Cell *159*, 857–868.

Bieniossek, C., Schalch, T., Bumann, M., Meister, M., Meier, R., and Baumann, U. (2006). The molecular architecture of the metalloprotease FtsH. Proc Natl Acad Sci USA *103*, 3066–3071.

Bochtler, M., Hartmann, C., Song, H.K., Bourenkov, G.P., Bartunik, H.D., and Huber, R. (2000). The structures of HsIU and the ATP-dependent protease HsIU-HsIV. Nature *403*, 800–805.

Bolon, D.N., Grant, R.A., Baker, T.A., and Sauer, R.T. (2004). Nucleotide-dependent substrate handoff from the SspB adaptor to the AAA+ ClpXP protease. Mol Cell *16*, 343–350.

Cha, S.-S., An, Y.J., Lee, C.R., Lee, H.S., Kim, Y.-G., Kim, S.J., Kwon, K.K., De Donatis, G.M., Lee, J.-H., Maurizi, M.R., et al. (2010). Crystal structure of Lon protease: molecular architecture of gated entry to a sequestered degradation chamber. Embo J *29*, 3520–3530.

Ciosk, R., Zachariae, W., Michaelis, C., Shevchenko, A., Mann, M., and Nasmyth, K. (1998). An ESP1/PDS1 complex regulates loss of sister chromatid cohesion at the metaphase to anaphase transition in yeast. Cell *93*, 1067–1076.

Cordova, J.C., Olivares, A.O., Shin, Y., Stinson, B.M., Calmat, S., Schmitz, K.R., Aubin-Tam, M.-E., Baker, T.A., Lang, M.J., and Sauer, R.T. (2014). Stochastic but highly coordinated protein unfolding and translocation by the ClpXP proteolytic machine. Cell *158*, 647–658.

Donaldson, L.W., Wojtyra, U., and Houry, W.A. (2003). Solution structure of the dimeric zinc binding domain of the chaperone ClpX. J Biol Chem *278*, 48991–48996.

Enemark, E.J., and Joshua-Tor, L. (2006). Mechanism of DNA translocation in a replicative hexameric helicase. Nature *442*, 270–275.

Farrell, C.M., Baker, T.A., and Sauer, R.T. (2007). Altered specificity of a AAA+ protease. Mol Cell *25*, 161–166.

Flynn, J.M., Levchenko, I., Seidel, M., Wickner, S.H., Sauer, R.T., and Baker, T.A. (2001). Overlapping recognition determinants within the ssrA degradation tag allow modulation of proteolysis. Proc Natl Acad Sci USA *98*, 10584–10589.

Gai, D., Zhao, R., Li, D., Finkielstein, C.V., and Chen, X.S. (2004). Mechanisms of conformational change for a replicative hexameric helicase of SV40 large tumor antigen. Cell *119*, 47–60.

Glynn, S.E., Martin, A., Nager, A.R., Baker, T.A., and Sauer, R.T. (2009). Structures of asymmetric ClpX hexamers reveal nucleotide-dependent motions in a AAA+ protein-unfolding machine. Cell *139*, 744–756.

Glynn, S.E., Nager, A.R., Baker, T.A., and Sauer, R.T. (2012). Dynamic and static components power unfolding in topologically closed rings of a AAA+ proteolytic machine. Nat Struct Mol Biol *19*, 616–622.

Gottesman, S., Clark, W.P., de Crecy-Lagard, V., and Maurizi, M.R. (1993). ClpX, an alternative subunit for the ATP-dependent Clp protease of Escherichia coli. Sequence and in vivo activities. J Biol Chem *268*, 22618–22626.

Hanson, P.I., and Whiteheart, S.W. (2005). AAA+ proteins: have engine, will work. Nat. Rev. Mol. Cell Biol. *6*, 519–529.

Hersch, G.L., Burton, R.E., Bolon, D.N., Baker, T.A., and Sauer, R.T. (2005). Asymmetric interactions of ATP with the AAA+ ClpX6 unfoldase: allosteric control of a protein machine. Cell *121*, 1017–1027.

Hershko, A., and Ciechanover, A. (1998). The ubiquitin system. Annu Rev Biochem *67*, 425–479.

Joshi, S.A., Hersch, G.L., Baker, T.A., and Sauer, R.T. (2004). Communication between ClpX and ClpP during substrate processing and degradation. Nat Struct Mol Biol *11*, 404–411.

Keiler, K.C., Waller, P.R., and Sauer, R.T. (1996). Role of a Peptide Tagging System in Degradation of Proteins Synthesized from Damaged Messenger RNA

. Science *271*, 990–993.

Kenniston, J.A., Baker, T.A., Fernandez, J.M., and Sauer, R.T. (2003). Linkage between ATP consumption and mechanical unfolding during the protein processing reactions of an AAA+ degradation machine. Cell *114*, 511–520.

Kenniston, J.A., Burton, R.E., Siddiqui, S.M., Baker, T.A., and Sauer, R.T. (2004). Effects of local protein stability and the geometric position of the substrate degradation

tag on the efficiency of ClpXP denaturation and degradation. J Struct Biol *146*, 130–140.

Kim, Y.I., Burton, R.E., Burton, B.M., Sauer, R.T., and Baker, T.A. (2000). Dynamics of substrate denaturation and translocation by the ClpXP degradation machine. Mol Cell *5*, 639–648.

Komine, Y., Kitabatake, M., Yokogawa, T., Nishikawa, K., and Inokuchi, H. (1994). A tRNA-like structure is present in 10Sa RNA, a small stable RNA from Escherichia coli. Proc Natl Acad Sci USA *91*, 9223–9227.

Kwon, A.-R., Kessler, B.M., Overkleeft, H.S., and McKay, D.B. (2003). Structure and reactivity of an asymmetric complex between HslV and I-domain deleted HslU, a prokaryotic homolog of the eukaryotic proteasome. J Mol Biol *330*, 185–195.

Lander, G.C., Estrin, E., Matyskiela, M.E., Bashore, C., Nogales, E., and Martin, A. (2012). Complete subunit architecture of the proteasome regulatory particle. Nature *482*, 186–191.

Lee, C., Schwartz, M.P., Prakash, S., Iwakura, M., and Matouschek, A. (2001). ATP-dependent proteases degrade their substrates by processively unraveling them from the degradation signal. Mol Cell *7*, 627–637.

Lee, M.E., Baker, T.A., and Sauer, R.T. (2010). Control of substrate gating and translocation into ClpP by channel residues and ClpX binding. J Mol Biol *399*, 707–718.

Levchenko, I., Seidel, M., Sauer, R.T., and Baker, T.A. (2000). A specificity-enhancing factor for the ClpXP degradation machine. Science *289*, 2354–2356.

Levchenko, I., Grant, R.A., Wah, D.A., Sauer, R.T., and Baker, T.A. (2003). Structure of a delivery protein for an AAA+ protease in complex with a peptide degradation tag. Mol Cell *12*, 365–372.

Lima, S., Guo, M.S., Chaba, R., Gross, C.A., and Sauer, R.T. (2013). Dual molecular signals mediate the bacterial response to outer-membrane stress. Science *340*, 837–841.

Maillard, R.A., Chistol, G., Sen, M., Righini, M., Tan, J., Kaiser, C.M., Hodges, C., Martin, A., and Bustamante, C. (2011). ClpX(P) generates mechanical force to unfold and translocate its protein substrates. Cell *145*, 459–469.

Martin, A., Baker, T.A., and Sauer, R.T. (2005). Rebuilt AAA + motors reveal operating principles for ATP-fuelled machines. Nature *437*, 1115–1120.

Martin, A., Baker, T.A., and Sauer, R.T. (2007). Distinct static and dynamic interactions control ATPase-peptidase communication in a AAA+ protease. Mol Cell *27*, 41–52.

Martin, A., Baker, T.A., and Sauer, R.T. (2008a). Diverse pore loops of the AAA+ ClpX

machine mediate unassisted and adaptor-dependent recognition of ssrA-tagged substrates. Mol Cell *29*, 441–450.

Martin, A., Baker, T.A., and Sauer, R.T. (2008b). Pore loops of the AAA+ ClpX machine grip substrates to drive translocation and unfolding. Nat Struct Mol Biol *15*, 1147–1151.

Mellman, I., Fuchs, R., and Helenius, A. (1986). Acidification of the endocytic and exocytic pathways. Annu Rev Biochem *55*, 663–700.

Nager, A.R., Baker, T.A., and Sauer, R.T. (2011). Stepwise unfolding of a β barrel protein by the AAA+ ClpXP protease. J Mol Biol *413*, 4–16.

Neuwald, A.F., Aravind, L., Spouge, J.L., and Koonin, E.V. (1999). AAA+: A class of chaperone-like ATPases associated with the assembly, operation, and disassembly of protein complexes. Genome Res *9*, 27–43.

Ogura, T., and Wilkinson, A.J. (2001). AAA+ superfamily ATPases: common structure--diverse function. Genes Cells *6*, 575–597.

Olivares, A.O., Nager, A.R., Iosefson, O., Sauer, R.T., and Baker, T.A. (2014). Mechanochemical basis of protein degradation by a double-ring AAA+ machine. Nat Struct Mol Biol *21*, 871–875.

Park, E.Y., Lee, B.-G., Hong, S.-B., Kim, H.-W., Jeon, H., and Song, H.K. (2007). Structural basis of SspB-tail recognition by the zinc binding domain of ClpX. J Mol Biol *367*, 514–526.

Prakash, S., Tian, L., Ratliff, K.S., Lehotzky, R.E., and Matouschek, A. (2004). An unstructured initiation site is required for efficient proteasome-mediated degradation. Nat Struct Mol Biol *11*, 830–837.

Sauer, R.T., and Baker, T.A. (2011). AAA+ proteases: ATP-fueled machines of protein destruction. Annu Rev Biochem *80*, 587–612.

Sauer, R.T., Bolon, D.N., Burton, B.M., Burton, R.E., Flynn, J.M., Grant, R.A., Hersch, G.L., Joshi, S.A., Kenniston, J.A., Levchenko, I., et al. (2004). Sculpting the proteome with AAA(+) proteases and disassembly machines. Cell *119*, 9–18.

Sen, M., Maillard, R.A., Nyquist, K., Rodriguez-Aliaga, P., Pressé, S., Martin, A., and Bustamante, C. (2013). The ClpXP protease unfolds substrates using a constant rate of pulling but different gears. Cell *155*, 636–646.

Smith, D.M., Fraga, H., Reis, C., Kafri, G., and Goldberg, A.L. (2011). ATP binds to proteasomal ATPases in pairs with distinct functional effects, implying an ordered reaction cycle. Cell *144*, 526–538.

Sousa, M.C., Trame, C.B., Tsuruta, H., Wilbanks, S.M., Reddy, V.S., and McKay, D.B. (2000). Crystal and solution structures of an HslUV protease-chaperone complex. Cell

103, 633–643.

Sousa, M.C., Kessler, B.M., Overkleeft, H.S., and McKay, D.B. (2002). Crystal structure of HslUV complexed with a vinyl sulfone inhibitor: corroboration of a proposed mechanism of allosteric activation of HslV by HslU. J Mol Biol *318*, 779–785.

Stinson, B.M., Nager, A.R., Glynn, S.E., Schmitz, K.R., Baker, T.A., and Sauer, R.T. (2013). Nucleotide Binding and Conformational Switching in the Hexameric Ring of a AAA+ Machine. Cell *153*, 628–639.

Thrower, J.S., Hoffman, L., Rechsteiner, M., and Pickart, C.M. (2000). Recognition of the polyubiquitin proteolytic signal. Embo J *19*, 94–102.

Tu, G.F., Reid, G.E., Zhang, J.G., Moritz, R.L., and Simpson, R.J. (1995). C-terminal extension of truncated recombinant proteins in Escherichia coli with a 10Sa RNA decapeptide. J Biol Chem *270*, 9322–9326.

Uhlmann, F., Lottspeich, F., and Nasmyth, K. (1999). Sister-chromatid separation at anaphase onset is promoted by cleavage of the cohesin subunit Scc1. Nature *400*, 37–42.

Wah, D.A., Levchenko, I., Baker, T.A., and Sauer, R.T. (2002). Characterization of a specificity factor for an AAA+ ATPase: assembly of SspB dimers with ssrA-tagged proteins and the ClpX hexamer. Chem Biol *9*, 1237–1245.

Walsh, N.P., Alba, B.M., Bose, B., Gross, C.A., and Sauer, R.T. (2003). OMP Peptide Signals Initiate the Envelope-Stress Response by Activating DegS Protease via Relief of Inhibition Mediated by Its PDZ Domain. Cell *113*, 61–71.

Wang, F., Mei, Z., Qi, Y., Yan, C., Hu, Q., Wang, J., and Shi, Y. (2011). Structure and mechanism of the hexameric MecA-ClpC molecular machine. Nature *471*, 331–335.

Wang, J., Song, J.J., Franklin, M.C., Kamtekar, S., Im, Y.J., Rho, S.H., Seong, I.S., Lee, C.S., Chung, C.H., and Eom, S.H. (2001). Crystal structures of the HslVU peptidase-ATPase complex reveal an ATP-dependent proteolysis mechanism. Structure *9*, 177–184.

White, S.R., and Lauring, B. (2007). AAA+ ATPases: achieving diversity of function with conserved machinery. Traffic *8*, 1657–1667.

Wojtyra, U.A., Thibault, G., Tuite, A., and Houry, W.A. (2003). The N-terminal zinc binding domain of ClpX is a dimerization domain that modulates the chaperone function. J Biol Chem *278*, 48981–48990.

Yakamavich, J.A., Baker, T.A., and Sauer, R.T. (2008). Asymmetric nucleotide transactions of the HslUV protease. J Mol Biol *380*, 946–957.

CHAPTER 2

Nucleotide binding and conformational switching

in the hexameric ring of a AAA+ machine

This chapter is published as referenced below:

* indicates equal contribution. I generated and characterized ClpX variants containing nucleotide-binding mutations (Figure 2), developed the nCoMET assay (Figure 3), and contributed to writing the manuscript.

INTRODUCTION

In all branches of life, AAA+ molecular machines harness the energy of ATP binding and hydrolysis to degrade, disaggregate, and secrete proteins, to remodel macromolecular complexes, to transport nucleic acids, and to drive vectorial transport along microtubules (Hanson and Whiteheart, 2005). A central unsolved challenge in dissecting the mechanisms of these complicated multi-protein machines is to determine how ATP interacts with different subunits and coordinates the conformational changes that ultimately power machine function. Although many different models for this orchestration are possible, most proposals in the literature depend upon multiple untested assumptions, and the paucity of methods to test specific models has limited understanding of these machines.

ClpXP is an ATP-dependent protease that consists of a self-compartmentalized barrel-shaped peptidase (ClpP) and a hexameric-ring AAA+ unfoldase (ClpX), which recognizes, unfolds, and translocates protein substrates into an internal ClpP chamber for degradation (for review, see Baker and Sauer, 2012). Insight into ClpX function has come from biochemistry, protein engineering, and single-molecule biophysics. For example, translocation of a peptide degron through the axial pore of the ClpX ring drives substrate unfolding, and processive translocation can occur against substantial resisting forces (Martin et al., 2008a; 2008b; Aubin-Tam et al., 2011; Maillard et al., 2011). Although ClpX is a homohexamer, it is asymmetric, and nucleotides fail to bind some ClpX subunits and bind other subunits with different affinities (Hersch et al., 2005). A single active subunit in the hexameric ring is sufficient to power mechanical unfolding and translocation, yet subunit-subunit communication appears to be important for

controlling and coupling ATP hydrolysis to function (Martin et al., 2005). Because processive ClpXP proteolysis of a single polypeptide can require hundreds of ATP-binding and hydrolysis events (Kenniston et al., 2003), understanding how these nucleotide transactions are coupled to mechanical work is a critical aspect of mechanism.

Crystal structures of the hexameric ClpX ring reveal two basic classes of subunits (Glynn et al., 2009). In four loadable (L) subunits, the orientation of the large and small AAA+ domains creates a binding cleft in which nucleotide can contact each domain, the intervening hinge, and a neighboring subunit (Fig. 1A). The exact structure and properties of these binding sites can differ depending upon the position in the hexamer and bound nucleotide. By contrast, these sites are destroyed in two unloadable (U) subunits by a hinge rotation that reorients the flanking domains. In the known hexamer structures, these subunits are arranged in an L/U/L/L/U/L pattern with approximate two-fold symmetry (Fig. 1B). For all subunits, the large AAA+ domain packs against the small AAA+ domain of the counterclockwise subunit in a conserved rigid-body fashion, and crosslinks across these interfaces are compatible with full ClpX function (Glynn et al., 2012). Thus, the functional ring can be viewed as six rigid-body units connected by hinges (Fig. 1B). Nucleotide-dependent changes in hinge geometry provide a potential way to couple ATP binding and hydrolysis in one subunit to conformational changes in neighboring subunits. However, direct evidence for such allosteric changes is lacking, and it is not known if L and U subunits interconvert and/or if a 4:2 ratio of L:U subunits is maintained during function.

To address these questions, we have developed and applied assays for subunit-specific nucleotide binding (nCoMET) and conformational changes (cCoMET), where CoMET signifies **co**ordinated **m**etal **e**nergy **t**ransfer, a method that relies on short-distance quenching of a fluorescent dye by a transition-metal ion (tmFRET; Taraska et al., 2009). Our results show that nucleotide binding to ClpX subunits with tight and weak affinities allosterically alters the conformations of neighboring subunits in a stepwise fashion, support a model in which L and U subunits in the ClpX ring dynamically interconvert during the functional cycle, and suggest that nucleotide binding stabilizes a ring with five L-like subunits, reminiscent of structures observed in the AAA+ rings of the E1 helicase and 26*S* proteasome (Enemark and Joshua-Tor, 2006; Lander et al., 2012). The operating principles and tools developed here should be broadly applicable to the study of other AAA+ machines and multimeric assemblies.

RESULTS

The N domain of ClpX is not required for machine function (Singh et al., 2001; Wojtyra et al., 2003) and was deleted in the variants used here. ClpX variants were typically expressed from genes encoding two, three, or six subunits connected by polypeptide tethers, as linking subunits in this way allows ClpP-mediated degradation of ssrA-tagged substrates, does not affect pseudo-hexamer formation, and permits mutations or fluorescent probes to be introduced into specific subunits (Martin et al., 2005).

New crystal structures

For crystallography, ClpX$^{\Delta N}$ variants were single-chain trimers or dimers. In addition, specific subunits were either wild-type (W), contained an E185Q (E) Walker-B mutation or R370K (R) sensor-2 mutation to eliminate ATP hydrolysis, or contained both ATPase mutations (ER). In previous structures with and without nucleotide, a covalently tethered E-E-ER ClpX$^{\Delta N}$ trimer crystallized as a pseudo hexamer with an L/U/L/L/U/L arrangement of subunits (Glynn et al., 2009). We obtained six new pseudo-hexamer structures. Most had the L/U/L/L/U/L pattern, including an E-E-ER trimer with bound ATPgS, E-R dimers, W-W-R trimers, W-W-W trimers, and W-W-W trimers with bound ADP (Table 1). Thus, the L/U/L/L/U/L arrangement is not a consequence of bound nucleotide, the number of covalent tethers, or the presence of specific mutations. However, one W-W-W structure revealed an L/L/L/L/L/L or 6L arrangement of subunits (Table 1; Fig. 2A).

We aligned the large domains of each subunit from the eight crystal structures and represented the small domains by vectors corresponding to one helix (Fig. 1C). As expected, there were two major categories, corresponding to L and U conformations, but substantial variations were evident in each class. For example, compared to single reference vectors, the average angular variability was 16 ± 7° (maximum 27°) among L subunits and 18 ± 13° (maximum 45°) among U subunits, highlighting the variability in the conformations of individual subunits that comprise the ClpX ring. This variability allowed us to model a plausible 5L:1U ring structure using subunits taken from the observed 4L:2U and 6L structures (Fig. 2A).
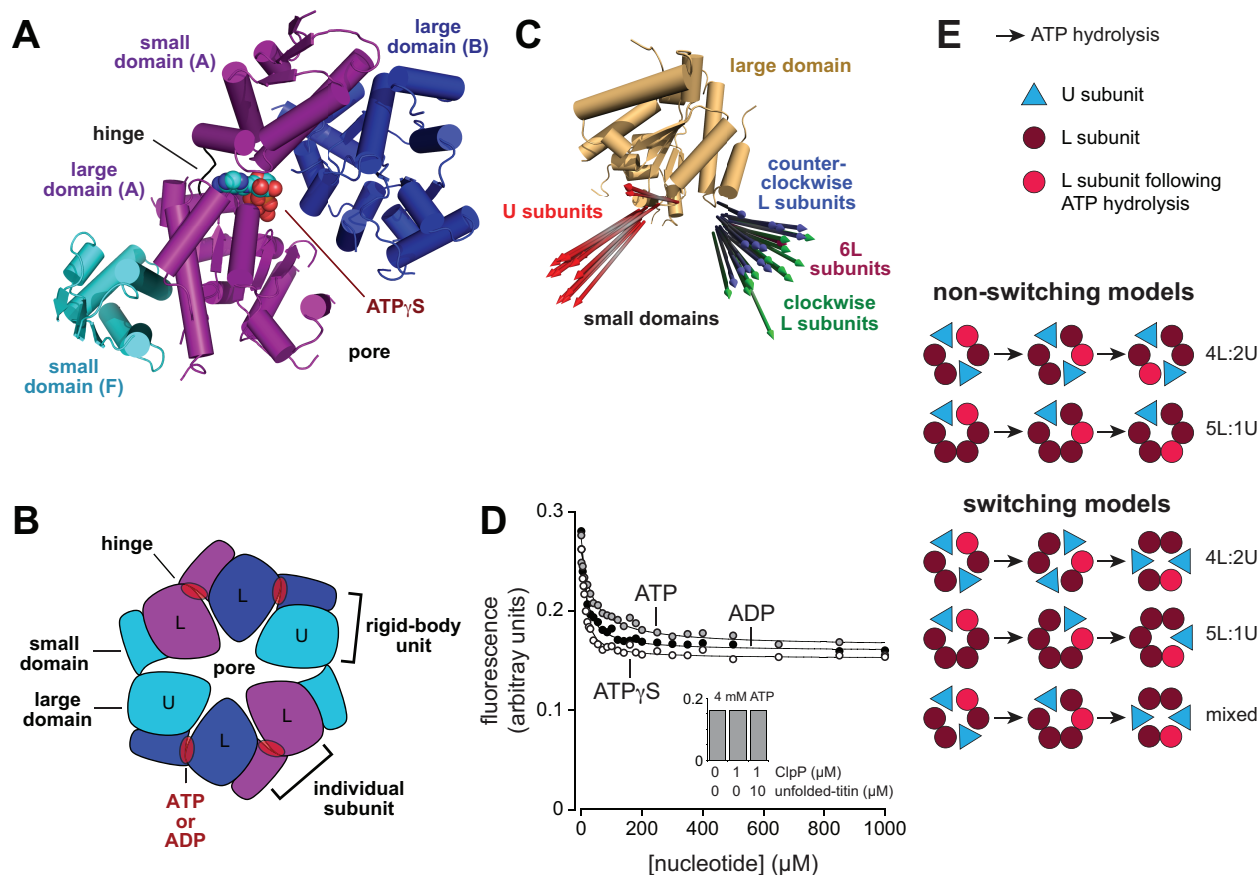
Figure 1. ClpX structure. **(A)** Nucleotide binds between the large and small AAA+ domains of a ClpX subunit and also contacts the neighboring large domain of the clockwise subunit. Each small domain and the large domain of the neighboring clockwise subunit form a rigid-body unit. The structure shown is from an ATPgS-bound hexamer (PDB code 4I81). **(B)** In most crystal structures, the ClpX ring consists of four L subunits, which can bind nucleotide, and two U subunits, which cannot bind nucleotide. The ring consists of six rigid-body units. Changes in the conformations of the hinges that connect the large and small domain of each subunit are responsible for major conformational changes in the hexameric ring. **(C)** After aligning the large AAA+ domains of each crystallographically independent subunit in eight crystal structures of *E. coli* ClpX hexamers (PDB codes 3HTE, 3HWS, 4I81, 4I4L, 4I34, 4I5O, 4I63, and 4I9K), the attached small domains were represented by a vector corresponding to a single a helix (residues 332-343). Although the vectors in U subunits are very different from those in L subunits, substantial variations within each subunit class are evident. **(D)** Addition of ATP, ATPgS, or ADP reduced the fluorescence of a W-W-W^{TT} pseudo hexamer (0.3 µM) to a level expected for a 5L:1U hexamer or a mixture of 4L:2U and 6L hexamers. The lines are fits to a hyperbolic equation with K_{app} values of 15 ± 2 µM for ADP, 41 ± 6 µM for ATP, and 9 ± 1 µM for ATPgS. **Inset**: The same final fluorescence value was observed in the presence of 4 mM ATP with or without ClpP (1 µM) and a titin^{I27} substrate (10 µM) unfolded by reaction with fluorescein-5-maleimide. **(E)** Models of ClpX function in which ClpX subunits retain their U or L identities (non-switching models) or subunits adopt U and L conformations at different points in the reaction cycle (switching models). See also Fig. S1 and Table S1.

Table 1. Crystallographic statistics.

ClpX variant	E-E-ER	W-W-W	W-W-W	W-W-R	E-R	W-W-W
PDB code	4I81	4I4L	4I34	4I5O	4I63	4I9K
tether length	20	20	20	20	20	0
bound nucleotide	ATPgS	ADP	none	none	none	none
crystallization well solution	*a*	*a*	*a*	*b*	*b*	*c*
Data collection						
space group	$P2_12_12_1$	$P2_12_12_1$	$P2_12_12_1$	$P2_12_12_1$	$P2_12_12_1$	$P6_3$
unit-cell lengths (a, b, c) (Å)	57.9 199.2 211.9	55.9 181.9 201.4	58.3 199.6 203.4	55.2 199.9 222.3	55.2 201.2 222.6	119.4 119.4 111.7
unit-cell angles (a,b,g) (°)	90, 90, 90	90, 90, 90	90, 90, 90	90, 90, 90	90, 90, 90	90, 90, 120
resolution (Å)	50.0 – 3.8	50 – 3.7	50.0 – 4.1	50.0 – 4.5	50.0 – 5.7	60.0 – 4.5
R_{sym} (%)	7.4 (84.3)	7.7 (30.9)	5.9 (29.4)	7.7 (27.8)	9.6 (35.2)	18.6 (27.2)
(I)/sig(I)	24.7 (1.6)	16.9 (3.1)	24.8 (3.8)	17.1 (4.3)	20.7 (2.9)	5.5 (4.1)
redundancy	6.7 (6.5)	3.8 (3.4)	5.7 (4.3)	4.0 (3.2)	8.5 (5.0)	6.4 (6.6)
completeness (%)	98.8 (95.5)	93.9 (95.3)	97.2 (84.1)	92.2 (80.4)	99.4 (96.2)	94.6 (95.7)
Refinement						
resolution (Å)	41.0 – 3.9	45.4 – 3.7	38.5 – 4.1	48.3 – 4.5	49.1 – 5.7	49.1 – 5.0
R_{work}/R_{free} (%)	26.2/29.6	27.5/33.4	27.4/30.8	28.6/32.3	30.7/31.5	32.2/35.2
rmsd bond angles (°)	0.452	0.508	0.499	0.452	0.449	0.613
rmsd bond lengths (Å)	0.002	0.003	0.003	0.002	0.002	0.004
allowed Ramachandran (%)	100	100	100	100	100	100

Well solution *a* is 1.9 M ammonium sulfate, 75 mM sodium acetate (pH 4.8). Well solution *b* is 2.2 M ammonium sulfate, 0.2 M ammonium bromide, 0.1 M bicine (pH 9.0). Well solution *c* is 2 M ammonium sulfate, 0.15 M potassium sulfate, 4 mM ATP, 4 mM $MgCl_2$ chloride, and 50 mM EDTA.
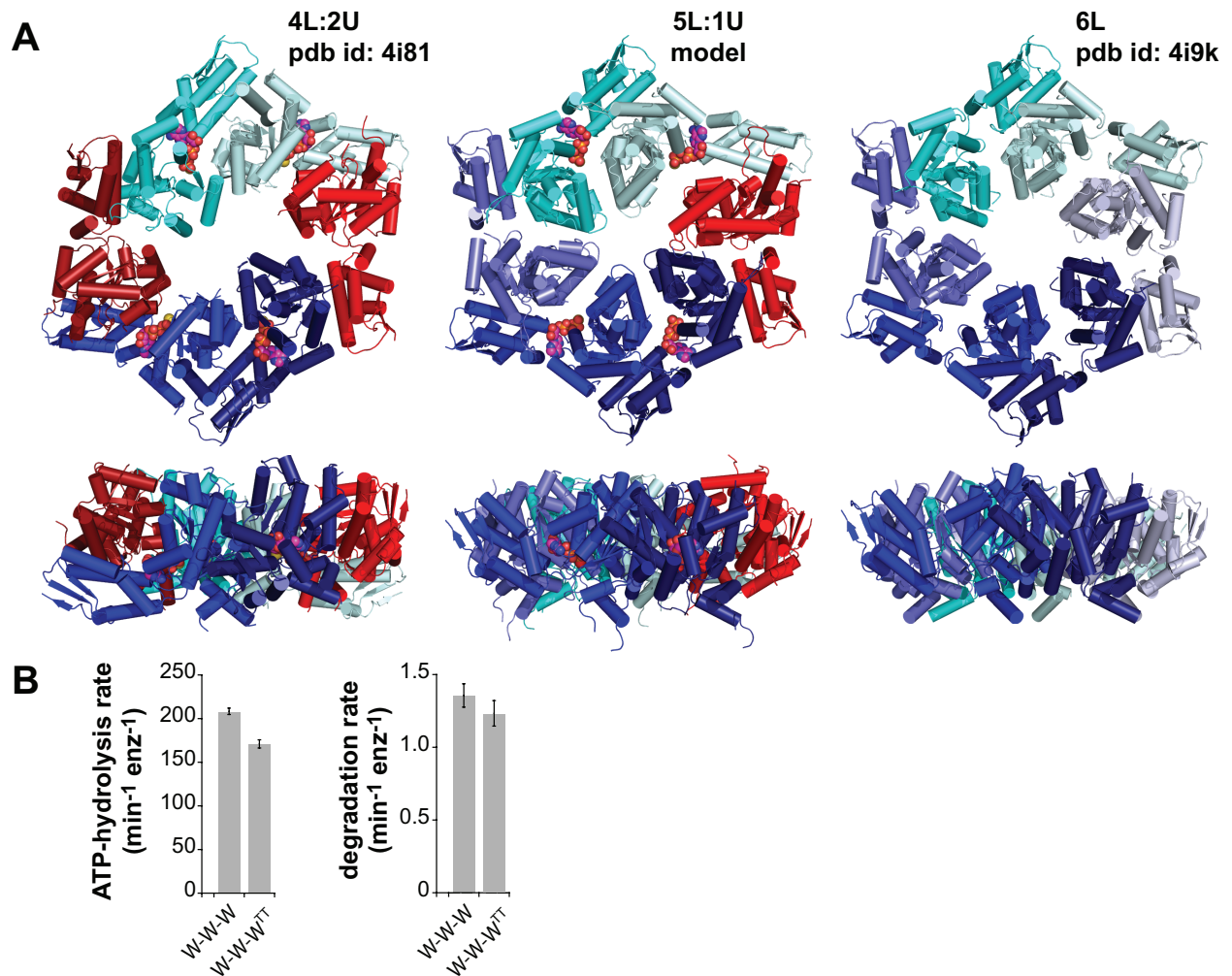
Figure 2. ClpX hexamer structures; W-W-W^{TT} activity. **(A)** Top and side views of structures (protein in cartoon representation; nucleotide in CPK representation) of a 4L:2U hexamer (left), the modeled 5L:1U hexamer (middle), and the 6L hexamer (right). The 4L:2U and 5L:1U structures are asymmetric, whereas the 6L structure is essentially 6-fold symmetric. **(B)** Tethered ClpX W-W-W^{TT} trimers (0.3 μM pseudo hexamer) containing the TT modifications (D76C^{TAMRA}; K330C^{TAMRA}) had activities similar to the parental W-W-W enzyme (0.3 μM pseudo hexamer) in hydrolyzing 4 mM ATP (left panel) and in supporting degradation of 10 μM cp7-GFP-ssrA by 0.5 μM ClpP (right panel). Data are shown as mean ± SD.

Evidence supporting 4L:2U and 5L:1U subunit arrangements

Contact between two rhodamine-family dyes, such as TAMRA, results in quenching that

displays an all-or-none character (Zhou et al., 2011). To address which arrangements of

ClpX subunits might be populated in solution, we produced a W-W-W^{TT} trimer in which

TT designates TAMRA dyes attached to K330C in the small domain and D76C in the large domain of the third subunit (the TAMRA-labeled protein was active in ATP hydrolysis and supported ClpP-mediated degradation; Fig. 2B). Modeling showed that the TAMRA dyes were close enough for contact quenching in L subunits but were >25 Å apart in U subunits. Compared to an unquenched control, we would therefore expect ~33% fluorescence for a population of 4L:2U hexamers, ~16% fluorescence for a population of 5L:1U hexamers, and no substantial fluorescence for a population of 6L hexamers. In the absence of nucleotide, the fluorescence of the W-W-W^{TT} pseudo hexamer was ~28% of a control sample of the same protein denatured in 3 M urea, as expected for a predominant population of 4L:2U structures (Fig. 1D). Addition of saturating concentrations of different nucleotides resulted in a decrease to ~16% of the unquenched control, consistent with a 5L:1U arrangement. These results are also consistent with a roughly equal mixture of 4L:2U and 6L hexamers at saturating nucleotide, but we consider this possibility less likely, as similar final fluorescence values at saturating ATP were also obtained when ClpX was bound to ClpP or was translocating an unfolded substrate into ClpP for degradation (Fig. 1D inset). Thus, if 4L:2U and 6L ClpX species were equally populated at saturating nucleotide, this equilibrium would have to be independent of the identity of the bound nucleotide and independent of ClpP binding and ATP-fueled protein degradation.

A test of subunit switching

In principle, L subunits and U subunits could either maintain their conformations during the chemo-mechanical cycle of ClpX or switch dynamically. Fig. 1E shows several non-

switching and switching models, but many more are possible, including variations in which ATP hydrolysis occurs sequentially or probabilistically among the L subunits that bind nucleotide and/or models in which subunit switching is not coupled to ATP hydrolysis.

One way to determine if L and U subunits maintain their conformations during ATP hydrolysis and protein unfolding by ClpX is to reduce ATP-binding affinity to one or a few subunits in the hexamer and test for effects on the ATP concentrations required for these activities. The logic is that non-switching models would allow low-affinity subunits to adopt U conformations, and thus the concentration of ATP required for activity should not be significantly altered. By contrast, if nucleotide must bind to each subunit in the ring at some point in a cycle, as required by most switching models, then substantially higher concentrations of ATP would be required for equivalent levels of ClpX activity. To weaken nucleotide affinity, we engineered V78A/I79A substitutions (hereafter called VI) to truncate the wild-type side chains and reduce packing with the adenine base of ATP (Fig. 3A). As anticipated, substantially higher concentrations of ATP were required to support ATP hydrolysis and ClpP-mediated protein degradation by the VI homohexamer compared to the parental enzyme (Fig. 3B; Table 2).
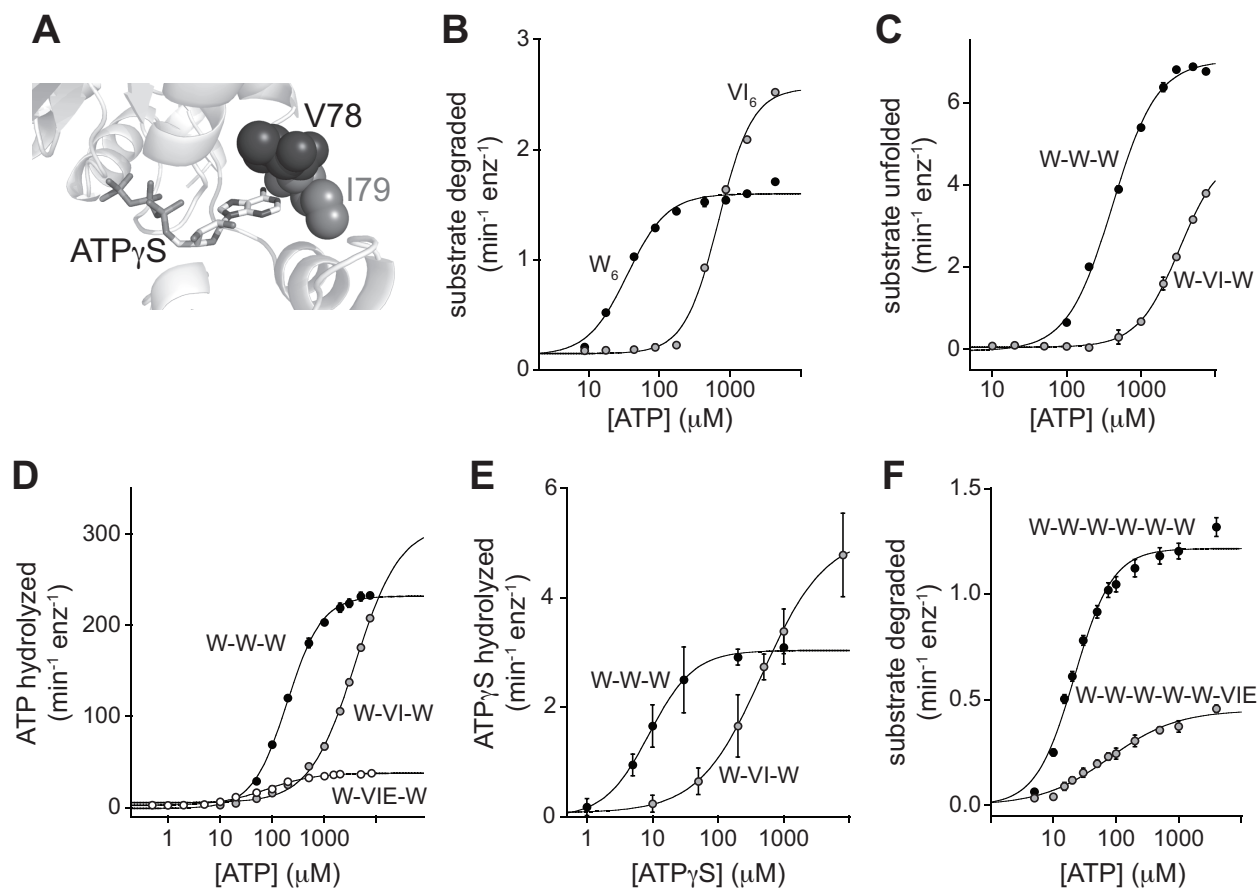
Figure 3. VI mutations alter the ATP dependence of ClpX function. **(A)** The side chains of Val78 and Ile79 contact the adenine base of bound nucleotide. **(B)** The VI mutations (V78A/I79A) in a non-tethered hexamer (VI_6) increased the concentration of ATP required to support degradation of cp7-CFP-ssrA (20 µM) by $ClpP_{14}$ (0.9 µM) compared to an otherwise identical hexamer (W_6) without the VI mutations. The VI_6 and W_6 concentrations were 0.3 µM. In panels B-F, data are shown as mean ± SD, and lines are fits to a Hill equation. Values of fitted parameters are listed in Table S2. **(C)** ATP dependence of the unfolding of cp7-CFP-ssrA (10 µM) by the W-W-W and W-VI-W ClpX variants (1 µM pseudo hexamer). This experiment and those in panels D and E contained 10 mM Co^{2+} and no Mg^{2+}. **(D)** ATP dependence of the rate of ATP hydrolysis for W-W-W, W-VI-W, or W-VIE-W (0.3 µM pseudo hexamer). **(E)** ATPgS dependence of the rate of ATPgS hydrolysis for W-W-W (0.1 µM pseudo hexamer) and W-VI-W (2 µM pseudo hexamer). **(F)** ATP dependence of the degradation of cp7-CFP-ssrA (20 µM) by ClpP (0.5 µM) supported by the W-W-W-W-W-W or W-W-W-W-W-VIE ClpX variants (0.2 µM pseudo hexamer). See also Fig. 3 and Table 2.

Table 2. Nucleotide-interaction parameters obtained from activity assays.

variant	nucleotide	assay	K_M or $K_{1/2}$ (µM)	Hill constant	R^2
W-W-W	ATP	hydrolysis	230 ± 3	1.3 ± 0.1	0.999
		unfolding	410 ± 23	1.4 ± 0.1	0.998
	ATPγS	hydrolysis	9 ± 1	1.3 ± 0.2	0.998
W-VI-W	ATP	hydrolysis	3900 ± 350	not determined	0.998
		unfolding	3300 ± 210	1.6 ± 0.1	0.999
	ATPγS	hydrolysis	470 ± 37	0.9 ± 0.1	0.999
W-VIE-W	ATP	hydrolysis	79 ± 7	0.9 ± 0.1	0.996
W-W-W-W-W-W	ATP	degradation	22 ± 2	1.4 ± 0.2	0.985
W-W-W-W-W-VI	ATP	degradation	40 ± 3	1.5 ± 0.2	0.987
W-W-W-W-W-VIE	ATP	hydrolysis	67 ± 11	1.3 ± 0.2	0.979
		degradation	79 ± 14	0.8 ± 0.1	0.987
W-W-VIE-W-W-W	ATP	hydrolysis	86 ± 16	1.1 ± 0.2	0.976
		degradation	98 ± 10	1.3 ± 0.1	0.993
W-W-W-W-W-VIK	ATP	degradation	400 ± 100	1.2 ± 0.2	0.972

VI – V78A/I79A
VIE – V78A/I79A/E185Q
VIK – V78A/I79A/K125M
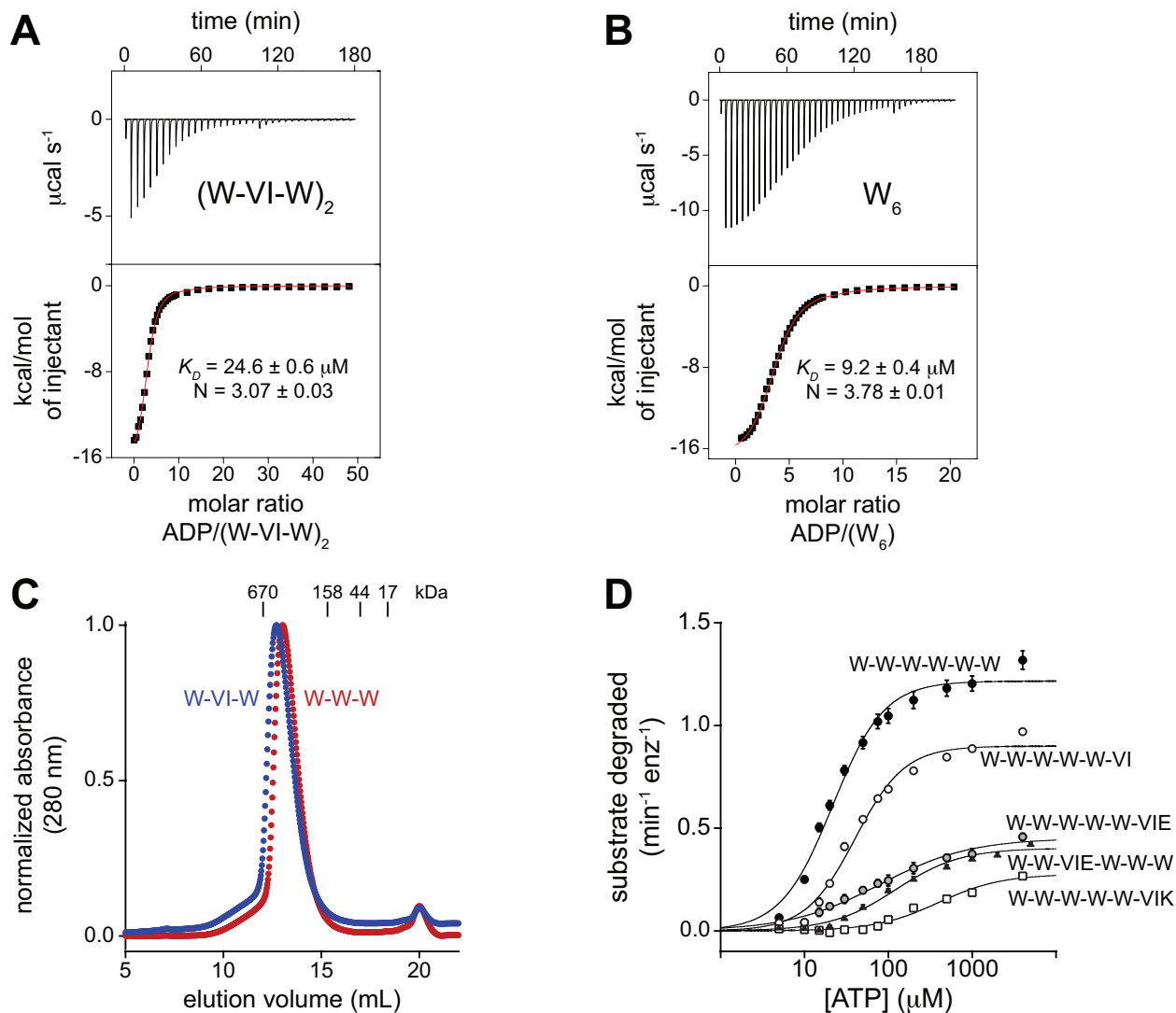
Figure 4. ADP binding and gel filtration; activity of covalent hexamers with one mutant subunit. (**A**) Binding of ADP to W-VI-W assayed by isothermal titration calorimetry. **(B)** Binding of ADP to W_6 ClpX assayed by isothermal titration calorimetry. In panels A and B, the initial concentrations in pseudo hexamer equivalents of the ClpX variants were 15.8 µM (W-VI-W) and 54.0 µM (W_6). Binding isotherms were fit to a one-site model using MicroCal Origin software. Data also fit well two a two-site model (W-VI-W; site 1: K_D = 3 ± 1 µM, N = 2.0 ± 0.6; site 2: K_D = 26 ± 10 µM, N = 1.3 ± 0.8; W6; site 1: K_D = 5 ± 2 µM, N = 2.0 ± 1.1; site 2: K_D = 46 ± 20 µM, N = 2.0 ± 0.8). **(C)** W-VI-W and W-W-W chromatographed at positions expected for pseudo hexamers on a Superose 6 gel-filtration column (loading concentration 15 µM). **(D)** ATP dependence of the rate of cp7-CFP-ssrA (20 µM) degradation by covalent ClpX hexamers (0.2 µM pseudo hexamer; 0.5 µM $ClpP_{14}$) containing all wild-type subunits or a single nucleotide-binding-deficient VI, VIE, or VIK subunit. The VIK subunit contains V78A/I79A and K125M, which alters the conserved lysine of the Walker-A motif and also prevents hydrolysis in the subunit bearing this substitution. The data for W-W-W-W-W-W and W-W-W-W-W-VIE are reproduced from Fig. 2F. The lines are fits to the Hill equation. Fitted parameters are listed in Table 2. Data are shown as mean ± SD.

To test the predictions of a 4L:2U non-switching model, we constructed a covalently tethered W-VI-W trimer and found that protein unfolding, ATP hydrolysis, and ATPgS hydrolysis all required ~10-fold higher ATP/ATPgS concentrations to achieve activities comparable to the W-W-W parent (Fig. 3C-E; Table 2). Like its wild-type counterparts, the W-VI-W enzyme ran as a pseudo hexamer in gel filtration and bound 3-4 ADPs in isothermal titration calorimetry (Fig. 4A-C). We also introduced the E185Q mutation into the VI subunit to generate W-VIE-W, as this mutation should only affect activity if nucleotide binds the VIE subunit, and found that W-VIE-W had much lower ATP-hydrolysis activity than W-VI-W (Fig. 3D). These results are inconsistent with a non-switching 4L:2U model and suggest that robust activity requires ATP occupancy and hydrolytic activity by at least one VI or VIE subunit in these pseudo hexamers.

To test a 5L:1U non-switching model, we constructed W-W-W-W-W-VIE and W-W-VIE-W-W-W enzymes, which had properties similar to each other (Table 2; Fig. 4D). In both cases, higher concentrations of ATP were required for function compared to the parental W-W-W-W-W-W enzyme and maximal activity was also reduced (Fig. 3F; Fig. 4D). These results suggest that ATP binds to the single VIE subunit of these pseudo hexamers, a result inconsistent with non-switching models. Additional pseudo hexamers with five wild-type subunits and one subunit with multiple mutations affecting ATP binding and/or hydrolysis also required increased concentrations of ATP for function (Fig. 4D).
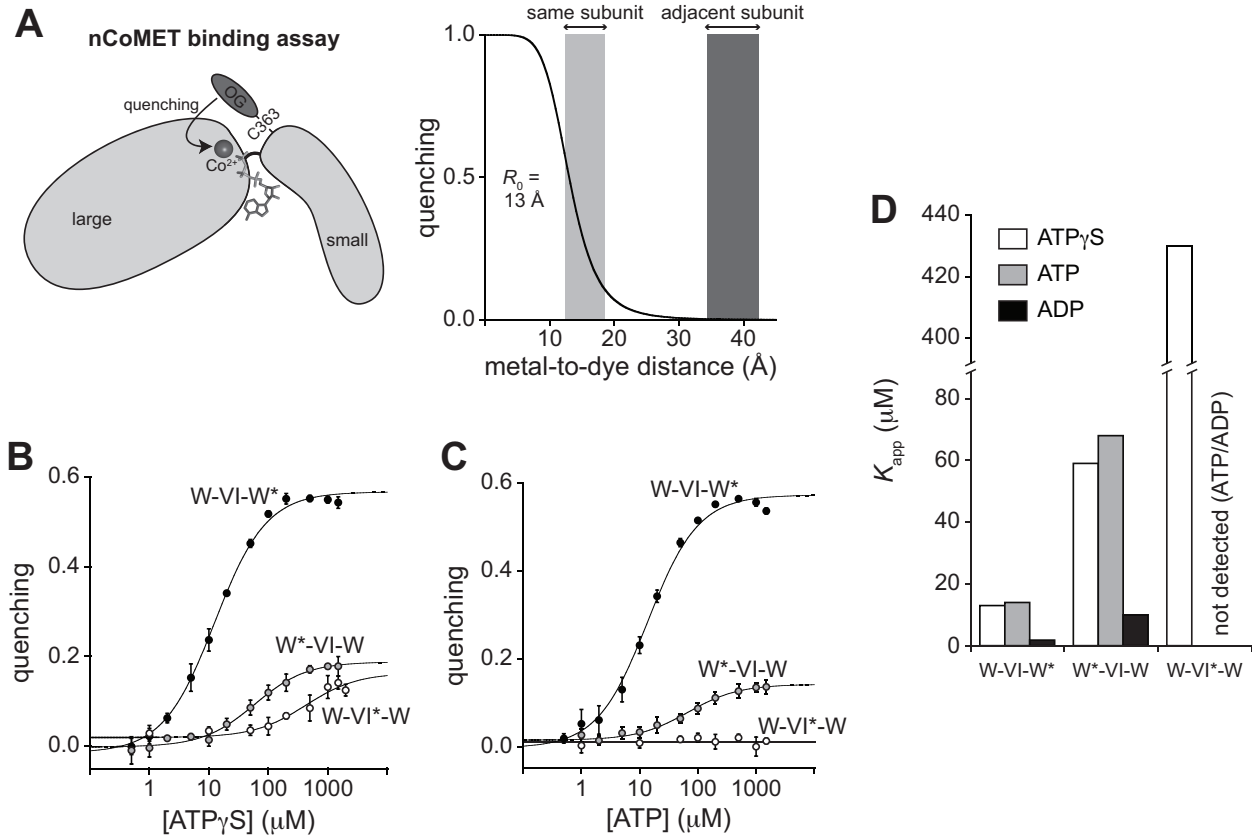
An assay for subunit-specific nucleotide binding

We developed nCoMET to measure nucleotide binding to specific sites in the ClpX ring. Mg^{2+} and nucleotide normally bind ClpX together, but Co^{2+} substitutes for Mg^{2+} and can quench the fluorescence of a nearby Oregon-Green dye with a calculated Förster radius (R_0) of ~13 Å (Fig. 5A). We attached this dye to ClpX residue M363C in just one subunit of the W-VI-W trimer, which should position the dye ~10-15 Å from the metal in the nucleotide-binding site of the same subunit. By contrast, the closest neighboring nucleotide-binding site is ~35 Å away, a distance at which nucleotide/Co^{2+} binding would cause less than 1% quenching. Although Mg^{2+} is normally required for ClpX function, Co^{2+} supported ATP/ATPgS hydrolysis and protein unfolding by W-VI-W and W-W-W (Fig. 6A-C), although it inhibited the ClpP peptidase (Fig. 6D). Indeed, the assays shown in Fig. 2C, 2D, and 2E contained Co^{2+} but no Mg^{2+} to allow comparisons of ClpX function and nucleotide binding under the same conditions. Modification of M363C with the Oregon-Green dye was also compatible with ClpX activity (Fig. 6E).

To allow nCoMET binding assays to different subunits, we generated and purified W*-VI-W, W-VI*-W, and W-VI-W* pseudo hexamers, where the asterisk indicates the subunit containing the nCoMET probe. Titration experiments were performed using ATP in the presence of protein substrate (Fig. 5B), ATPgS without substrate (Fig. 5C), or ADP without substrate (Fig. 6F). In each case, binding to the rightmost W* subunit was tight (K_{app} 2-14 µM), binding to the leftmost W* subunit was weaker (K_{app} 60-90 µM), and binding to the VI* subunit was even weaker (K_{app} 430 µM) or undetectable (Fig. 5D; Table 3). For ATP and ATPgS, K_{app} values are a function of the rate constants for nucleotide association and dissociation, the rate constant for hydrolysis, and the rate

45

constant for ADP dissociation, and thus are greater than true K_D's. Nevertheless, ADP

and ATP/ATPgS bound ClpX subunits over similar concentration ranges (Fig. 5D), a

finding we return to in the Discussion.

Figure 5. nCoMET detects nucleotide binding to specific subunits. **(A)** In the nCoMET assay, nucleotide binds ClpX and coordinates a Co^{2+} ion, which quenches the fluorescence of an Oregon-Green dye attached to M363C in the small AAA+ domain of a ClpX subunit. Given the calculated R_0, quenching would be substantial from nucleotide/Co^{2+} bound in the same subunit but minimal from nucleotide/Co^{2+} bound in neighboring subunits. **(B)–(C)** ATPgS and ATP binding to pseudo hexamers of W*-VI-W, W-VI*-W, and W-VI-W* assayed by nCoMET. Data are shown as mean ± SD, and the lines are fits to a hyperbolic equation. K_{app} values are listed in Table S2. The panel-B experiment contained 0.1 μM nCoMET variants (pseudo hexamer equivalents). The panel-C experiment contained 0.5 μM pseudo hexamer and 10 μM cp7-CFP-ssrA. **(D)** Summary of fitted K_{app} values for nucleotide binding to different classes of subunits. See also Fig. 6 and Table 3.

For ATPγS hydrolysis by W-VI-W, K_M (470 μM) was similar to K_{app} (430 μM) for

nCoMET binding to the VI subunit in W-VI*-W (Tables 2,3). For ATP hydrolysis by W-VI-

W in the presence of protein substrate, K_M (~4 mM) was 20-fold greater than the ATP

concentration required for nCoMET binding to the weakest wild-type subunits in W*-VI-W or W-VI-W* (Fig. 5D; Tables 2,3). Thus, as expected for a subunit-switching model, the high ATP/ATPgS concentrations required to support W-VI-W function appear to reflect binding of these nucleotides to the VI subunit.
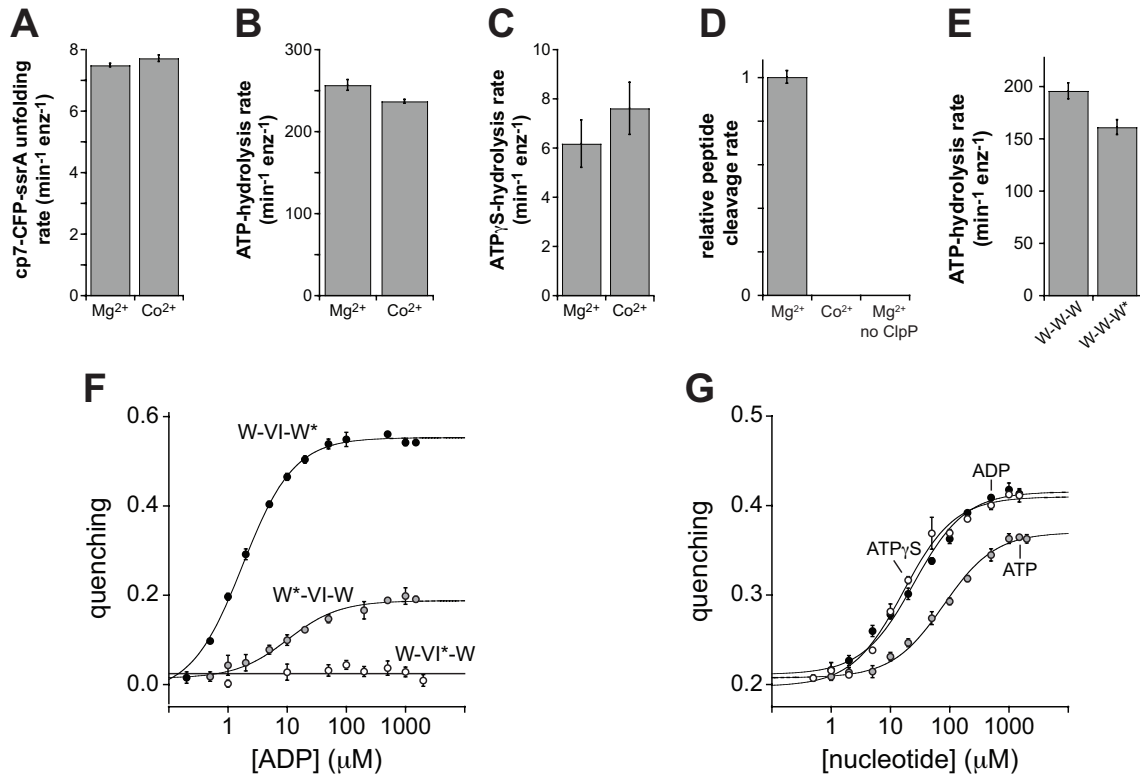
Figure 6. Metal dependence of ClpX and ClpP activity; ATP hydrolysis and nucleotide binding of nCoMET variants. (**A**) Mg^{2+} and Co^{2+} supported activity of W-W-W ClpX (1 µM pseudo hexamer) in unfolding 10 µM cp7-CFP-ssrA. **(B)** Mg^{2+} and Co^{2+} supported activity of W-W-W (0.3 µM pseudo hexamer) in hydrolysis of ATP in the presence of 10 µM cp7-CFP-ssrA. **(C)** Mg^{2+} and Co^{2+} supported activity of W-W-W (1 µM pseudo hexamer) in hydrolysis of ATPgS. In panels A-C, assays were performed in PD buffer supplemented with the appropriate divalent metal (10 mM) at room temperature. **(D)** Co^{2+} inhibits ClpP cleavage. The rate of cleavage of a succinyl-Leu-Tyr-AMC dipeptide (50 µM) by $ClpP_{14}$ (1 µM) was assayed by changes in fluorescence (excitation 345 nm; emission 440 nm) in PD buffer supplemented with 10 mM $MgCl_2$ or 10 mM $CoCl_2$. Rates were normalized to the rate with 10 mM $MgCl_2$. **(E)** Rates of hydrolysis of ATP (5 mM) by W-W-W and the Oregon-Green labeled W-W-W* variant (0.3 µM pseudo hexamer) in the presence of cp7-CFP-ssrA (10 µM). **(F)** ADP binding to pseudo hexamers (0.1 µM) of W*-VI-W, W-VI*-W, and W-VI-W* assayed by nCoMET. The lines are fits to a hyperbolic equation. K_{app} values are listed in Table S3. **(G)** Nucleotide binding to W-W-W* (0.1 µM pseudo hexamer for ATPγS and ADP titrations; 0.5 µM pseudo hexamer plus 10 µM cp7-CFP-ssrA for ATP titration) assayed by nCoMET. Lines are fits to a hyperbolic function. K_{app} values are listed in Table S3. Data are represented as mean ± SD.

Table 3. Nucleotide-interaction parameters obtained from nCoMET assays of binding.

| variant	nucleotide	K_{app} (µM)	R^2
W-W-W*	ADP	25 ± 4	0.990
	ATP	79 ± 8	0.996
	ATPγS	17 ± 2	0.994
W-VI-W*	ADP	1.8 ± 0.1	0.998
	ATP	14 ± 1	0.996
	ATPγS	13 ± 1	0.998
W*-VI-W	ADP	10 ± 2	0.982
	ATP	68 ± 14	0.984
	ATPγS	59 ± 8	0.992
W-VI*-W	ADP	not detected	
	ATP	not detected	
	ATPγS	430 ± 200	0.947

VI – V78A/I79A

Subunit-specific conformational changes

We developed cCoMET to assay how the conformations of specific subunits in the ClpX ring were altered by nucleotide binding. In this variation of tmFRET (Taraska et al., 2009), quenching is determined by the distance between a TAMRA dye attached to K330C in the small AAA+ domain and a Ni^{2+} ion bound to an a-helical His-X_3-His motif in the large domain of the same subunit (Fig. 7A). The His-X_3-His site was engineered by introducing N72H and D76H mutations in combination with H68Q to remove an alternative Ni^{2+}-binding site, and nitrilotriacetic acid (NTA) was included in assays to minimize Ni^{2+} binding to nucleotides. The calculated R_0 for the Ni^{2+}-TAMRA pair is ~14 Å, and thus strong quenching should occur in L subunits (modeled distance 8-15 Å) and weak or no quenching should occur in U subunits (19-31 Å). The mutations and modifications required for this assay did not affect ATP hydrolysis or protein degradation (Fig. 8A,B).

We introduced the cCoMET modifications (§) to generate W§-VI-W, W-VI§-W, and W-VI-W§ pseudo hexamers and assayed the nucleotide dependence of fluorescence quenching using conditions differing from nCoMET only in the divalent metals. Changes in cCoMET quenching were determined as a function of ATP with protein substrate present (Fig. 7B), as a function of ATPgS without substrate (Fig. 7C), and as a function of ADP without substrate (Fig. 8C). As nucleotide increased, quenching generally increased from an initial value to a plateau that depended upon the variant and nucleotide. Several conclusions follow from these assay results. (*a*) At saturating nucleotide, the average distance between the dye and Ni^{2+} decreased both in W§ and in VI§ subunits. (*b*) Conformational changes in both the leftmost and rightmost W§ subunits occurred at low nucleotide concentrations, where only the rightmost subunits were substantially occupied in nCoMET assays (Fig. 7B,C). Thus, the first nucleotide-binding events cause allosteric changes in both bound (rightmost W) and unbound (leftmost W) subunits of the ring, possibly altering the hinge conformations and rigidifying the domain-domain interfaces in L subunits. (*c*) In VI§ subunits, the Ni^{2+}-dye distance increased slightly at low ATP concentrations and then decreased substantially at higher ATP concentrations (Fig. 7C). The low-ATP transition corresponds to binding to tight W sites in nCoMET assays, whereas the high-ATP transition occurred at concentrations at which ATP binding to both weak W subunits as well as VI subunits was observed. Thus, nucleotide binding to weak W and VI subunits stabilizes a different conformation (possibly a 5L:1U ring) than binding to tight subunits. (*d*) Although there were small differences depending on the nucleotide, the magnitude of maximal quenching in VI§ and W§ subunits was generally similar, suggesting that these subunits spend roughly

comparable amounts of time in L and U conformations because of switching.
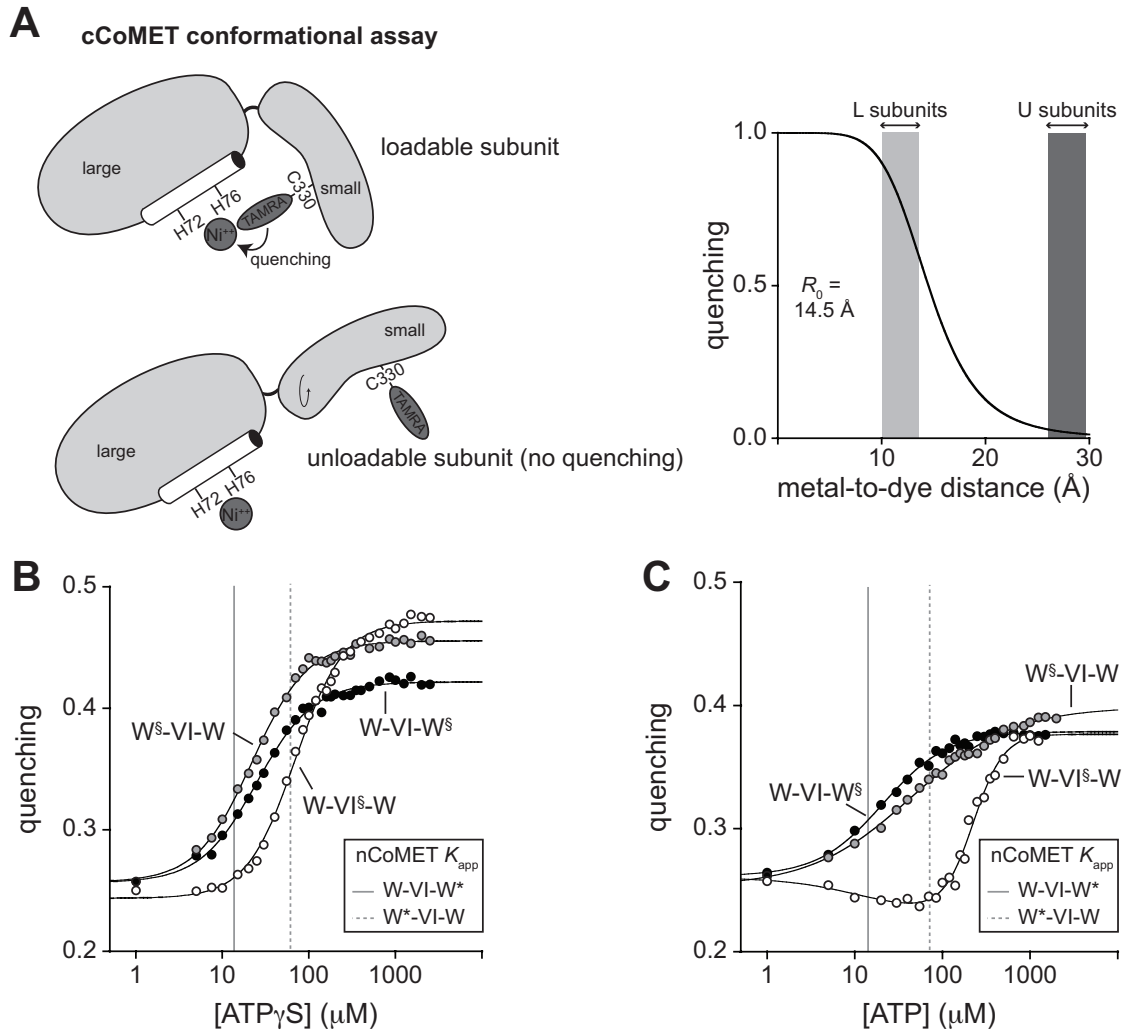
Figure 7. cCoMET detects conformational changes in specific subunits. **(A)** The cCoMET assay measures quenching of a TAMRA dye attached to K330C in the small domain of a ClpX subunit by a Ni^{2+} ion bound to an a-helical His-X_3-His motif in the large domain. Based on distances estimated from crystal structures and a calculated R_0, L subunits should display moderate quenching and U subunits should display little or no quenching. **(B)** ATPgS-dependent changes in the conformations of subunits containing cCoMET probes (§) were assayed for pseudo hexamers (0.3 µM). Lines are fits to a Hill equation with K_{app} and n values of 22 ± 1 µM and 1.4 ± 0.1 (W§-VI-W), 70 ± 2 µM and 1.5 ± 0.1 (W-VI§-W), or 25 ± 1 µM and 1.3 ± 0.1 (W-VI-W§). The solid gray vertical line represents K_{app} for tight binding to the rightmost subunit of W-VI-W* in nCoMET experiments, whereas the dashed vertical line represents K_{app} for weak binding to the leftmost subunit in W*-VI-W. **(C)** ATP-dependent cCoMET conformational changes using 0.3 µM pseudo hexamers and 10 µM cp7-CFP-ssrA. Lines are either fits to a Hill equation (K_{app} and n values of 45 ± 4 µM and 0.8 ± 0.1 for W§-VI-W, and 21 ± 1 µM and 1.2 ± 0.1 for W-VI-W§) or a hyperbolic plus Hill equation for W-VI§-W (hyperbolic phase, K_{app} = 12 ± 18 µM, amplitude = -0.03; Hill phase, K_{app} = 230 ± 13 µM, n = 2.5 ± 0.3, amplitude = 0.15). The solid gray and dashed vertical lines represent K_{app} values for binding to tight and weak subunits as defined in panel B. See also Fig. 8.
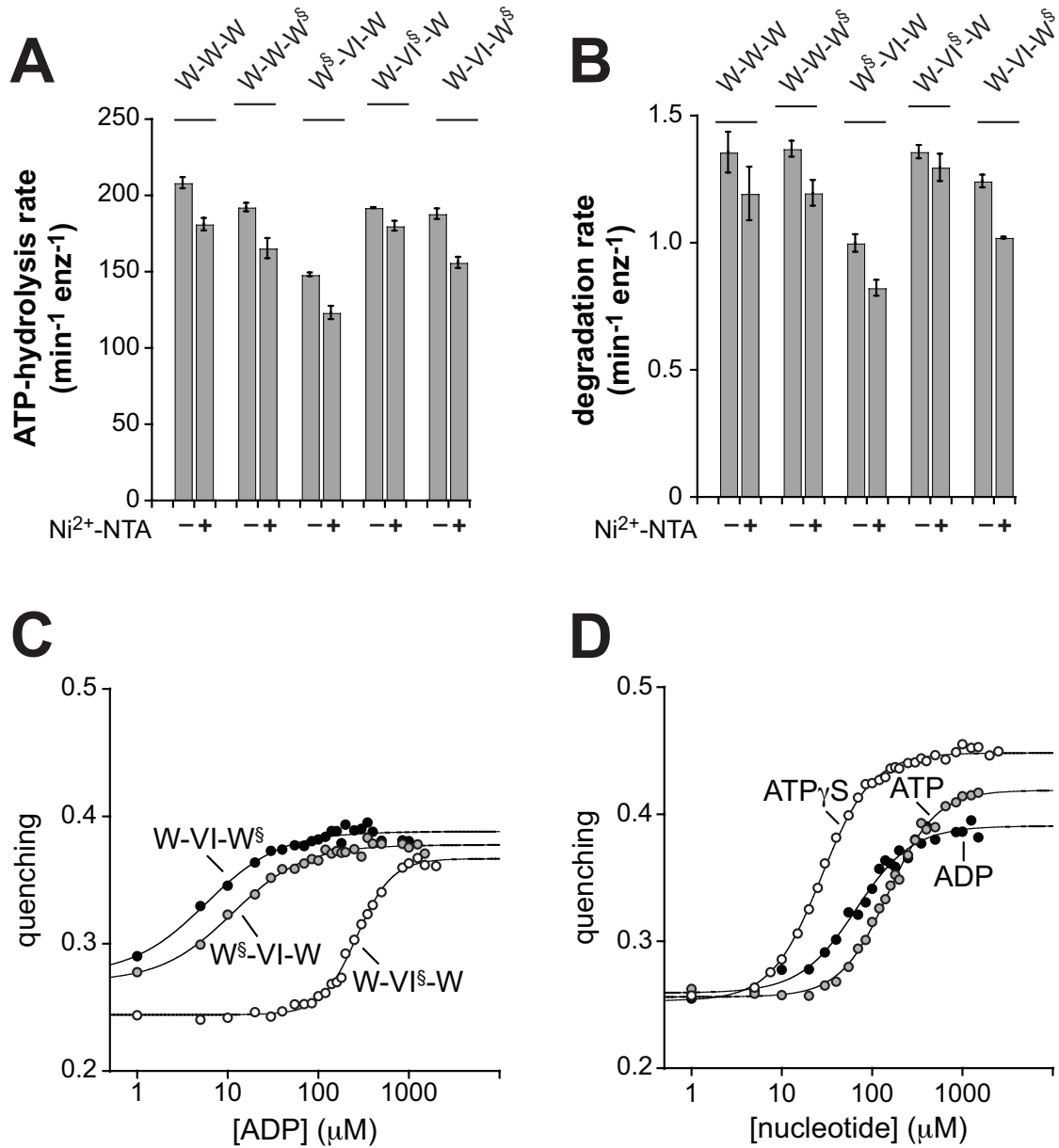
Figure 8. Activity and nucleotide dependence of cCoMET variants. (**A**) Tethered ClpX trimers (0.3 μM pseudo hexamer) containing the cCoMET (§) modifications (K330C^{TAMRA}; H68Q/N72H/D76H) were active in hydrolyzing 4 mM ATP in the presence or absence of Ni^{2+}-NTA (500 μM). (**B**) Modified variants were also active in supporting degradation of 10 μM cp7-GFP-ssrA by 0.5 μM ClpP. Same conditions as panel A. (**C**) ADP-dependent changes in the conformations of subunits containing cCoMET probes were assayed for pseudo hexamers (0.3 μM) of W§-VI-W, W-VI§-W, and W-VI-W§. Lines are fits to a Hill equation. The values of K_{app} and n were 11 ± 1 μM and 1.1 ± 0.1 for W§-VI-W, 270 ± 8 μM and 2.2 ± 0.1 for W-VI§-W, and 6 ± 2 μM and 1.1 ± 0.2 for W-VI-W§. (**D**) Nucleotide-dependent changes in the rightmost subunit of W-W-W§ (0.3 μM pseudo hexamer for ATPγS and ADP titrations; 0.3 μM pseudo hexamer plus 10 μM cp7-CFP-ssrA for ATP titration) assayed by cCoMET. Lines are fits to a Hill equation. K_{app} and n values were 66 ± 5 μM and 1.4 ± 0.1 for ADP, 150 ± 5 μM and 1.6 ± 0.1 for ATP, and 27 ± 1 μM and 1.6 ± 0.1 μM for ATPgS. Data are represented as mean ± SD.

51

We also performed cCoMET and nCoMET assays using W-W-W§ and W-W-W* constructs (Fig. 6G, Fig. 8D). In these cases, signal amplitudes were similar to those observed with the W-VI-W proteins, but averaging over all types of subunits precluded rigorous determination of interaction constants for individual classes.
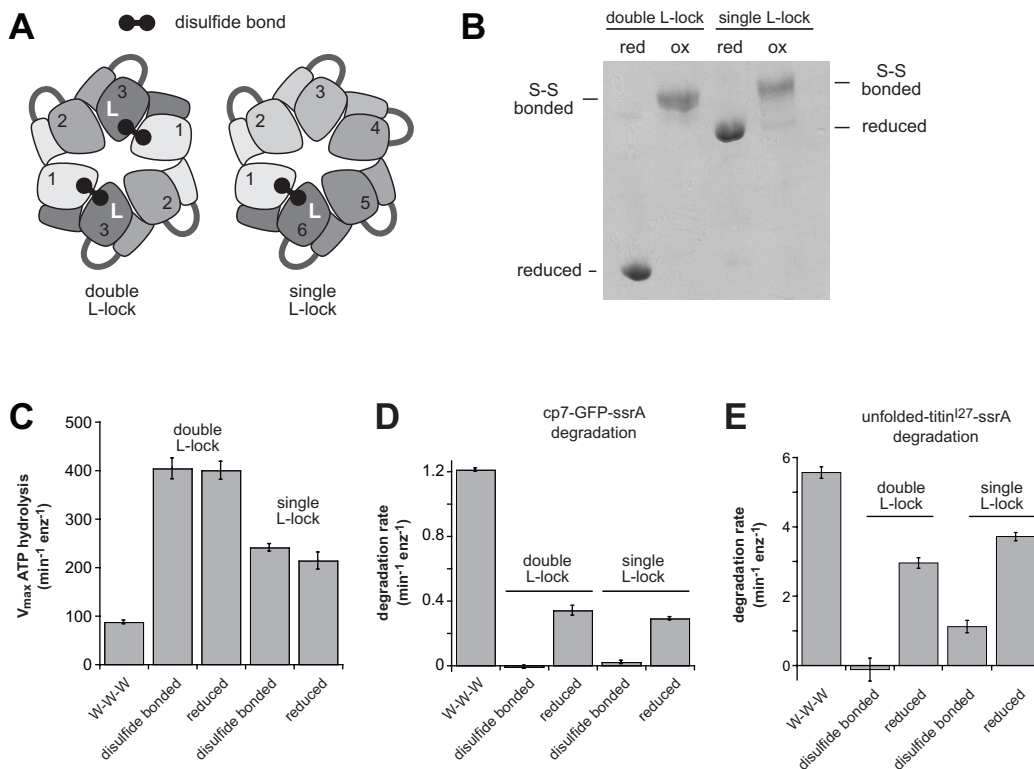
Locking subunits in the L conformation prevents unfolding and degradation

To prevent L→U switching, we engineered disulfide bonds to lock a single subunit or two opposed subunits of a pseudo hexamer in the L conformation. A T147C cysteine (TC) in the large domain of one subunit can form a disulfide with an E205C cysteine (EC) in the large domain of the clockwise subunit, only when the TC subunit adopts the L conformation. We constructed a linked trimer, with the EC mutation in the first subunit and the TC mutation in the third subunit, and we also constructed a linked hexamer, with the EC mutation in the first subunit and the TC mutation in the sixth subunit. Disulfide formation between two trimers forms a covalently closed hexameric ring, with subunit 3 of each trimer in the L-lock conformation (called double L-lock; Fig. 9A). Disulfide formation in the linked hexamer covalently closes the ring and locks subunit 6 in the L conformation (called single L-lock; Fig. 9A).

We purified these variants, catalyzed oxidation with copper phenanthroline, and confirmed that disulfides were formed by non-reducing SDS-PAGE (Fig. 9B), although 10-15% of the single L-lock protein remained reduced. The disulfide-bonded L-lock enzymes hydrolyzed ATP (Fig. 9C) at maximum rates comparable to the reduced

enzymes but faster than a W-W-W control. In the presence of ClpP, which binds both variants (Fig. 10), the disulfide-bonded enzymes showed poor or undetectable degradation of a folded protein substrate (cp7-GFP-ssrA) compared to the reduced proteins or W-W-W (Fig. 9D). Similarly, the disulfide bonded double L-lock enzyme failed to degrade an unfolded substrate (titin[I27]-ssrA with core cysteines modified by fluorescein) at an appreciable rate in the presence of ClpP, but degraded this substrate well following reduction (Fig. 9E). Following oxidation, the single L-lock enzyme displayed a low level of degradation of the unfolded substrate (Fig. 9E), although some of this activity may result from the reduced protein still present (Fig. 9B). ClpX rings topologically closed by formation of different disulfide bonds are fully active (Glynn et al., 2012). Thus, disulfide crosslinks that block L→U switching in one or two subunits of the ClpX ring uncouple ATP hydrolysis from efficient substrate unfolding and translocation.

Figure 9. Effects of L-lock disulfides on ClpX function. (A) Cartoon depiction of L-lock disulfide bonds between cysteines in the adjacent large AAA+ domains of subunits in the L conformation. (B) Non-reducing SDS-PAGE of the single and double L-lock proteins before and after treatment with 20 mM copper phenanthroline. For the single L-lock enzyme, ~15% of the sample was not disulfide bonded after oxidation. (C) Maximal rates of ATP hydrolysis were determined by Michaelis-Menten experiments using the indicated ClpX variants (0.3 µM pseudo hexamers). K_M values were 100 ± 19 µM (W-W-W), 2700 ± 350 µM (disulfide bonded double L-lock), 1250 ± 190 µM (reduced double L-lock), 440 ± 45 µM (disulfide bonded single L-lock), and 490 ± 120 µM (reduced single L-lock). (D) Rates of degradation of cp7-GFP-ssrA (10 µM) by the indicated ClpX variants (0.3 µM pseudo hexamers) and $ClpP_{14}$ (0.5 µM) in the presence of ATP (4 mM) and an ATP-regeneration system. (E) Rates of degradation of titin^{I27}-ssrA (20 µM) denatured by reaction with fluorescein-iodoacetamide by the indicated ClpX variants (0.3 µM pseudo hexamers) and $ClpP_{14}$ (0.9 µM) in the presence of ATP (10 mM) and an ATP-regeneration system. In panels C-E, data are shown as mean ± SD. See also Fig. S5.
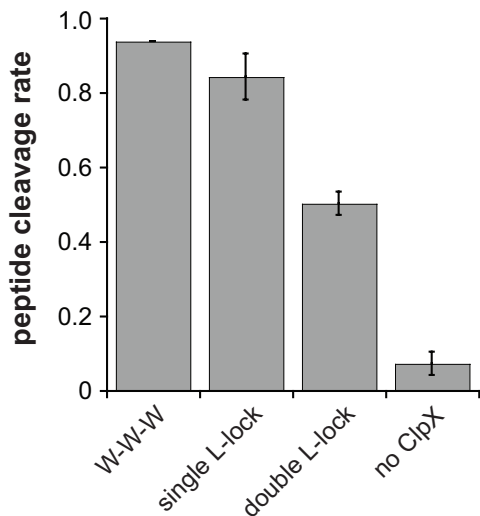
Figure 10. L-lock variants bind ClpP. Rates of cleavage of a fluorescent decapeptide (15 µM) by a cysteine-free $ClpP_{14}$ variant (50 nM) were determined in the presence of different ClpX variants (0.2 µM pseudo hexamer) and 1 mM ATPgS. The disulfide-bonded L-lock enzymes bind ClpP and enhance peptide cleavage, although they do not support degradation of protein substrates. Data are represented as mean ± SD.

Subunit communication and ATP hydrolysis

To determine if ATP hydrolysis requires communication between different nucleotide-binding sites, we designed mini-ClpX$^{\Delta N}$, which contains two rigid-body units that encompass a single nucleotide-binding site (Fig. 11A). We expected that a mini-ClpX$^{\Delta N}$ pseudo hexamer would not be stable because the surface buried between different

rigid-body units is small (Glynn et al., 2009). Indeed, mini-ClpX$^{\Delta N}$ eluted at a position expected for a molecule with two subunits in gel-filtration experiments (Fig. 11B). Mini-ClpX$^{\Delta N}$ hydrolyzed ATP at approximately 75% of the basal rate of a ClpX$^{\Delta N}$ hexamer on a per site basis, the K_M for ATP was similar for mini-ClpX$^{\Delta N}$ (210 µM) and W-W-W (230 µM; Table 2), and hydrolysis activity was abolished by an E185Q mutation in the single nucleotide-binding site in mini-ClpX$^{\Delta N}$ (Fig. 11C). Thus, hexamer formation and communication between different nucleotide-binding sites are not required for ATP binding and hydrolysis. However, mini-ClpX$^{\Delta N}$ did not bind ClpP (Fig. 11D) and exhibited no evidence of interacting with or unfolding protein substrates (Fig. 11C, 11E), suggesting that hexamer formation is required for these activities.
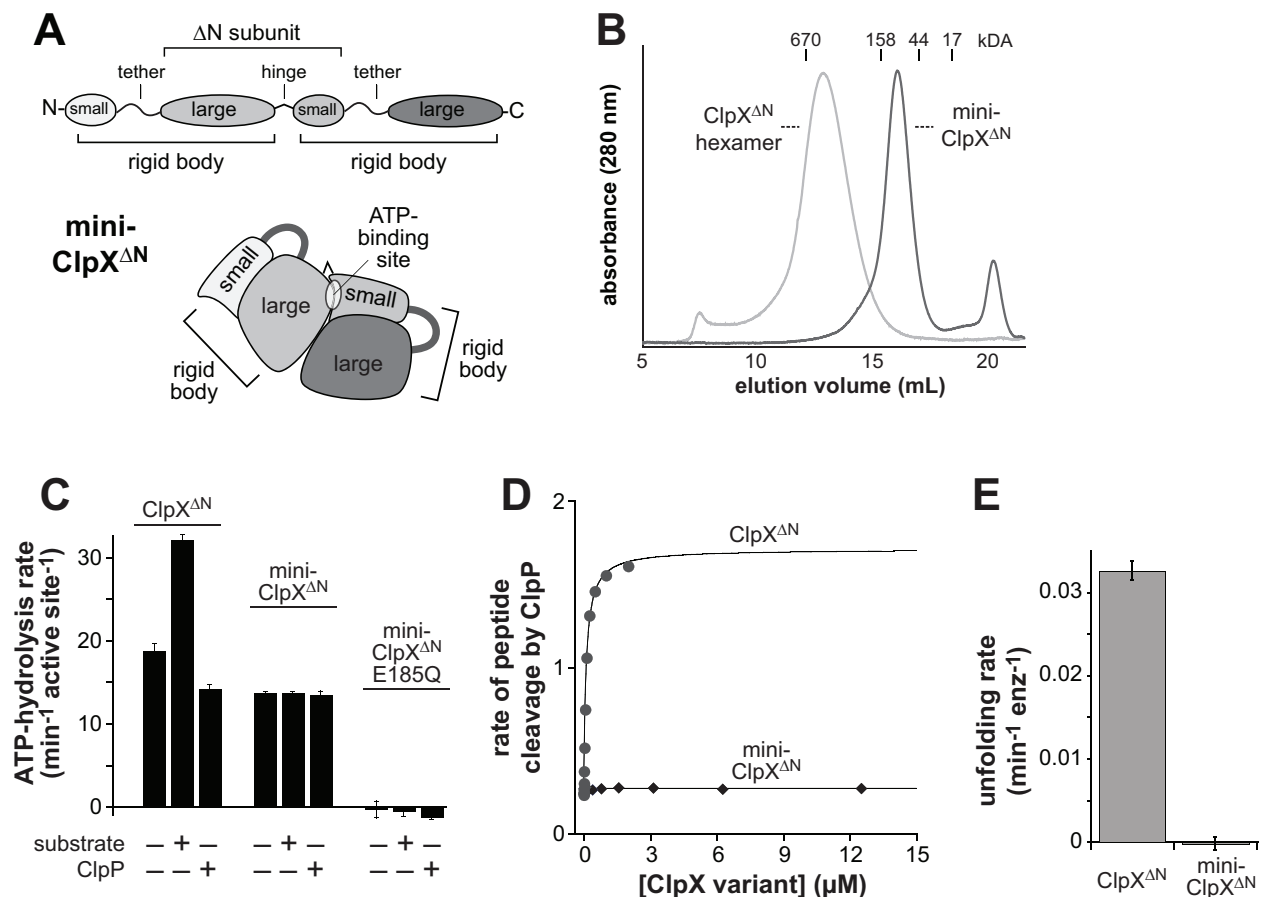
Figure 11. ATP hydrolysis by a variant with one binding site does not support function. (A) Cartoon depiction of the domain structure of mini-ClpX$^{\Delta N}$. This variant contains two rigid-body units but only one complete ATP-binding site. (B) Mini-ClpX$^{\Delta N}$ (loading concentration 12 µM) chromatographed at a position expected for a pseudo dimer on a Superose 6 gel-filtration column. The elution position of a single-chain ClpX$^{\Delta N}$ hexamer is shown for reference. (C) Mini-ClpX$^{\Delta N}$ hydrolyzed ATP at approximately 75% of the basal rate of single-chain ClpX$^{\Delta N}$ when activities were normalized for the number of active sites. Unlike ClpX$^{\Delta N}$, ATP hydrolysis by mini-ClpX$^{\Delta N}$ was not stimulated by protein substrate (10 µM V15P-titin^{I27}-ssrA) or repressed by ClpP$_{14}$ (3 µM). In panels C and E, data are shown as mean ± SD. (D) The rate of cleavage of a fluorescent decapeptide (15 µM) by ClpP$_{14}$ (50 nM) in the presence of increasing concentrations of single-chain ClpX$^{\Delta N}$ or mini-ClpX$^{\Delta N}$ was determined in the presence of 1 mM ATPgS. (E) Unfolding rates of photo-cleaved Kaede-ssrA (5 µM; Glynn et al., 2012) by single-chain ClpX$^{\Delta N}$ or mini-ClpX$^{\Delta N}$ (2 µM) were determined in the presence of 2.5 mM ATP and a regeneration system.

DISCUSSION

Setting and resetting the configuration of the ClpX ring

Our results support a model in which (*i*) the conformation of the hexameric ClpX ring is initially "set" in a staged nucleotide-binding reaction to allow ATP hydrolysis, and (*ii*) the configuration of the nucleotide-loaded ring is subsequently "reset" via isomerization that involves changes in the nucleotide-binding properties of subunits and reciprocal U→L and L→U subunit switching events that occur synchronously. Fig. 12 shows a model for ring-setting and ring-resetting reactions in which ATP binding causes one ClpX subunit in a 4L:2U ring to switch from a U→L conformation, resulting in a 5L:1U ring. We expect the 5L:1U structure to persist as long as ATP is plentiful but cannot exclude models in which the ring occasionally reverts to a 4L:2U structure. More complicated models in which the active enzyme is a 6L ring that switches through a 4L:2U intermediate, or that involve mixtures of 4L:2U, 5L:1U, and 6L rings are also possible. We favor the 5L:1U model shown, in part, because structures with five L-like subunits and one U-like subunit are observed in the AAA+ rings of the E1 helicase and 26*S* proteasome (Enemark and Joshua-Tor, 2006; Lander et al., 2012), and a 5L:1U ClpX ring is

structurally plausible. Because a maximum of ~4 nucleotides bind to the ClpX hexamer (Hersch et al. 2005; Fig. S2B), we also posit that a 5L:1U ring contains one L subunit that is nucleotide free or binds nucleotide only transiently.
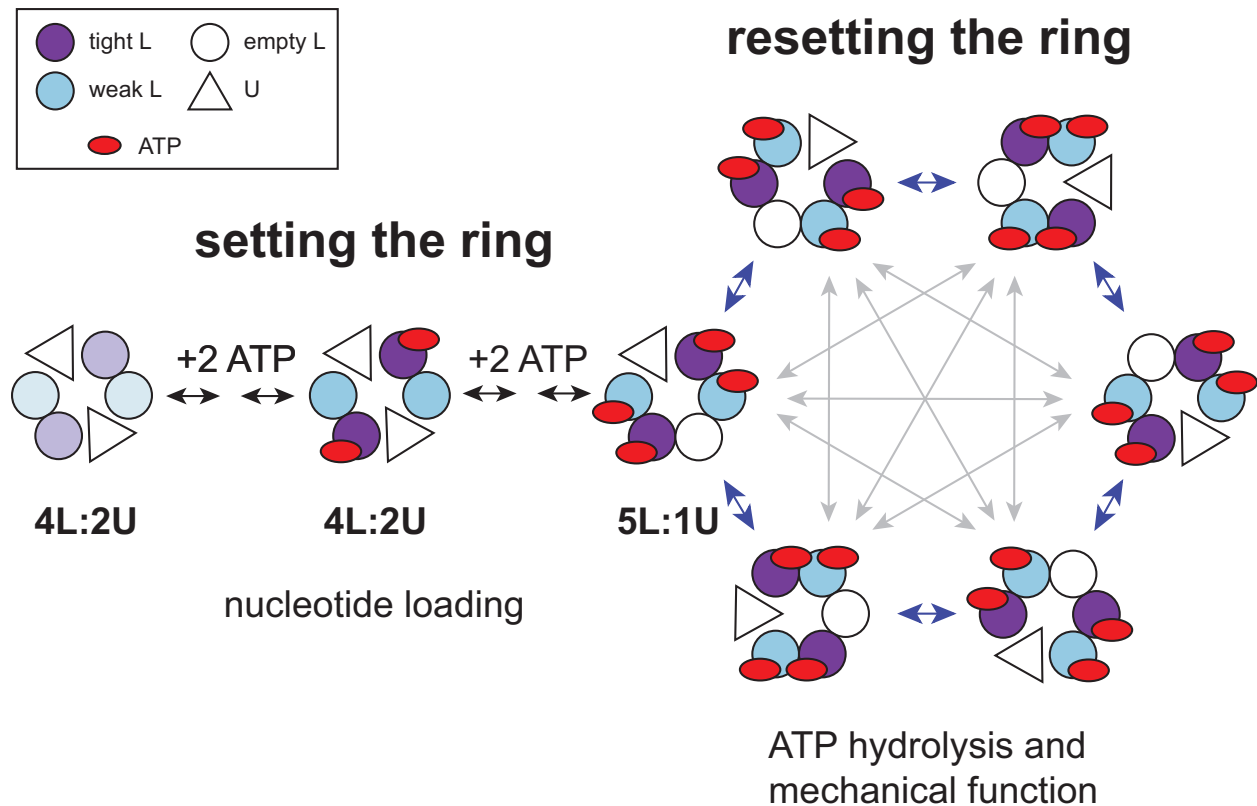
Figure 12. Model for ring-setting and ring-resetting reactions. The left side of the figure shows the proposed ring-setting reaction. In the absence of nucleotide, ClpX hexamers mainly adopt a 4L:2U ring structure with two U subunits (triangles), two L subunits with high affinity for nucleotide (light purple circles), and two L subunits with low affinity for nucleotide (light blue circles). ATP (red oval) binding to the high-affinity subunits changes the conformations of both classes of loadable subunits (designated by color darkening), but this intermediate is inactive in ATP hydrolysis. Subsequent ATP binding to the low-affinity L subunits stabilizes a 5L:1U configuration of the ring, which is active in ATP hydrolysis, but the new L subunit (white circle) has very low nucleotide affinity and is generally empty. The right side of the figure shows ring-resetting reactions (gray arrows), in which reciprocal L⇔U subunit switching changes the configuration of the ring. These isomerization reactions are required for efficient protein unfolding and translocation of substrates by ClpX. Resetting of the ring could occur sequentially, with subunit switching proceeding clockwise or counterclockwise in rotary order around the perimeter (blue arrows), or stochastically, with subunits switching in a probabilistic fashion (gray arrows). Many variations of the model shown are possible.

Stepwise conformational changes, driven initially by ATP binding to high-affinity subunits and subsequently by binding to lower-affinity subunits, are key features of the ring-setting reaction. Our results indicate that only the fully loaded ring can perform mechanical work and show that little or no ATP hydrolysis occurs in the partially loaded intermediate with just the high-affinity ATP sites occupied. Thus, the ring-setting reaction minimizes ATP hydrolysis before it can be coupled to functional work. However, the mini-ClpX$^{\Delta N}$ pseudo dimer, which has just one nucleotide-binding site, hydrolyzes ATP efficiently with a K_M similar to wild-type hexamers. Thus, structural constraints imposed by formation of the hexameric ring appear to keep the high-affinity subunits in the partially loaded intermediate in a conformation poorly suited for ATP hydrolysis.

In our model, ring resetting involves synchronous and paired U→L and L→ subunit switching in the nucleotide-loaded ClpX hexamer, resulting in new isomers or ring configurations with individual subunits having redefined nucleotide-binding properties determined by their position with respect to the U and/or empty L subunits (Fig. 12). As we discuss below, resetting the ring appears to be required for the mechanical functions of the ClpX machine. Ring resetting could be linked to ClpX activity in two ways. First, coupled L→U and U→L switching could be a normal consequence of ATP hydrolysis, occurring with each power stroke or some fixed number of power strokes. Alternatively, ring resetting could be independent of a fixed number of hydrolysis events. Such probabilistic resetting could provide a way to escape stalling in situations in which machine function might otherwise be compromised. These situations could include

failed protein-unfolding attempts, as for very stable proteins fewer than 1% of ClpX ATP-hydrolysis events result in unfolding (Kenniston et al., 2003), or binding of an inappropriate nucleotide. For example, ADP binds ClpX subunits over concentration ranges similar to or lower than ATP, yet ClpX functions well in the presence of equimolar ATP and ADP (Chapter 3). Ring isomerization might allow ClpX to eject improperly bound ADP and avoid prolonged stalling and could also help explain how ClpX hexamers with only one or two hydrolytically active subunits escape stalling as they unfold and translocate protein substrates (Martin et al., 2005).

Evidence for subunit switching

Our results support L⇔U switching during ClpX function. For example, we find that weakening the nucleotide affinity of one or two subunits in a hexamer increases the concentration of ATP/ATPgS required for ClpX activity, a result expected for a switching model in which nucleotide must bind to every subunit in the hexameric ring at some time during the multiple enzyme cycles required for protein unfolding and translocation. In a non-switching model, by contrast, a low-affinity subunit could simply assume a U or empty L conformation and would only alter the ATP dependence of enzyme function by restricting the number of active ring configurations, which would produce much smaller activity effects than those we observe. Moreover, when we crosslink one or two ClpX subunits in the L conformation using disulfide bonds, these enzymes hydrolyze ATP and bind ClpP but do not efficiently unfold protein substrates and/or translocate unfolded substrates into ClpP, a result that suggests that ATP hydrolysis is not tightly coupled to mechanical work.

L⇔U switching is also supported by cCoMET results. Each type of subunit in the W-VI-W pseudo hexamer displayed roughly similar quenching at saturating concentrations of nucleotide. Thus, in a nucleotide-loaded ring, the average Ni^{2+}-TAMRA distance must be similar in high-affinity and low-affinity W subunits as well as in VI subunits. Based on crystal structures, moderate quenching is expected for loadable subunits and very low quenching for unloadable subunits. Thus, our cCoMET results suggest that no single type of subunit in W-VI-W adopts just an L conformation or just a U conformation, but rather that all subunits sample both conformations. This result is inconsistent with non-switching models, in which the VI subunits would preferentially adopt the U conformation. For ATP and ATPgS, hydrolysis-powered L⇔U switching could explain these results. For ADP, however, subunit switching would need to be thermally driven. Indeed, ongoing single-molecule studies using the assays described here show subunit switching in the presence of saturating ADP (A.R.N., T.A.B., R.T.S., Y. Shin, H. Manning, and M. Lang, unpublished).

Structural and functional classes of ClpX subunits

In our crystal structures, substantial conformational variations occur within the general L and U classes of ClpX subunits. Indeed, this variation could allow each L subunit in a 4L:2U or 5L:1U ring to have different nucleotide-binding properties. In previous studies of nucleotide binding to ClpX hexamers, evidence was presented for tight, weak, and empty sites with an approximate ratio of four binding to two non-binding subunits (Hersch et al., 2005). Subsequent studies with the hexameric HslU and PAN AAA+

60

unfoldases revealed similar nucleotide-binding categories and ratios (Yakamavich et al., 2008; Smith et al., 2011). Our current studies support multiple classes of nucleotide-binding sites, and suggest a basic ring pattern of [weak-empty-tight-weak-empty-tight] sites, with the proviso that empty sites may bind nucleotide transiently and very weakly. Based on our nCoMET and cCoMET studies, ATP binding to tight subunits alters the conformations of weak subunits, whereas ATP binding to weak subunits alters the conformations of empty subunits. These allosteric effects can be viewed as being propagated to the subunit clockwise from the bound subunit, probably through the shared rigid-body unit. Because the conformational changes observed in different classes of subunits occur over different ranges of nucleotide, allosteric models in which there are just two conformations of the ClpX ring can be rejected.

Sequential versus probabilistic models

Subunits of hexameric AAA+ and related enzymes may be coordinated by either a sequential model, in which ATP hydrolysis and conformational changes occur in an ordered progression around the ring, or by a probabilistic model, in which sequential events are possible but not obligatory. In the tightly coupled chemical and mechanical cycles of the F_1 ATPase, for example, the hydrolytic b subunits switch in a strictly sequential reaction between conformations with different nucleotide-binding properties (Kinosita et al., 2000; Leslie and Walker, 2000). The structural changes in different classes of F_1 subunits are less dramatic than L⇔U switching in ClpX subunits and can be considered analogous to the modest structural changes between different classes of L subunits. Our results suggest that ATP must bind to every subunit in the ClpX ring at

some point during the multiple cycles required to unfold and translocate protein substrates and that these activities require U⇔L subunit switching. Whether these binding, hydrolysis, and switching reactions occur sequentially or probabilistically is unresolved, but several factors suggest that ClpX may operate by a mechanism that is at least partially probabilistic. First, as noted above, ClpX is rather insensitive to ADP inhibition, whereas inappropriate ADP binding stalls the F_1 motor for very long periods (Hirono et al., 2001). Second, unlike F_1, the ATP-hydrolysis and mechanical functions of ClpX are not tightly coupled. ClpX does not stall when unfolding fails, and our L-lock variants hydrolyze ATP rapidly without doing mechanical work. Third, previous studies showed that R-W-E-R-W-E rings, containing two non-adjacent W subunits that are hydrolytically active and four R or E subunits that are ATPase-defective, have ~30% of wild-type ClpX activity in ClpP-mediated degradation (Martin et al., 2005). Given our current results, ATP binding to non-hydrolytic subunits in R-W-E-R-W-E is likely to be important for setting the active conformation of the ring, and probabilistic subunit switching could then permit the two hydrolytic subunits to power substrate unfolding and translocation in a non-sequential reaction. We anticipate that assays at the single-molecule level, potentially using multi-color CoMET pairs in different subunits to establish how nucleotide binding and conformational switching are coordinated, will establish if ClpX and other AAA+ machines operate as strictly sequential motors, as probabilistic motors, or operate sequentially some of the time and probabilistically when necessary.

EXPERIMENTAL PROCEDURES

Materials

PD buffer contained 25 mM HEPES-KOH (pH 7.5), 100 mM KCl, 10% (v/v) glycerol, and 0.5 mM EDTA. IEXA buffer contained 20 mM HEPES (pH 7.8), 150 mM KCl, 10% (v/v) glycerol, and 1 mM EDTA. GF buffer contained 50 mM Tris (pH 7.0), 300 mM KCl, and 10% (v/v) glycerol. ATP (Sigma), ADP (Sigma), ATPγS (Roche), and GTP (Sigma) were dissolved in PD buffer, and adjusted to pH 7.0 by addition of NaOH.

Proteins

Unless noted, all ClpX variants were derived from *E. coli* ClpX$^{\Delta N}$ (residues 61-423), contained the C169S mutation to remove an accessible cysteine, and were constructed by PCR and purified generally as described (Martin et al., 2005; 2007). During purification of variants with reactive cysteines, buffers were degassed, argon sparged, and contained 0.5 mM EDTA to minimize oxidation. Buffer exchange and desalting steps were performed using a PD10 column (GE Healthcare).

ClpX variants used for nCoMET experiments initially contained an N-terminal His$_6$-SUMO domain. After Ni^{2+}-NTA affinity chromatography (Qiagen), these variants were exchanged into IEXA buffer, and the H$_6$-SUMO domain was cleaved by incubation with equimolar Ulp1 protease for 2 h at room temperature. Cleavage was confirmed by SDS-PAGE, and the mixture was chromatographed on a MonoQ column (GE Healthcare) using a gradient from 150 to 500 mM KCl. Fractions containing the nCoMET variant were incubated with Oregon Green 488 Maleimide (Invitrogen; 3 equivalents for each cysteine) for 30 min at room temperature and separated from unreacted dye on a Superdex S-200 column (GE Healthcare) equilibrated in GF buffer. The extent of

labeling was > 90% as determined by absorbance of the purified protein at the maximum of the dye and at 280 nm for this reaction and those described below.

ClpX variants used for cCoMET initially contained a TEV-cleavable C-terminal His$_6$ tag. After Ni^{2+}-NTA affinity chromatography, these variants were exchanged into PD buffer, incubated with TAMRA-5-maleimide (1.5 equivalents for each cysteine) for 30 min at room temperature, dithiothreitol (1 mM) was added to quench the reaction, and excess dye was removed by desalting. Proteins were incubated with equimolar TEV protease for ~1 h at room temperature to remove the His$_6$ tag, and a final purification step was performed using a Superdex S-200 column equilibrated in PD buffer. Disulfide-bond formation in L-lock variants was performed as described (Glynn et al., 2012).

The cp7-CFP-ssrA substrate was generated from cp7-GFP-ssrA (Nager et al., 2011) by PCR incorporation of the Y66W, A206K, and N146I mutations and initially contained a cleavable N-terminal His$_6$ tag. cp7-CFP-ssrA was purified by Ni-NTA^{2+} affinity chromatography, exchanged into IEXA buffer, incubated with 10 units of PreScission protease (GE Healthcare) for 2 h at room temperature to remove the His$_6$ tag, and the sample was diluted 5-fold into water and purified on a MonoQ column using a gradient from 30 to 500 mM KCl.

Crystallization and structure determination

Detailed methods are presented in the Supplement.

Fluorescence assays

Unless noted, assays were performed at room temperature in PD buffer, with nucleotides, metals, and substrate added as required. All nCoMET assays contained 10 mM $CoCl_2$, and nucleotide-dependent changes in fluorescence were measured using a PTI QM-20000-4SE spectrofluorimeter (excitation 500 nm; emission: 520 nm). Signal contamination from fluorescent CFP substrates, when present, was less than 2%. Addition of 1 mM GTP did not result in nCoMET quenching (Fig. 13A), confirming specificity. Ni^{2+} can also be used for nCoMET and supports ClpX function, but Co^{2+} results in a larger R_0 when paired with the Oregon-Green dye. nCoMET assays were limited to nucleotide concentrations below 2 mM, as higher concentrations appeared to alter fluorescence indirectly by binding Co^{2+}.

All cCoMET assays contained 500 μM Ni^{2+}, 500 μM NTA, and 10 mM $MgCl_2$. NTA was included because it binds Ni^{2+} ($K_D \sim 1$ nM) and reduces its affinity for free and ClpX-bound nucleotides but does not prevent binding to the His-X_3-His motif. Titration of ATP against W-W-W[§] in the absence of Ni^{2+}-NTA resulted in no quenching (Fig. 13B). Titration of Ni^{2+}-NTA against W-W-W[§] resulted in ~30% quenching with an affinity of 25 ± 2 μM (Fig. 13C). cCoMET can detect small conformational changes. For example, when a cCoMET pair was placed within a single rigid-body unit, ATP binding to high-affinity subunits resulted in quenching (Fig. 13D). Conformational changes of 3-4 Å caused by a minor change in the rigid body or side-chain movements that alter the dye-quencher distance, could account for these results.

The degree of TAMRA-TAMRA contact quenching for W-W-W[TT] was determined

relative to a control experiment with W-W-W^{TT} in 3 M urea (a W-W-W^{TT} sample degraded with elastase showed the same fluorescence as the sample in urea).
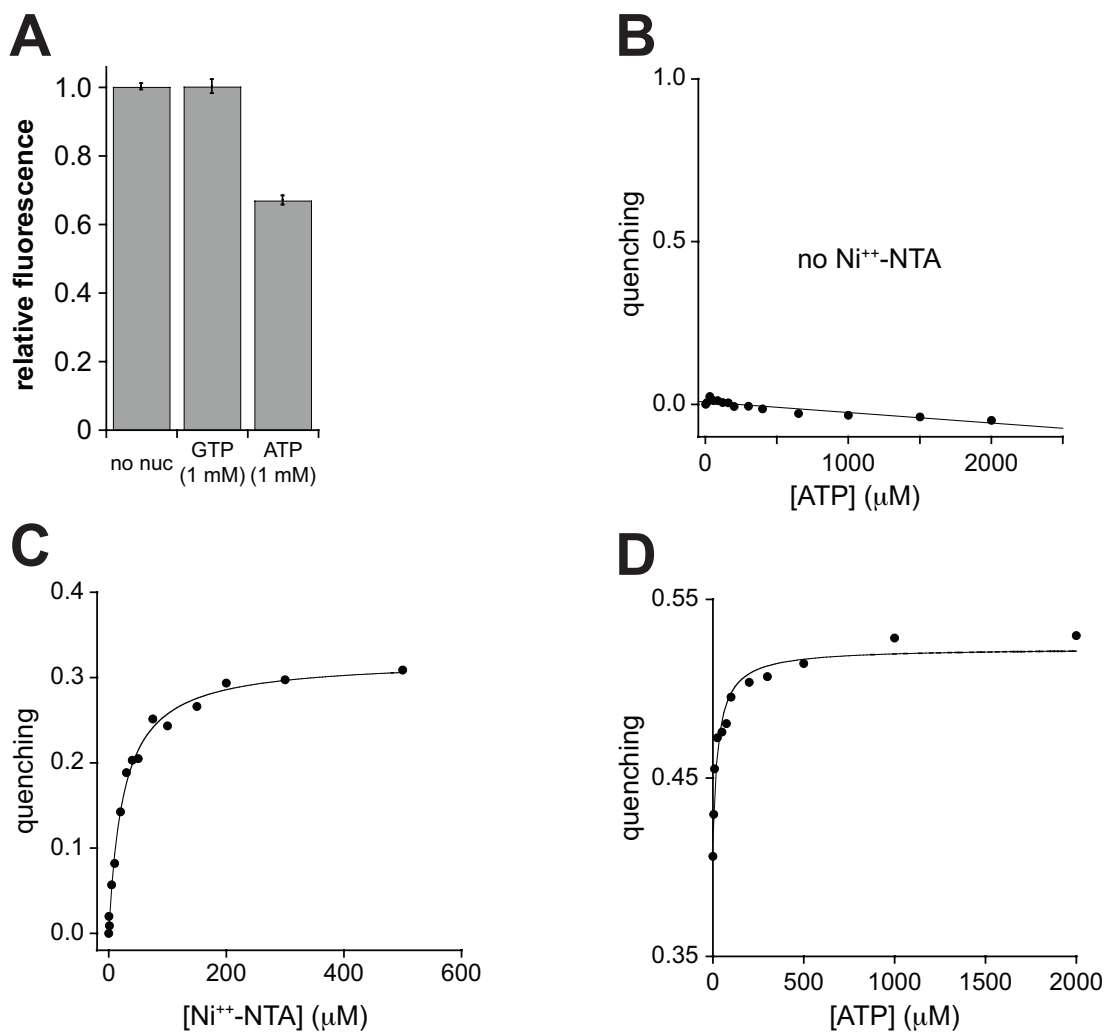
Figure 13. Specificity of nCoMET quenching; cCoMET controls. **(A)** Specificity of nCoMET quenching. In PD buffer plus 10 mM CoCl$_2$, ATP reduced the fluorescence of W-W-W*, but GTP or buffer with no nucleotide did not result in quenching. Data are shown as mean ± SD. **(B)** In the absence of Ni^{2+}-NTA, titration of ATP against W-W-W§ (0.3 µM) did not result in quenching. **(C)** Titration of Ni^{2+}-NTA against W-W-W§ (0.1 µM) gave ~30% quenching The line is a single hyperbolic fit with K_{app} = 25 ± 2 µM. **(D)** ATP dependence of cCoMET quenching for a W-W-W variant containing TAMRA-labeled S389C in the small AAA+ domain of the second subunit and the His^{72}-X$_3$-His^{76} mutations in the large domain of the third subunit. This cCoMET pair spans a single rigid-body unit. The line is a single hyperbolic fit with K_{app} = 30 ± 9 µM. At nucleotide concentrations at which the low-affinity sites are occupied and ATP hydrolysis occurs, no major changes were observed indicating that the conformational changes monitored with other cCoMET pairs, which correlate with ATP hydrolysis, involve changes across the hinged interfaces of ClpX rather than the rigid-body interfaces.

The apparent nucleotide affinities of individual subunits observed using nCoMET represent a time-weighted average over multiple conformations that occur as a consequence of subunit switching and other conformational changes. Thus, nCoMET may detect ATPgS but not ATP binding to the VI subunits of W-VI*-W because these subunits spend very little time in an ATP-bound state as a consequence of rapid hydrolysis and subsequent ADP dissociation. Alternatively, nCoMET would fail to detect a nucleotide bound without a companion Co^{2+} ion. This situation is unlikely to occur for ATP, because Co^{2+} binding is also required for hydrolysis, but could explain why no ADP binding to VI subunits was detected.

Biochemical assays

ATP hydrolysis was measured by a coupled assay (Nørby, 1988). ATPγS hydrolysis was analyzed by ion-pair chromatography on a Shimadzu Class-VP HPLC. Time points were taken by quenching the reaction with excess dithiothreitol (when Co^{2+} was present) or by the addition of one-quarter volume of 50% trichloroacetic acid. Samples were directly loaded onto a Waters Delta-Pak C18 column (300 Å, 5 µM, 3.9 x 150 mm) equilibrated in 30 mM triethylammonium phosphate (pH 5.5) and eluted isocratically. Hydrolysis was measured by quantifying the ADP and ATPγS peaks (retention times ~6 min and ~15 min, respectively) and calculating the amount of ADP formed as a fraction of total nucleotide. ATP-hydrolysis rates measured by the coupled assay and the HPLC assay were within experimental error.

The rate of cp7-CFP-ssrA unfolding was calculated from the initial rate of loss of

fluorescence measured with an SF-300X stopped flow instrument (KinTek). Pre-mixed ClpX and substrate were rapidly mixed with an equal volume of ATP solution and substrate fluorescence was monitored (excitation 435 nm; emission 495 nm long-pass filter).

ClpP peptide-cleavage assays were performed using a succinyl-Leu-Tyr-AMC dipeptide or a decapeptide containing an N-terminal 2-aminobenzoic acid fluorophore and nitro-tyrosine quencher at residue nine as described (Lee et al., 2010).

Crystallization and structure determination

Crystallized proteins included a tethered E-R dimer and tethered W-W-W, W-W-R and E-E-ER trimers, where ER designates E185Q/R370K subunits (Table 1). These proteins did not contain the C169S mutation. Polypeptide tethers were twenty (T_{20}) or zero (T_0) residues and compatible with ClpX function (Glynn et al., 2012). Variants were crystallized at room temperature by hanging-drop vapor diffusion after mixing 1 µL of well solution with 1 µL of protein solution (~40 µM pseudo hexamer). The composition of well solutions are listed in Table 1. The nucleotide-bound form of W-W-W with T_{20} tethers was obtained using a soaking procedure similar to one described previously (Glynn et al., 2009) but limited to 5 min. To obtain the structure of E-E-ER bound to ATPgS, nucleotide-free crystals were soaked in 3.4 M sodium malonate, 75 mM sodium acetate (pH 4.8), 4 mM ATPgS, and 4 mM $MgCl_2$ for approximately 2 h. All crystals were cryo-protected by coating in Paratone-N (Hampton Research) and flash-frozen in liquid nitrogen. Data were collected at the 24-ID-C beamline of the Advanced Photon Source, Argonne National Laboratories. Unit-cell volumes indicated that crystals with

the space groups $P2_12_12_1$ and $P6_3$ contained six and two subunits in the asymmetric unit, respectively. Data collection and refinement statistics are listed in Table S1.

Diffraction data were integrated and scaled using HKL2000 (Otwinowski and Minor, 1997), TRUNCATE (Winn et al., 2011), MOSFLM (Leslie and Powell, 2007) and SCALA (Winn et al., 2011). The structures of the large and small AAA+ domains of *E. coli* ClpX (Glynn et al., 2009) were used as molecular-replacement search models in PHASER (McCoy et al., 2007). Each domain was placed independently to avoid bias towards previously observed conformations. Manual model building and real-space refinement were carried out in COOT (Emsley et al., 2010). Rigid-body refinement, TLS refinement, and grouped atomic displacement parameter refinement were performed using PHENIX (Adams et al., 2010). Individual large and small AAA+ domains were defined as rigid bodies and TLS groups, with either individual domains or individual residues defined as atomic displacement parameter groups based on the resolution and quality of the data.

For crystals soaked in nucleotide, examination of calculated mF_o-DF_c maps revealed strong peaks of positive density in the nucleotide-binding pockets of loadable subunits. The single bound nucleotide in the ATPgS-soaked W-W-W (T_{20}) structure could not be determined unambiguously, probably because of mixed occupancy by nucleotide and sulfate ions, and ADP provided the best fit for the electron density. For the E-E-ER crystal soaked in sodium malonate and ATPgS, the bound nucleotides were unambiguously modeled as ATPgS.

Structural validation was performed using MolProbity (Chen et al., 2010). Superposition of structures was carried out using LSKQAB (Winn et al., 2011). The atomic coordinates for all structures have been deposited in the Protein Data Bank, with accession codes listed in Table S1.

ACCESSION NUMBERS

The Protein Data Bank accession codes for the new ClpX hexamer structures are 4I81, 4I4L, 4I34, 4I5O, 4I63, and 4I9K (Table 1).

REFERENCES

Adams, P.D., Afonine, P.V., Bunkoczi, G., Chen, V.B., Davis, I.W., Echols, N., Headd, J.J., Hung, L.W., Kapral, G.J., Grosse-Kunstleve, R.W., McCoy, A.J., Moriarty, N.W., Oeffner, R., Read, R.J., Richardson, D.C., Richardson, J.S., Terwilliger, T.C. and Zwart, P.H. (2010). PHENIX: a comprehensive Python-based system for macromolecular structure solution. Acta Cryst., *D66*, 213-221.

Aubin-Tam, M.E., Olivares, A.O., Sauer, R.T., Baker, T.A., and Lang, M.J. (2011). Single-molecule protein unfolding and translocation by an ATP-fueled proteolytic machine. Cell *145*, 257-67.

Baker, T.A., and Sauer, R.T. (2012) ClpXP, an ATP-powered unfolding and protein-degradation machine. Biochim. Biophys. Acta. *1823*, 15-28.

Chen, V.B. Arendall, W.B. 3rd, Headd, J.J., Keedy, D.A., Immormino, R.M., Kapral, G.J., Murray, L.W., Richardson, J.S., & Richardson, D.C. (2010). MolProbity: all-atom structure validation for macromolecular crystallography. Acta. Cryst., *D66*, 12-21.

Emsley, P., Lohkamp, B., Scott, W.G. and Cowtan, K. (2010). Features and development of Coot. Acta Cryst., *D66*, 486-501.

Enemark, E.J., and Joshua-Tor, L. (2006). Mechanism of DNA translocation in a replicative hexameric helicase. Nature *442*, 270-275.

Glynn, S.E., Martin, A., Nager, A.R., Baker, T.A., and Sauer, R.T. (2009). Crystal structures of asymmetric ClpX hexamers reveal nucleotide-dependent motions in a AAA+ protein-unfolding machine. Cell *139*, 744-756.

Glynn, S.E., Nager, A.R., Baker, T.A., and Sauer, R.T. (2012). Dynamic and static components power unfolding in topologically closed rings of a AAA+ proteolytic machine. Nat. Struct. Mol. Biol. *19*, 616-622.

Hanson, P.I., and Whiteheart, S.W. (2005). AAA+ proteins: have engine, will work. Nat. Rev. Mol. Cell. Biol. *6*, 519-529.

Hersch, G.L., Burton, R.E., Bolon, D.N., Baker, T.A. and Sauer, R.T. (2005). Asymmetric interactions of ATP with the AAA+ ClpX$_6$ unfoldase: allosteric control of a protein machine. Cell *121*, 1017-1027.

Hirono-Hara, Y., *et al*. (2001). Pause and rotation of F(1)-ATPase during catalysis. Proc. Natl. Acad. Sci. USA. *98*, 13649-54.

Kenniston, J.A., Baker, T.A., Fernandez, J.M., and Sauer, R.T. (2003). Linkage between ATP consumption and mechanical unfolding during the protein processing reactions of an AAA+ degradation machine. Cell *114*, 511-520.

Kinosita, K., Yasuda, R., Noji, H., and Adachi, K. (2000) A rotary molecular motor that can work at near 100% efficiency. Philos. Trans. R. Soc. Lond. B Biol. Sci. *355*, 473-489.

Lander, G.C., Estrin, E., Matyskiela, M.E., Bashore, C., Nogales, E., and Martin, A. (2012). Complete subunit architecture of the proteasome regulatory particle. Nature *482*, 186-191.

Lee, M.E., Baker, T.A., Sauer, R.T. (2010). Control of substrate gating and translocation into ClpP by channel residues and ClpX binding. J. Mol. Biol. *399*, 707-718.

Leslie, A.G. and Walker, J.E. (2000) Structural model of F1-ATPase and the implications for rotary catalysis. Philos. Trans. R. Soc. Lond. B Biol. Sci. *355*, 465-471.

Leslie, A.G.W. and Powell, H.R. (2007). Processing Diffraction Data with Mosflm. Evolving Methods for Macromolecular Crystallography, *245*, 41-51.

Maillard, R.A., Chistol, G., Sen, M., Righini, M., Tan, J., Kaiser, C.M., Hodges, C., Martin, A., and Bustamante, C. (2011). ClpX(P) generates mechanical force to unfold and translocate its protein substrates. Cell *145*, 459-469.

Martin, A., Baker, T.A., and Sauer, R.T. (2005). Rebuilt AAA+ motors reveal operating principles for ATP-fueled machines. Nature *437*, 1115-1120.

Martin, A., Baker, T.A., and Sauer, R.T. (2007). Distinct static and dynamic interactions control ATPase-peptidase communication in a AAA+ protease. Mol. Cell *27*, 41-52.

Martin, A., Baker, T.A. and Sauer, R.T. (2008a). Diverse pore loops of the AAA+ ClpX machine mediate unassisted and adaptor-dependent recognition of ssrA-tagged substrates. Mol. Cell *29*, 441-450.

Martin, A., Baker, T.A. and Sauer, R.T. (2008b). Pore loops of the AAA+ ClpX machine grip substrates to drive translocation and unfolding. Nat. Struct. Mol. Biol. *15*, 1147-1151.

McCoy, A.J., Grosse-Kunstleve, R.W., Adams, P.D., Winn, M.D., Storoni, L.C. and Read, R.J. (2007). Phaser crystallographic software. J. Appl. Cryst. *40*, 658-674.

Nager, A.R., Baker, T.A., and Sauer, R.T. (2011) Stepwise unfolding of a β barrel protein by the AAA+ ClpXP protease. J. Mol. Biol. *413*, 4-16.

Nørby, J.G. (1988). Coupled assay of Na^+,K^+-ATPase activity. Methods Enzymol. *156*, 116–119.

Otwinowski, Z., and Minor, W. (1997). Processing of X-ray diffraction data collected in oscillation mode. Methods Enzymol. *276*, 307-326.

Singh, S.K., Rozycki, J., Ortega, J., Ishikawa, T., Lo, J., Steven, A.C. and Maurizi, M.R. (2001). Functional domains of the ClpA and ClpX molecular chaperones identified by limited proteolysis and deletion analysis. J. Biol. Chem. *276*, 29420-29429.

Smith, D.M., Fraga, H., Reis, C., Kafri, G., and Goldberg AL. (2011). ATP binds to proteasomal ATPases in pairs with distinct functional effects, implying an ordered reaction cycle. Cell *144*, 526-538.

Taraska, J.W., Puljung, M.C., Olivier, N.B., Flynn, G.E., and Zagotta, W.N. (2009) Mapping the structure and conformational movements of proteins with transition metal ion FRET. Nat. Methods. *6*, 532-537.

Winn, M.D., Ballard, C.C., Cowtan, K.D., Dodson, E.J., Emsley, P., Evans, P.R., Keegan, R.M., Krissinel, E.B., Leslie, A.G.W., McCoy, A., McNicholas, S.J., Murshudov, G.N., Pannu, N.S., Potterton, E.A., Powell, H.R., Read, R.J., Vagin, A. and Wilson, K.S. (2011). Overview of the *CCP*4 suite and current developments. Acta Cryst. *D67*, 235-242.

Wojtyra, U.A., Thibault, G., Tuite, A. and Houry, W.A. (2003). The N-terminal zinc binding domain of ClpX is a dimerization domain that modulates the chaperone function. J. Biol. Chem. *278*, 48981-48990.

Yakamavich, J.A., Baker, T.A., and Sauer, R.T. (2008). Asymmetric nucleotide

transactions of the HslUV protease. J. Mol. Biol. *380*, 946-957.

Zhou, R., Kunzelmann, S., Webb, M.R., and Ha, T. (2011). Detecting intramolecular conformational dynamics of single molecules in short distance range with subnanometer sensitivity. Nano Lett. *11*, 5482-5488.

CHAPTER 3

Subunit asymmetry and roles of conformational switching

in the hexameric AAA+ ring of ClpX

INTRODUCTION

The hexameric AAA+ ring of *Escherichia coli* ClpX recognizes protein substrates via a peptide degron, uses cycles of ATP binding and hydrolysis to unfold the substrate, and then translocates the denatured polypeptide through an axial pore and into the ClpP degradation chamber, which lies within a barrel-shaped structure formed by the stacking of two heptameric rings (Baker and Sauer, 2011). Although ClpX is a homohexamer, biochemical and structural experiments reveal differences among the subunits. For example, some subunits bind nucleotide with higher affinities than others, and some subunits fail to bind nucleotide (Hersch et al., 2005; Stinson et al., 2013). Crystal structures of ClpX hexamers show two major classes of subunits, typically arranged with approximate two-fold symmetry (Glynn et al., 2009; Stinson et al., 2013). Four loadable (L) subunits bind nucleotide in the cleft between the large and small AAA+ domains, whereas repositioning of these domains in two symmetrically opposed unloadable (U) subunits destroys the nucleotide-binding site (Fig. 1A). However, the functional relevance of the pseudo symmetric L4:2U subunit arrangement observed in most crystal structures is unclear. Indeed, biochemical experiments suggest that an L5:1U configuration may predominate in the presence of nucleotide (Stinson et al., 2013). The issue of subunit symmetry in working hexameric rings applies to other AAA+ enzymes that remodel proteins, as some models of ring function require symmetric subunit function (Smith et al., 2011), and crystal structures of many of these enzymes show 2-fold, 3-fold, or 6-fold symmetry (Sauer and Baker, 2011).

Previous studies provide evidence that dynamic interconversion between the L and U

conformations of ClpX subunits is necessary for efficient coupling of ATP hydrolysis to mechanical work (Stinson et al., 2013). The precise roles of conformational switching, however, remain poorly understood. Here, we use crosslinking to prevent U→L switching in one subunit of variants of a covalent ClpX hexamer, and characterize the resulting conformationally restricted enzymes. A ClpX ring with one U-locked subunit catalyzes robust ATP hydrolysis. Experiments examining the nucleotide binding and hydrolytic properties of the unlocked subunits reveal that each one can bind and hydrolyze ATP, albeit with position-specific affinities that are highly asymmetric. U-locking one subunit in the ClpX ring compromises multiple facets of function, including the binding, unfolding, and degradation of protein substrates, and the cooperativity of ATP hydrolysis. These results support an asymmetric and probabilistic model of ring activity and the importance of conformational switching for robust activity. They also constrain models for conformational coordination among ClpX subunits, and illustrate strategies that should be useful for dissection of mechanism in other AAA+ ring systems.

RESULTS

Constraining one subunit to the U conformation by covalent crosslinking

All experiments used *E. coli* ClpX$^{\Delta N}$ variants containing the complete AAA+ module (residues 61-424) but lacking the family-specific N domain, which is dispensable for machine function (Wojtyra et al., 2003). To permit introduction of mutations into specific subunits, variants were expressed from genes encoding three ClpX$^{\Delta N}$ subunits linked into trimers, which form pseudo hexamers that bind ClpP and mediate degradation of

ssrA-tagged substrates (Martin et al., 2005). To assemble fully covalent hexamers, we linked trimers via sortase ligation (Popp et al., 2007). In all subunits, the only endogenous reactive cysteine was mutated (C169S) to allow introduction of specific cysteine substitutions, which could then be modified by bismaleimide crosslinking or attachment to maleimide-conjugated fluorescent dyes.

In ClpX crystal structures, the beta-carbons of residues D144 and K330 are separated by ~13 Å in U subunits and ~27 Å in L subunits (Fig. 1B). We introduced the D144C and K330C substitutions into the N-terminal subunit of a covalent ClpX trimer, and crosslinked the cysteines by addition of 1,6-bismaleimidohexane (BMH), which has a length of ~16 Å (Fig. 1C). This distance allows crosslinking of cysteines 144 and 330 in U subunits but is too short for crosslinking in L subunits. Thus, BMH-crosslinking generates a U-locked subunit. Using the strategy diagrammed in Fig. 1D, we linked this BMH-crosslinked trimer to a wild-type trimer via Sortase ligation to create a covalent hexamer. To determine the degree of crosslinking, a TEV-protease cleavage site was introduced into the flexible peptide tether between the cysteine-modified subunit and the neighboring subunit (Fig. 1D), allowing resolution of crosslinked and uncrosslinked subunits by SDS-PAGE after TEV cleavage. This assay showed a complete shift in electrophoretic mobility of the modified subunit upon addition of BMH, indicating very efficient crosslinking (Fig. 1E). Modification with *N*-propylmaleimide (NPM, Fig. 1C), which mimics modification by BMH without covalent crosslinking of the two cysteines, did not produce a shift in mobility (Fig. 1E).
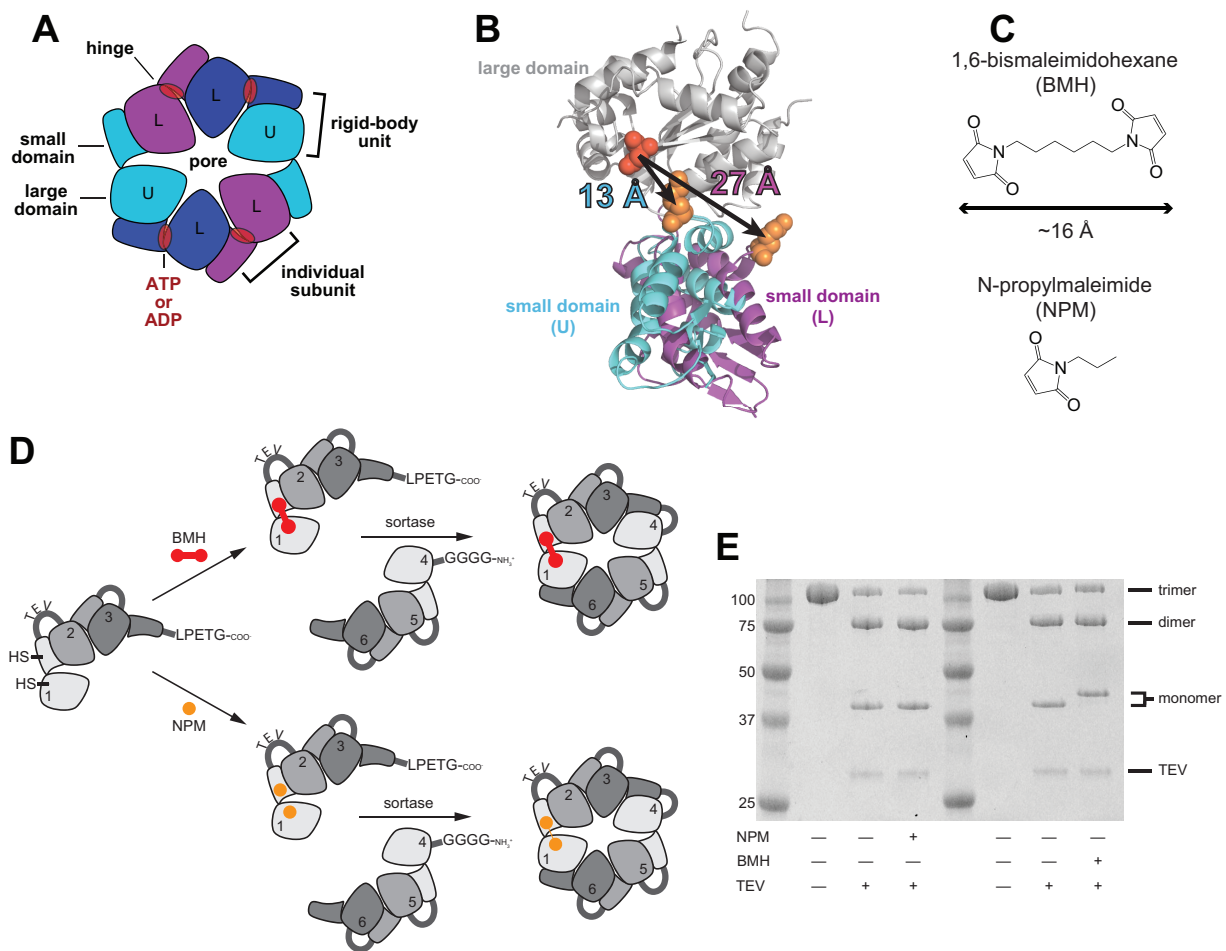
Figure 1. ATP binding and subunit conformations in ring hexamers of ClpX. **(A)** In most crystal structures, differences in the orientation of the large and small AAA+ domains result in four L subunits that bind nucleotide and two U subunits that do not bind nucleotide. Because each small AAA+ domain packs in a rigid-body interaction with the large AAA+ domain of its clockwise neighbor, nucleotide-dependent changes in the conformation of any subunit are propagated around the topologically closed ring. **(B)** Structures of an L and U subunit (PDB code, 4I81) were aligned by their large domains (gray). The beta carbons of D144 in the large domain and K330 in the small domain are separated by ~13 Å in U subunits (cyan) and ~27 Å in L subunits (purple). **(C)** Bifunctional (BMH; top) or monofunctional (NPM; bottom) maleimides used to crosslink or modify D144C and K330C in ClpX variants. **(D)** Construction of modified covalent hexamers. A ClpX covalent trimer containing D144C and K330C mutations in a single subunit was modified with either BMH of NPM and subsequently ligated via sortase to a second ClpX trimer. Crosslinking with BMH restricts the D144C/K330C subunit to the U conformation; modification with NPM serves as a non-crosslinked control. A TEV-protease site was engineered into the linker between the D144C/K330C and clockwise neighboring subunit to monitor crosslinking efficiency. **(E)** SDS-PAGE after TEV digestion of ClpX covalent trimers containing one NPM/BMH modified subunit shows that >95% of BMH-modified subunits display reduced electrophoretic mobility compared to NPM-modified subunits, indicating that crosslinking is essentially complete in BMH-modified subunits.

Table 1

ATP hydrolysis

	V_{max} (ATP min^{-1} enz^{-1})	K_M (μM)	n
parental	69 ± 2	25 ± 2	3.6 ± 0.9*
NPM	136 ± 2	94 ± 2	1.2 ± 0.1
BMH	500 ± 90	4000 ± 3000	0.5 ± 0.1
1EQ	320 ± 60	2000 ± 1000	0.5 ± 0.1
2EQ	250 ± 40	4000 ± 2000	0.5 ± 0.1
3EQ	113 ± 4	140 ± 10	0.9 ± 0.1
4EQ	92 ± 2	180 ± 10	1.0 ± 0.1
5EQ	240 ± 20	1000 ± 200	0.6 ± 0.1
parental (Co^{2+})**	340 ± 10	170 ± 20	1.3 ± 0.2
BMH (Co^{2+})**	420 ± 90	3000 ± 2000	0.8 ± 0.1

ADP inhibition

	IC_{50} (mM)
parental	1.4
NPM	0.5
BMH	0.6

nCoMET

	ATP		**ATPγS**		**ADP**	
	K_{app} (μM)	n	K_{app} (μM)	n	K_{app} (μM)	n
parental	102	0.8 ± 0.1	11	1.0 ± 0.1	13	0.6 ± 0.1
subunit 1	14	0.8 ± 0.1	10	1.1 ± 0.1	4	0.9 ± 0.1
subunit 2	410	0.6 ± 0.1	38	0.8 ± 0.1	21	0.6 ± 0.1
subunit 3	56	0.6 ± 0.1	52	0.6 ± 0.1	5	0.6 ± 0.1
subunit 4	35	0.8 ± 0.1	21	0.8 ± 0.1	7	0.7 ± 0.1
subunit 5	56	1.0 ± 0.1	120	0.7 ± 0.1	4	0.9 ± 0.1

protein substrate binding

	K_{app} (μM)	maximal quenching
parental	0.32 ± 0.05	0.71 ± 0.02
NPM	3.8 ± 0.5	0.45 ± 0.02
BMH	11 ± 4	0.11 ± 0.02

protein substrate degradation

	unfolded titin-ssrA (min^{-1} enz^{-1})	Arc-GCN4-ssrA (min^{-1} enz^{-1})
parental	6.3 ± 0.7	1.1 ± 0.1
NPM	3.0 ± 0.1	0.40 ± 0.05
BMH	0.90 ± 0.05	0.07 ± 0.04

Parameters were determined by fitting of experimental data as described in figure legends. Errors are from nonlinear least-squares fitting. For ADP-inhibition experiments, IC_{50} is defined as the concentration of ADP resulting in 50% hydrolysis relative to the initial rate. For nCoMET experiments, errors in K_{app} are estimated as ±50% on the basis of independent protein preparations. * Hill constants of ~1.4 were reported in experiments containing saturating substrate (Stinson et al., 2013), which is absent in the present experiment, suggesting substrate affects positive cooperativity in ATP hydrolysis. ** Parameters for experiments in the lower panel of Fig. 3B, which were performed in the presence of Co^{2+} rather than Mg^{2+} for comparison to nCoMET experiments.

One U-locked subunit permits robust ATP hydrolysis

We assayed hydrolysis of different concentrations of ATP by covalent hexamers composed of parental C169S ClpX subunits or variants containing a single D144C/K330C subunit modified with BMH or NPM and fit curves to the Hill form of the Michaelis-Menten equation to determine V_{max}, K_M, and the Hill constant (Fig. 2A; Table 1). V_{max} for the BMH variant was ~5-fold higher than the parent. For the NPM variant, V_{max} was intermediate between the parent and BMH suggesting that NPM modification biases subunit conformation without generating a fully U-locked subunit. Parental ClpX displayed strong positive cooperativity in ATP hydrolysis, the NPM variant showed almost no cooperativity, and the BMH variant displayed negative cooperativity (Table 1). Thus, U-locking even one subunit in the ClpX ring alters subunit-subunit communication. K_M for ATP hydrolysis by the parent and NPM variant was ≤ 100 µM but increased to ~4 mM for the BMH variant, presumably as a consequence of faster ATP hydrolysis and/or weaker binding. An unfolded titin[I27]-ssrA protein substrate substantially stimulated the ATPase activity of the parental enzyme as expected (Kenniston et al., 2003) but did not appreciably stimulate ATP hydrolysis by the NPM or BMH enzymes (Fig. 2B).
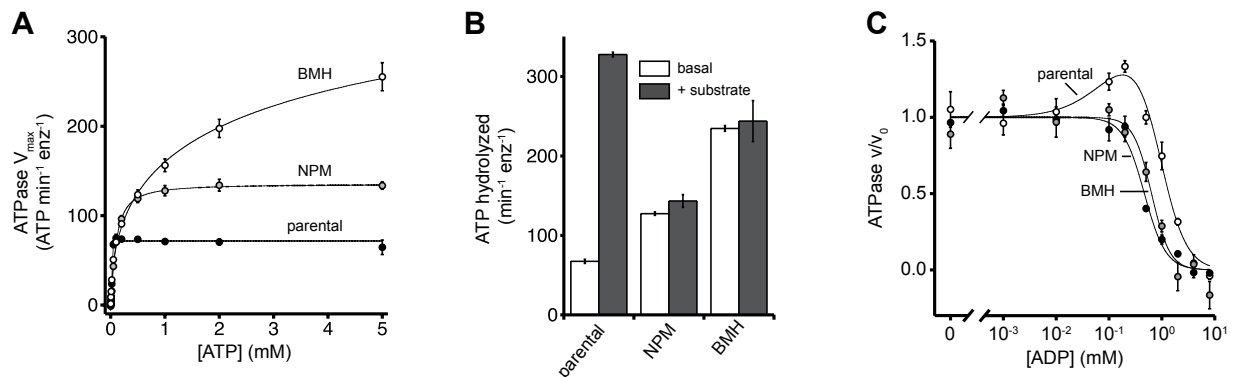
Figure 2. ATP hydrolysis. **(A)** ATP hydrolysis by parental and BMH or NPM modified ClpX variants (50 nM). **(B)** Rates of hydrolysis of 5 mM ATP by parental and NPM or BMH ClpX variants (50 nM) in the absence and presence of unfolded titin^{I27}-ssrA protein substrate (20 µM). **(C)** Inhibition of hydrolysis of ATP (2 mM) by different concentrations of ADP for parental and NPM or BMH variants (50 nM). For the NPM or BMH variants, the lines are fits to the equation $V_{max} = (1 - [ADP]^n/([ADP]^n + IC_{50}^n))$. For the parental enzyme, the line is a fit to a biphasic binding equation $(1+a*[ADP]/([ADP]+K_1)-(1+a)*[ADP]^n/([ADP]^n+K_2^n))$. IC_{50} values are shown in Table 1. In all panels, values represent means ± SD (N = 3).

Conformationally restricted variants are more susceptible to ADP inhibition

ADP is a competitive inhibitor of ATP binding and hydrolysis. To test the possibility that conformational switching helps the ClpX hexamer escape an unproductive ADP-bound state, we measured hydrolysis of 2 mM ATP in the presence of increasing ADP (Fig. 2C). For the parental enzyme, ADP stimulated hydrolysis at low concentrations, suggesting that a ring with one or a few bound ADPs is more active, and inhibited hydrolysis at higher concentrations with an IC_{50} of 1.4 mM. By contrast, ADP did not significantly stimulate the NPM or BMH variants and inhibited these variants more strongly with IC_{50} values of 0.5-0.6 mM. Thus, restriction of subunit switching renders the hexamer more susceptible to ADP inhibition.

Subunit-specific nucleotide binding and hydrolysis in a U-locked hexamer

How does U-locking of one subunit in the BMH hexamer affect nucleotide binding in the remaining five subunits? To address this question, we measured binding to each unlocked subunit by nucleotide-coordinated metal energy transfer (nCoMET), which measures quenching of a nearby fluorophore upon binding of a nucleotide•Co^{2+} complex (Stinson et al., 2013). The nucleotide-binding sites in adjacent subunits of ClpX are ~35 Å apart, whereas the Co^{2+} metal only quenches fluorophores within ~25 Å (Taraska et al., 2009). Thus, judicious placement of a fluorophore in one subunit permits

measurement of nucleotide binding to just that subunit. For these studies, we constructed and purified five variants of BMH hexamers in which a single unlocked subunit contained an M363C substitution (see Methods for construction strategy), which we modified with an Oregon-Green fluorophore. We refer to each unlocked subunit by its numbered position clockwise from the U-locked subunit, as shown in Fig. 3A (left panel).

We measured ATP, ATPγS, and ADP binding to the Oregon-Green modified subunits at positions 1-5 of the U-locked variants by nCoMET. Fig. 3A (top panel) shows apparent ATP, ATPγS, and ADP affinities for each of these subunits, which varied in an asymmetric fashion. Individual ATP-binding curves for each subunit are shown in the upper panel of Fig. 3B. For each nucleotide, the apparent affinity for one Oregon-Green modified subunit of the parental unlocked enzyme (an average over all ring configurations) was similar to the average of the five unlocked subunits in the different BMH variants (Fig. 3A; bottom panel). Importantly, nucleotide bound each unlocked subunit, indicating that they all assume a loadable conformation in some fraction of the population. For ATP and ATPγS, apparent affinities are not equilibrium dissociation constants, as these nucleotides can leave by hydrolysis and ADP/P_i dissociation in addition to simple dissociation. In most cases, ATP and ATPγS bound with similar apparent affinities to a given subunit. However, subunit 2 bound ATP ~10-fold more weakly than ATPγS. Because ClpX hydrolyzes ATP faster than ATPγS (Burton et al., 2003), which would result in a lower apparent affinity, this difference could arise because subunit 2 hydrolyzes ATP much faster than other subunits or because

hydrolysis elsewhere in the ring weakens binding to subunit 2. ADP bound each subunit in the U-locked hexamer with apparent affinities from 2- to 20 fold tighter than ATP or ATPγS, which might be expected to lead to more potent ADP inhibition than that observed in the Fig. 2C experiment. It is possible, however, that ATP binds more tightly or ADP binds more weakly to a ClpX hexamer with some ATP-bound and some ADP-bound subunits.

We measured Co^{2+}-supported ATP hydrolysis by the parental and BMH enzymes (lower panel, Fig. 3B) for comparison with the nCoMET results. Previous studies suggest that occupancy of weak ATP-binding sites is necessary for robust ATP hydrolysis by ClpX (Stinson et al., 2013). Consistently, the K_M for ATP hydrolysis for the parental enzyme (~170 µM) was higher than the average affinity measured by nCoMET (~100 µM). This difference was more extreme for the U-locked BMH variant, with a K_M in excess of 1 mM compared to an average affinity of ~110 µM. Although the nCoMET assay measures binding to specific subunits, the degree of saturation of any single subunit is not determined. Notably, both the ATPase and nCoMET binding curves for the U-locked variants were negatively cooperative. Even though each unlocked subunit binds nucleotide in some fraction of the population, it is plausible that negative cooperativity prevents any single hexamer from binding four or five nucleotides and hydrolyzing ATP efficiently except at very high concentrations.
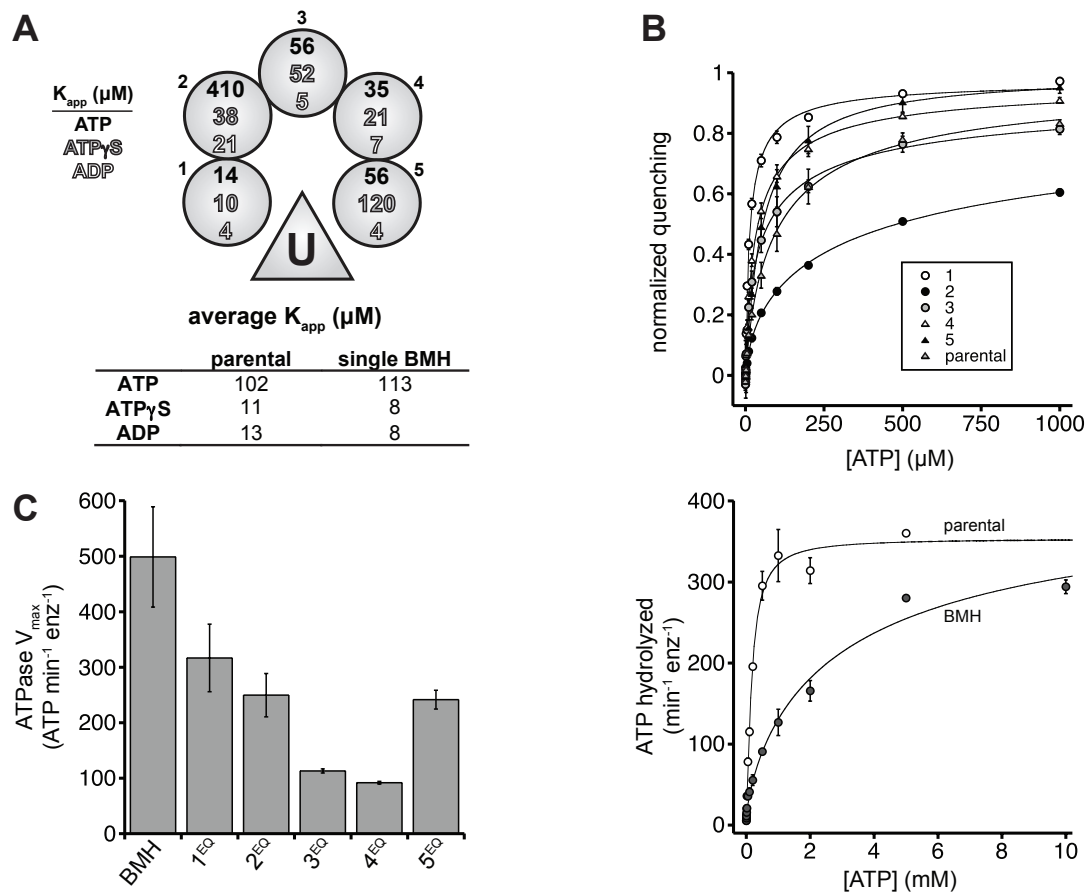
Figure 3. Subunit-specific nucleotide binding and effects on ATP hydrolysis in BMH U-locked hexamers. nCoMET variants were generated as shown in Figure 1D, but the second trimer contained the M363C substitution in a single subunit which was modified with Oregon Green prior to sortase ligation. **(A)** Apparent ATP, ATPγS and ADP affinities determined by nCOMET experiments for one subunit of the parental enzyme and each unlocked subunit of BMH ClpX (100 nM). Labeled unlocked subunits are numbered based on their clockwise position from the U-locked subunit. K_{app} was determined using fits to $[nuc]^n/([nuc]^n + K_{app}^n)$, and errors in K_{app} were estimated as ± 50% based on measurements from independent protein preparations. Values of n are shown in Table 1. Bottom panel shows values of K_{app} averaged over all subunits. **(B)** Upper panel: ATP binding isotherms for parental and BMH variants, numbered as in (A). Quenching amplitudes were normalized to 1.0. Values represent means ± SD (N = 3). Lower panel: ATP hydrolysis supported by 20 mM Co^{2+} for parental and BMH enzymes (25 nM pseudo hexamer). Solid lines are fits to $[ATP]^n/([ADP]^n + K_M^n)$. Fitted parameters are shown in Table 1. Data represent means ± SD (N = 2). **(C)** V_{max} values for ATP hydrolysis by single BMH and variants with a single E185Q mutation in one of the five unlocked subunits (50 nM). Fitted parameters from full Michaelis-Menten curves are shown in Table 1. Values represent means ± SD (N = 3).

To assess the importance of ATP hydrolysis in different subunits of BMH ClpX, we

introduced single E185Q (EQ) Walker-B mutations to inactivate ATP hydrolysis (Hersch

et al., 2005) in subunits 1, 2, 3, 4, or 5 in different U-locked BMH variants. Each single

EQ mutation decreased the maximal ATP-hydrolysis rate relative to the BMH hexamer,

suggesting that each unlocked subunit contributes to hydrolysis (Fig. 3C). The

dependence of hydrolysis on ATP concentration was negatively cooperative for variants

with EQ mutations in subunits 1, 2, or 5 and non-cooperative for subunits 3 and 4 (Fig.

3D; Table 1), suggesting that these mutations affect subunit-subunit communication in a

position-specific manner.

U-locking reduces the efficiency of substrate binding, unfolding, and degradation

We assayed binding of a native titin[I27]-ssrA protein substrate labeled with a BHQ3

quencher to fluorescent variants of BMH ClpX, NPM ClpX, or the parental enzyme.

Compared to the parent, the BMH and NPM variants showed substantially weaker

binding and lower levels of maximal quenching (Fig. 4A). These results are consistent

with a multi-step model of substrate binding and release (lower panel, Fig. 4A),

suggesting that U-locking hinders binding of protein substrates.
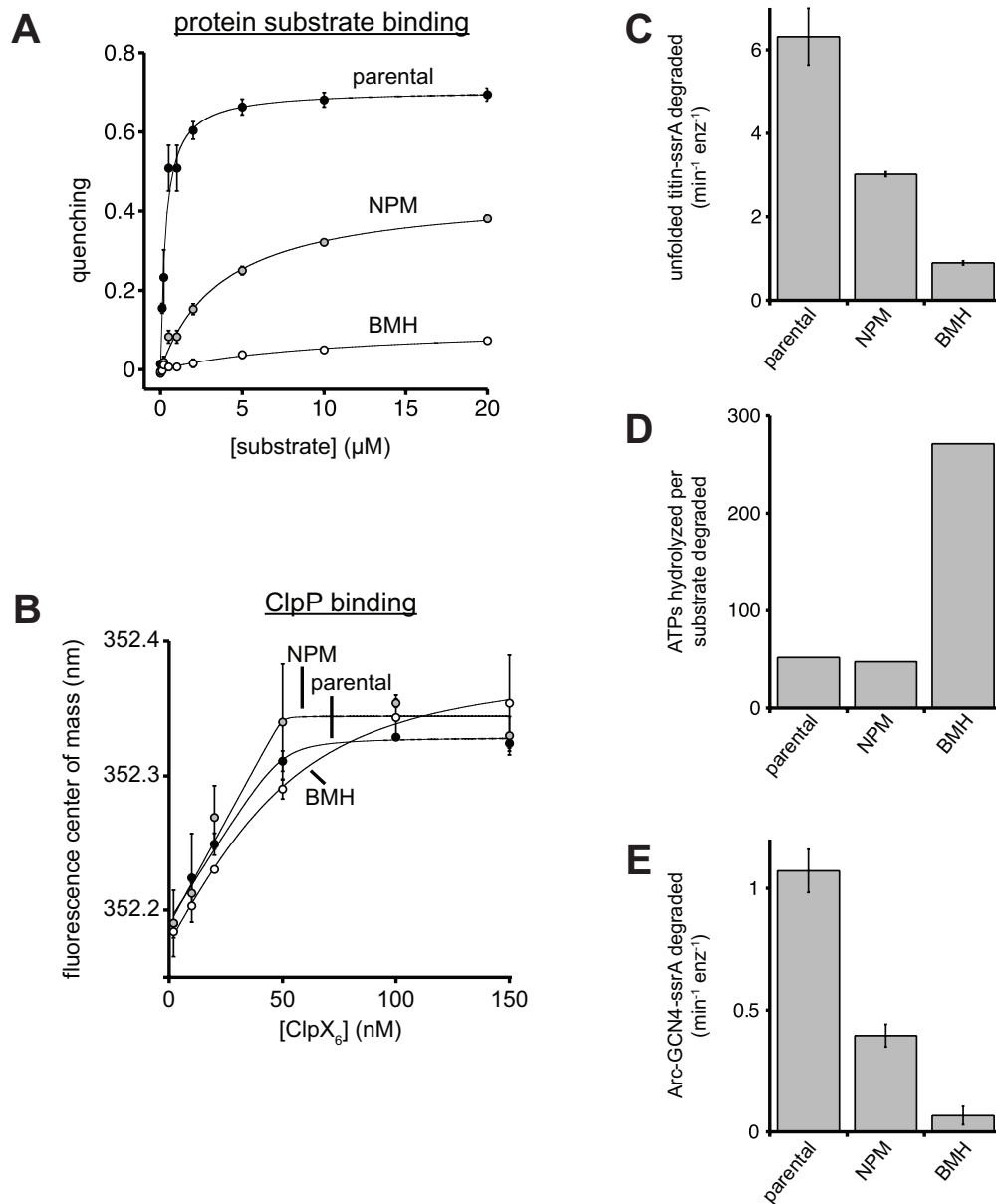
Figure 4. Binding, unfolding, and degradation of protein substrate by ClpX variants. **(A)** Binding of quencher-labeled titin^{I27}-ssrA to ClpX variants labeled with Alexa 555 at D170C (25 nM; 10 mM ATP). Solid lines are fits to a hyperbolic equation. Apparent affinities and amplitudes are shown in Table 1. **(B)** Binding of parental and NPM or BMH variants to Y60W ClpP$_{14}$ (25 nM) in the presence of 2 mM ATP. Solid lines are fits to a quadratic equation for near stoichiometric binding. K_D's were less than 25 nM for all variants (signal-to-noise problems precluded using sufficiently low ClpP concentrations for precise determination of K_D). **(C)** Rates of degradation of unfolded titin^{I27}-ssrA (20 µM) by parental and NPM or BMH enzymes (300 nM) and ClpP$_{14}$ (900 nM). Values are shown in Table 1. **(D)** Energetic efficiency of unfolded titin^{I27}-ssrA degradation calculated as the ratio of the ATPase rate in the presence of unfolded titin^{I27}-ssrA (Fig. 2B) to the rate of degradation in panel A. **(E)** Degradation of dimeric Arc-GCN4-ssrA (15 µM dimer) by parental and NPM/BMH enzymes (100 nM) and ClpP$_{14}$ (300 nM). Values are shown in Table 1. For the experiments in panels A, C and D, the ATP concentration was 10 mM and values represent means ± SD (N ≥ 2).

U-locking did not substantially affect binding to the ClpP peptidase. As assayed by changes in the tryptophan fluorescence emission spectrum, the BMH and NPM enzymes bound Y60W ClpP in a manner similar to parental ClpX (Fig. 4B). In combination with ClpP, the NPM variant degraded unfolded titin[I27]-ssrA protein at ~50% of the parental rate and the BMH variant degraded this substrate at ~15% of the parental rate (Fig. 4C). Thus, U-locking one subunit of the ClpX ring diminishes but does not prevent substrate engagement and translocation into ClpP. Notably, however, degradation by ClpP and the BMH enzyme was ~5-fold less energetically efficient than degradation by the NPM or parental enzymes in terms of the number of ATP molecules hydrolyzed per substrate degraded (Fig. 4D), suggesting that many power strokes in the U-locked enzyme do not result in productive work. In assays of degradation of a native substrate (Arc-GCN4-ssrA), the NPM enzyme had ~40% of the parental activity, whereas the BMH hexamer had ~10% activity (Fig. 4E). Relative to the parental enzyme, the BMH enzyme degraded the native substrate less efficiently than the unfolded substrate, suggesting that U-locking impairs protein unfolding.

DISCUSSION

U-locking partially uncouples ATP hydrolysis from machine function

In the presence of an unfolded protein substrate, U-locked BMH ClpX hydrolyzes ATP at a rate similar to the parental enzyme but degrades the substrate at a ~6-fold slower rate. Thus, the majority of ATP-hydrolysis events in the modified enzyme appear to be uncoupled from power strokes that result in mechanical work. A similar uncoupling of most power strokes from machine function is observed when disulfide bonds lock one or

two ClpX subunit in the L conformation (Stinson et al., 2013). These results emphasize the importance of U⇔L conformational switching in the ClpX ring for robust mechanical activity.

U-locking of a single subunit alters communication between subunits and interferes with normal coordination of ATP hydrolysis. For example, ATP hydrolysis by the parental enzyme shows modest positive cooperativity, whereas hydrolysis by the U-locked BMH variant is negatively cooperative. Positive cooperativity might normally result from conversion of a subunit with low ATP affinity to one with high affinity as a consequence conformational switching. ATP hydrolysis by the BMH variant is also inhibited at lower ADP concentrations than the parental enzyme, suggesting that U-locking may slow ADP ejection from ClpX subunits that need to be cleared and reloaded with ATP before mechanical work can continue.

U-locking alters multiple aspects of ClpX function

Restricting a single subunit in the ClpX ring to the U conformation affects binding to protein substrates, reducing both the apparent affinity and the extent of binding at substrate saturation. As substrate engagement appears to be a slow step in ClpXP degradation (Cordova et al., 2014), these changes in substrate binding almost certainly contribute to the defects in degradation of unfolded substrates by BMH ClpX and ClpP. However, the defects in native substrate unfolding and degradation are larger than expected from the reduced fraction of substrate bound at saturation. Thus, restricting the conformation of one ClpX subunit to a U conformation seems to reduce the rate at

which native substrates can be unfolded and then degraded. Population and single-molecule studies indicate that multiple ClpX power strokes are required, on average, before unfolding of a native substrate occurs (Kenniston et al., 2003; Aubin-Tam et al., 2011; Maillard et al., 2011; Sen et al., 2013; Cordova et al., 2014). Moreover, stably folded substrates are often released from ClpX when an unfolding attempt fails (Kenniston et al., 2005). Thus, it is plausible that the unfolding defect caused by U-locking is related to the substrate-binding defect. Specifically, more frequent release of native substrates from U-locked ClpX after a failed power stroke would result in weaker observed binding and require a larger number of rebinding events, on average, prior to successful unfolding. Restrictions in subunit conformation caused by U-locking might prevent the enzyme from readjusting its grip on an engaged substrate, leading both to the defects in substrate binding and unfolding, either because U⇔L switching is abolished and/or because other important conformational states become inaccessible.

Models of ring architecture and subunit coordination

Most crystal structures of ClpX hexamers have four L subunits and two U subunits, arranged with approximate 2-fold symmetry as shown in Fig. 1A (Glynn et al., 2009; Stinson et al., 2013). Whether this 4L:2U arrangement represents a "working" configuration has been questioned, as experiments based on contact quenching of rhodamine dyes support the presence of a 5L:1U hexamer in the presence of nucleotide, protein substrate, and ClpP (Stinson et al., 2013). Although our results do not settle this issue, restricting one subunit in the ClpX ring to the U conformation, as expected in a 5L:1U ring, allows robust ATP hydrolysis and permits the unfolding and

degradation of protein substrates, albeit at diminished levels compared to wild type presumably because U⇔L switching is compromised.

How subunits with different ATP-binding and hydrolysis properties are arranged and coordinated in working AAA+ hexamers is controversial. For example, studies with the AAA+ PAN and 26S Rpt_{1-6} unfolding rings have been interpreted as support for a model in which high-affinity, moderate-affinity, and ATP-free subunits are always arranged with two-fold symmetry around the hexameric ring but interconvert or switch in a strictly sequential fashion (Smith et al., 2011). If ClpX functioned according to this model, the subunit opposite the U-locked subunit in BMH ClpX should be forced into an ATP-free U conformation. However, our nCoMET results show that this subunit binds ATP, ADP and ATPγS, with affinities similar to or tighter than neighboring subunits. Our experiments also show that this subunit contributes to ATP hydrolysis. Finally, the pattern of nucleotide affinities that we measure for different subunits in the BMH hexamer is inconsistent with functional symmetry of any type in the hexameric ring of ClpX. Similarly, asymmetry in the Rpt_{1-6} unfolding ring of the 26S proteasome is supported both directly by EM structures and indirectly by biochemical experiments analyzing the functional contributions of specific subunits (Lander et al., 2011; Matyskiela et al., 2013; Beckwith et al., 2013).

Because ClpX rings with only one or two hydrolytically active subunits are active in substrate unfolding and degradation, Martin et al. (2005) proposed an asymmetric and probabilistic model of ring function. Single-molecule optical trapping studies of ClpXP

unfolding and translocation provide strong support for this model (Kenniston et al., 2003; Aubin-Tam et al., 2011; Maillard et al., 2011; Sen et al., 2013; Cordova et al., 2014) as do our current studies. For example, we find that each unlocked subunit in a ClpX ring with one U-locked subunit can bind and hydrolyze ATP with some probability. Thus, ATP hydrolysis is not restricted to a subset of subunits at certain positions in the ring relative to the U-locked subunit. Our current and prior results (Stinson et al., 2013) also show that subunits in the ClpX ring must be able to switch between U and L conformations to allow efficient substrate binding, unfolding, and degradation. Switching may ensure that the machine is both robust to failure by ejecting improperly bound nucleotides and opportunistic by allowing well-positioned subunits to switch into conformations allowing productive contacts with protein substrate.

EXPERIMENTAL PROCEDURES

Materials

PD buffer contained 25 mM HEPES (pH 7.0), 100 mM KCl, 10 mM $MgCl_2$, and 10% (v/v) glycerol. IEXA, IEXB, and IEXC buffers contained 20 mM HEPES (pH 7.8), 0.5 mM EDTA, 10% (v/v) glycerol, 1 M urea, with 150 mM KCl, 500 mM KCl, or 20 mM KCl, respectively. Xlink buffer contained 20 mM HEPES (pH 7.8), 300 mM KCl, 0.5 mM EDTA, and 10% (v/v) glycerol. ATP (Sigma), ADP (Sigma), and ATPγS (Roche) were dissolved in PD buffer and adjusted to pH 7.0 by addition of NaOH. Alexa 555 C_2 maleimide (Molecular Probes), Alexa 647 C_2 maleimide (Molecular Probes), Oregon Green 488 maleimide (Molecular Probes), and BHQ3 carboxylic acid succinimidyl ester (Biosearch Technologies) were dissolved in DMSO and stored desiccated at –20 °C.

Proteins

All ClpX variants were derived from *E. coli* ClpX$^{\Delta N}$ (residues 61-424), contained a C169S substitution to remove an accessible cysteine, and were constructed by polymerase chain reactions. Linked ClpX trimers were purified using Ni-NTA and Superdex-200 chromatography generally as described (Martin et al., 2005). Superdex-200 chromatography was carried out in Xlink buffer, and fractions containing ClpX were concentrated with Millipore Amicon 10,000 MWCO spin concentrators. During purification of variants with reactive cysteines, buffers were supplemented with 0.5 mM ethylenediaminetetraacetic acid (EDTA) and 1 mM dithiothreitol (DTT), kept at 4 °C, degassed, and sparged with argon to minimize oxidation. ClpX concentrations were calculated in pseudo-hexamer equivalents based on absorbance at 280 nm.

NPM- or BMH-modified variants were constructed as shown in Fig. 1D. A pseudo-hexamer consisting of linked ClpX trimer containing the D144C and K330C substitutions in the N-terminal subunit (trimer A) was purified as described above in buffer containing DTT and was desalted into degassed, argon-sparged Xlink buffer using an 10 x 100 mm Sephadex G-25 column, diluted to a concentration of 1 µM pseudo hexamer with Xlink buffer, placed in a 37 °C water bath for ~10 min, and reacted with either 10 µM BMH or 500 µM NPM for 15 min before quenching with 5 mM DTT. The modified samples were then desalted and concentrated. BMH-crosslinking efficiency was assessed by TEV digestion and subsequent SDS-PAGE on a 15% polyacrylamide gel. Digestion reactions contained 1 µM modified pseudo hexamer and equimolar TEV and were digested with equimolar TEV at room temperature for 30 min before quenching with SDS-sample

buffer (final concentrations 50 mM Tris-HCl pH 6.8, 2% SDS, 10% glycerol, 1% β-mercaptoethanol, 0.02% bromophenol blue).

An evolved *S. aureus* sortase-A enzyme with P94S/D160N/K194T substitutions (Chen et al., 2011) was used to ligate trimer A, which contained a C-terminal LPETG sortase recognition site, to one of several different linked trimers that contained an N-terminal poly-glycine motif after TEV protease cleavage (trimer B). These experiments rely on dissociation of pseudo-hexamers into trimers and reassembly. Trimer-B variants were desalted after initial Ni-NTA chromatography, cleaved with equimolar TEV at room temperature for 2 h, passed over a small Ni-NTA column to remove H_6-tagged TEV, and further purified by Sephadex-200 chromatography. One subunit of trimer B contained a M363C substitution for nCoMET experiments, a D170C substitution for substrate-binding experiments, or an E185Q mutation for ATP-hydrolysis experiments. For fluorophore-labeled ClpX variants, prior to sortase ligation, linked trimers stored in DTT were desalted and reacted with a 3-fold excess of the appropriate maleimide-functionalized fluorophore at room temperature for 30 min before quenching with 1 mM DTT and desalting into Xlink buffer using a PD10 column (GE Healthcare). For nCoMET experiments, trimer A constructs contained a BMH modification in either the first or third subunit, and trimer B constructs contained the M363C-Oregon Green modification in the first, second, or third subunit. For example, the subunit 1-labeled ClpX variant shown in Fig. 3 was constructed from trimer A with the BMH modification in the third subunit and trimer B with the fluorophore in the first subunit, and the subunit 5 variant contained BMH in the first subunit of trimer A and the fluorophore in the third subunit of trimer B.

ClpX variants with single E185Q mutations were constructed similarly. For substrate binding experiments, the first subunit of trimer A contained the BMH modification and the first subunit of trimer B contained the Alexa 555 modification.

Sortase-ligation reactions contained 5 µM trimer A, 5 µM trimer B, and 1 µM sortase, and were carried out at room temperature for 2-4 hours in Xlink buffer supplemented with 5 mM $CaCl_2$ and 1 mM DTT. Reactions were then diluted 5-fold with IEXC buffer and chromatographed on a Source 15Q column (GE Healthcare) using a linear gradient from 100% IEXA buffer to 100% IEXB buffer. The presence of 1 M urea in the chromatography buffers was required to separate fully covalent hexamers from linked trimers. Fractions containing fully linked hexamers were identified by SDS-PAGE, concentrated, and desalted into Xlink buffer. The parental ClpX variant was constructed as described above with otherwise unmodified trimers A and B and had ATPase and degradation activities similar to other $ClpX^{\Delta N}$ pseudo hexamers.

ClpP and $titin^{I27}$-ssrA variants were purified as described (Kim et al., 2000; Kenniston et al., 2003). Unfolded $titin^{I27}$-ssrA was prepared by reacting native cysteines with either fluorescein-iodoacetamide or iodoacetic acid as described (Kenniston et al., 2003). For $titin^{I27}$-ssrA binding experiments, PCR mutagenesis was used to mutate the GLG linker between the $titin^{I27}$ sequence and the ssrA tag to GCG. Purification buffers for this variant were designed to minimize oxidation as described above for reactive-cysteine ClpX preparations. A slight excess of BHQ3 carboxylic acid succinimidyl ester was reacted with 2-maleimidoethylamine (Sigma) for 2 h at room temperature in DMSO.

Cys-containing titin[I27]-ssrA was desalted and reacted with a 3-fold excess of the resulting maleimide-functionalized BHQ3 quencher for 30 min at room temperature in Xlink buffer supplemented with 5 mM Tris to quench unreacted BHQ3 carboxylic acid succinimidyl ester, quenched with 1 mM DTT, and desalted using a PD10 column.

Assays

Unless noted, experiments were performed at room temperature in PD buffer. Fluorescence experiments were performed using a SpectraMax M5 plate reader (Molecular Devices) or a PTI QM-20000-4SE spectrofluorimeter. ATP hydrolysis by ClpX variants was measured by a coupled assay (Nørby, 1988). ADP inhibition of ATP hydrolysis was measured by a colorimetric assay using malachite green in PD buffer lacking glycerol (Geladopoulos et al., 1991). Reactions were quenched at various time points by addition of EDTA to 20 mM. Solution A was freshly prepared 7.5% (w/v) ammonium molybdate, solution B was 0.122% (w/v) malachite green in 6 N sulfuric acid, and solution C was 11% (v/v) Tween-20. A 5x working solution was prepared immediately prior to the experiment by mixing 2.5 mL solution A, 10 mL solution B, and 0.2 mL solution C. 6 µL of this working solution was mixed with 24 µL of quenched reaction sample or phosphate standard in a 384-well microplate, incubated at room temperature for 15 min, and absorbance at 620 nm was measured. ATP hydrolysis rates were calculated by constructing a standard curve and calculating organic phosphate concentrations across reaction time points. nCoMET assays were performed as described (Stinson et al., 2013) in PD buffer containing 20 mM $CoCl_2$ in place of $MgCl_2$.

For substrate-binding experiments, increasing concentrations of quencher-labeled titin[I27]-ssrA were incubated with a fixed concentration of an Alexa 555-labeled ClpX variant (25 nM) for ~5 min in the presence of ATP (10 mM), ATPγS (1 mM), or no nucleotide and the fluorescence emission spectra (excitation 485 nm; emission 520-530 nm) was averaged across the emission range.

To assay the binding of different concentrations of ClpX variants to Y60W ClpP (25 nM tetradecamer, 50 nM binding sites), samples were incubated for ~5 min in PD buffer plus 2 mM ATP, the tryptophan-emission spectrum (excitation 295 nm; emission 345-360 nm) was averaged for across the emission range, and the center of spectral mass was calculated, plotted against ClpX concentration, and fitted to a quadratic equation for near-stoichiometric binding.

Degradation of unfolded titin[I27]-ssrA was measured by increases in fluorescence anisotropy (Stinson et al., 2013). Reactions contained 2 µM titin[I27]-ssrA unfolded by reaction with fluorescein-iodoacetamide and 18 µM titin[I27]-ssrA unfolded by carboxymethylation, 0.3 µM ClpX pseudohexamer and 0.9 µM ClpP$_{14}$. Arc(R23C)-GCN4-ssrA dimers were labeled with either Alexa 488 or Alexa 647 and then allowed to equilibrate to form an equilibrium mixture of homodimers and heterodimers. ClpX (0.1 µM pseudohexmaer) variants and ClpP$_{14}$ (0.3 uM) were added together with ATP and a regeneration system (16 mM phosphocreatine, 0.032 mg/mL creatine kinase; Sigma) and the decrease in fluorescence (excitation 494 nm; emission 668 nm) caused by loss

of FRET was measured to determine the degradation rate.

REFERENCES

Aubin-Tam, M.-E., Olivares, A.O., Sauer, R.T., Baker, T.A., and Lang, M.J. (2011). Single-molecule protein unfolding and translocation by an ATP-fueled proteolytic machine. Cell *145*, 257–267.

Baker, T.A., and Sauer, R.T. (2011). ClpXP, an ATP-powered unfolding and protein-degradation machine. Biochimica Et Biophysica Acta (BBA) - Molecular Cell Research.

Burton, R.E., Baker, T.A., and Sauer, R.T. (2003). Energy-dependent degradation: Linkage between ClpX-catalyzed nucleotide hydrolysis and protein-substrate processing. Protein Sci *12*, 893–902.

Chen, I., Dorr, B.M., and Liu, D.R. (2011). A general strategy for the evolution of bond-forming enzymes using yeast display. Proceedings of the National Academy of Sciences *108*, 11399–11404.

Cordova, J.C., Olivares, A.O., Shin, Y., Stinson, B.M., Calmat, S., Schmitz, K.R., Aubin-Tam, M.-E., Baker, T.A., Lang, M.J., and Sauer, R.T. (2014). Stochastic but highly coordinated protein unfolding and translocation by the ClpXP proteolytic machine. Cell *158*, 647–658.

Geladopoulos, T.P., Sotiroudis, T.G., and Evangelopoulos, A.E. (1991). A malachite green colorimetric assay for protein phosphatase activity. Anal. Biochem. *192*, 112–116.

Glynn, S.E., Martin, A., Nager, A.R., Baker, T.A., and Sauer, R.T. (2009). Structures of asymmetric ClpX hexamers reveal nucleotide-dependent motions in a AAA+ protein-unfolding machine. Cell *139*, 744–756.

Hersch, G.L., Burton, R.E., Bolon, D.N., Baker, T.A., and Sauer, R.T. (2005). Asymmetric interactions of ATP with the AAA+ ClpX6 unfoldase: allosteric control of a protein machine. Cell *121*, 1017–1027.

Joshi, S.A., Hersch, G.L., Baker, T.A., and Sauer, R.T. (2004). Communication between ClpX and ClpP during substrate processing and degradation. Nat Struct Mol Biol *11*, 404–411.

Kenniston, J.A., Baker, T.A., and Sauer, R.T. (2005). Partitioning between unfolding and release of native domains during ClpXP degradation determines substrate selectivity and partial processing. Proc Natl Acad Sci USA *102*, 1390–1395.

Kenniston, J.A., Baker, T.A., Fernandez, J.M., and Sauer, R.T. (2003). Linkage between ATP consumption and mechanical unfolding during the protein processing reactions of an AAA+ degradation machine. Cell *114*, 511–520.

Kim, Y.I., Burton, R.E., Burton, B.M., Sauer, R.T., and Baker, T.A. (2000). Dynamics of substrate denaturation and translocation by the ClpXP degradation machine. Mol Cell *5*, 639–648.

Kim, Y.I., Levchenko, I., Fraczkowska, K., Woodruff, R.V., Sauer, R.T., and Baker, T.A. (2001). Molecular determinants of complex formation between Clp/Hsp100 ATPases and the ClpP peptidase. Nat. Struct. Biol. *8*, 230–233.

Lander, G.C., Estrin, E., Matyskiela, M.E., Bashore, C., Nogales, E., and Martin, A. (2012). Complete subunit architecture of the proteasome regulatory particle. Nature *482*, 186–191.

Maillard, R.A., Chistol, G., Sen, M., Righini, M., Tan, J., Kaiser, C.M., Hodges, C., Martin, A., and Bustamante, C. (2011). ClpX(P) generates mechanical force to unfold and translocate its protein substrates. Cell *145*, 459–469.

Martin, A., Baker, T.A., and Sauer, R.T. (2005). Rebuilt AAA + motors reveal operating principles for ATP-fuelled machines. Nature *437*, 1115–1120.

Nørby, J.G. (1988). Coupled assay of Na+,K+-ATPase activity. Meth. Enzymol. *156*, 116–119.

Popp, M.W., Antos, J.M., Grotenbreg, G.M., Spooner, E., and Ploegh, H.L. (2007). Sortagging: a versatile method for protein labeling. Nat. Chem. Biol. *3*, 707–708.

Sauer, R.T., and Baker, T.A. (2011). AAA+ proteases: ATP-fueled machines of protein destruction. Annu Rev Biochem *80*, 587–612.

Sen, M., Maillard, R.A., Nyquist, K., Rodriguez-Aliaga, P., Pressé, S., Martin, A., and Bustamante, C. (2013). The ClpXP protease unfolds substrates using a constant rate of pulling but different gears. Cell *155*, 636–646.

Smith, D.M., Fraga, H., Reis, C., Kafri, G., and Goldberg, A.L. (2011). ATP binds to proteasomal ATPases in pairs with distinct functional effects, implying an ordered reaction cycle. Cell *144*, 526–538.

Stinson, B.M., Nager, A.R., Glynn, S.E., Schmitz, K.R., Baker, T.A., and Sauer, R.T. (2013). Nucleotide Binding and Conformational Switching in the Hexameric Ring of a AAA+ Machine. Cell *153*, 628–639.

Taraska, J.W., Puljung, M.C., Olivier, N.B., Flynn, G.E., and Zagotta, W.N. (2009). Mapping the structure and conformational movements of proteins with transition metal ion FRET. Nature Publishing Group *6*, 532–537.

Wojtyra, U.A., Thibault, G., Tuite, A., and Houry, W.A. (2003). The N-terminal zinc binding domain of ClpX is a dimerization domain that modulates the chaperone function. J Biol Chem *278*, 48981–48990.

CHAPTER 4

Single molecule FRET measurements of ClpX subunit conformation

INTRODUCTION

AAA+ enzymes are multimeric ATP-fueled machines that unwind DNA and RNA, remodel macromolecular complexes, and disaggregate or unfold proteins by utilizing the energy of ATP binding and hydrolysis to drive conformational changes that power mechanical work (Hanson and Whiteheart, 2005). Characterization of these conformational changes is central to understanding the molecular mechanisms of these important enzymes.

Escherichia coli ClpX is a AAA+ protein unfolding and translocation machine, which functions as a ring hexamer (for review, see Baker and Sauer, 2011). Each ClpX subunit has a AAA+ module consisting of a large domain and a small domain connected by a flexible hinge. Nucleotides bind at the hinged interface and drive conformational changes that are propagated around the ring via rigid-body interactions between subunits (Glynn et al., 2009). ClpX recognizes a peptide degron in a protein substrate and then unfolds the protein by pulling the degron through a narrow axial pore (Gottesman et al., 1998; Martin et al., 2008a; 2008b). Unfolding typically requires multiple cycles of ATP binding and hydrolysis (Kenniston et al., 2003). After unfolding, ClpX translocates the denatured polypeptide into the degradation chamber of ClpP, a barrel-shaped protease formed by two stacked heptameric rings (Wang et al., 1997).

Although each ClpX subunit has the same amino-acid sequence, there is evidence for functional and conformational asymmetry. For example, biochemical experiments demonstrate that some ClpX subunits bind nucleotide with varying affinities and other

subunits fail to bind nucleotide entirely (Hersch et al., 2005; Stinson et al., 2013). Moreover, two basic classes of subunits are observed in a set of crystal structures of ClpX hexamers in different nucleotide states (Glynn et al., 2009; Stinson et al., 2013). Loadable (L) subunits bind nucleotide in the cleft between large and small domains, whereas unloadable (U) subunits have no binding site as a consequence of a rotation between these domains. Most crystal structures contain four L and two U subunits, arranged with approximate 2-fold symmetry in a L/L/U/L/L/U pattern. However, within the L and U classes, substantial structural variability is observed.

Previous studies suggest that individual ClpX subunits convert dynamically between the L and U conformations, with "switching" being required for robust machine function (Stinson et al., 2013). The kinetics of conformational switching and its dependence on nucleotide and protein substrate remain unknown. To address these questions, we developed a single-molecule FRET (smFRET) assay to observe conformational changes in a single subunit of the ClpX ring by total internal reflection fluorescence (TIRF) microscopy. Our results directly show conformational switching at the single-molecule level and demonstrate that the kinetics of switching depend on the type of nucleotide and substrate present.

**RESULTS**

Engineering a ClpX variant for smFRET

To allow observation of the conformational dynamics of a single subunit in a ClpX ring hexamer, we sought to introduce one acceptor and one donor dye at positions that

would result in different FRET signals in U versus L subunits. Unique cysteine substitutions for labeling with maleimide-functionalized fluorophores were introduced into genes encoding three linked ClpX$^{\Delta N}$ subunits containing the C169S mutation, which removes the only endogenous surface-accessible cysteine. We constructed one linked trimer containing the Q174C substitution in the large AAA+ domain of the third subunit and another trimer containing the D170C substitution in the large AAA+ domain of the first subunit (Martin et al., 2005). We refer to these trimers as W-W-Q and D-W-W, respectively, where W indicates an otherwise wild-type C169S ClpX$^{\Delta N}$ subunit. We labeled purified W-W-Q with Alexa 647 maleimide to generate W-W-Q^{647}, labeled purified D-W-W with Cy3 maleimide to obtain D^{Cy3}-W-W, and then joined these labeled trimers via sortase ligation to generate a W-W-Q^{647}-D^{Cy3}-W-W covalent hexamer for single-molecule analysis. The D^{Cy3}-W-W trimer also contained a C-terminal biotin-acceptor sequence to allow biotinylation and attachment to the TIRF coverslip via streptavidin linkage. In crystal structures, the distance between the beta carbons of Q174 and D170 in adjacent subunits is ~40 Å when small AAA+ domain between them assumes an L conformation and ~60 Å when it adopts a U conformation (Figure 1A). The Förster radius calculated for the Cy3 and Alexa 647 dye pair is ~50 Å. Thus, an L subunit should display higher FRET efficiency than a U subunit.

Bulk experiments

The W-W-Q^{647}-D^{Cy3}-W-W ClpX hexamer supported ClpP degradation of a folded protein substrate similar at a rate similar to W-W-W-W-W-W ClpX, indicating that the cysteine substitutions and attached fluorophores did not affect machine function (Figure 1B). We

excited the donor fluorophore (Cy3) and determined emission spectra for the W-W-Q^{647}-D^{Cy3}-W-W hexamer and for an equimolar mixture of control W-W-Q^{647}-W-W-W and W-W-W-D^{Cy3}-W-W hexamers (Figure 1C). Compared to the mixture of control hexamers, the W-W-Q^{647}-D^{Cy3}-W-W hexamer showed a decrease in donor-emission intensity and an increase in acceptor-emission intensity, as expected if FRET occurs between the dyes in this molecule.
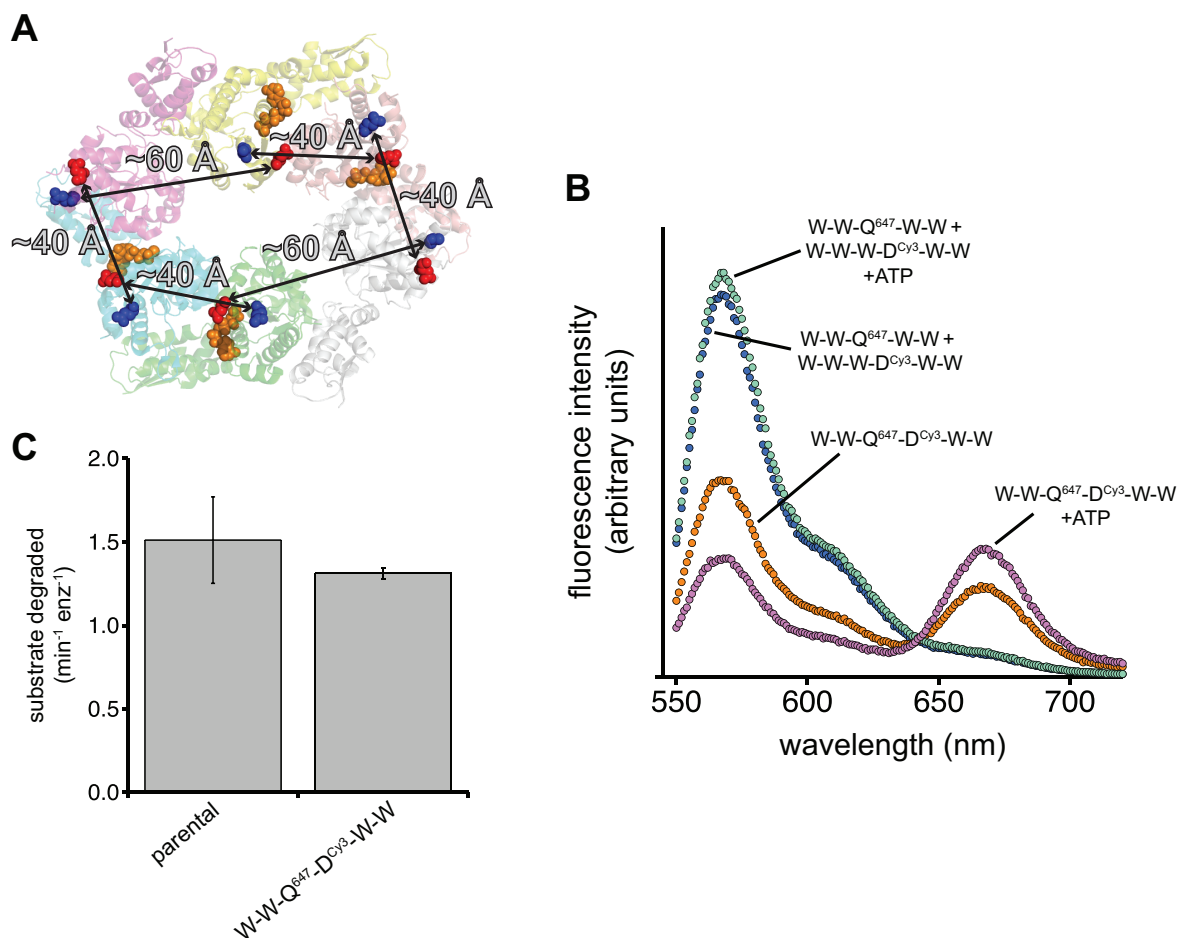

Figure 1. Design and biochemical properties of a ClpX hexamer used for smFRET. **(A)** Crystal structure of a ClpX hexamer (PDB 4I81), showing distances between residue Q174 (blue) in each subunit and residue D170 (red) in the clockwise adjacent subunit. ATPγS is shown in orange in four L subunits. **(B)** Degradation of a protein substrate (cp7-CFP-ssrA; 15 µM) by ClpX variants (0.1 µM) and ClpP$_{14}$ (0.3 µM). Reactions were performed in PD buffer plus 5 mM ATP and contained an ATP-regeneration system. **(C)** Fluorescence-emission spectra (excitation 520 nm) of W-W-Q^{647}-D^{Cy3}-W-W (0.1 µM) or a mixture of W-W-Q^{647}-W-W-W and W-W-W-D^{Cy3}-W-W hexamers (both 0.1 µM) in the absence and presence of ATP (5 mM).

A previous experiment based on contact quenching of rhodamine dyes suggested that the ClpX hexamer predominantly assumes a 4L:2U arrangement of subunits in the absence of nucleotide and a 5L:1U arrangement in the presence of nucleotide (Stinson et al., 2013). Addition of ATP to W-W-Q^{647}-D^{Cy3}-W-W resulted in a decrease in donor emission and concomitant increase in acceptor emission (Figure 1C). This result is consistent with an increase in the average number of L subunits upon addition of nucleotide.

Single molecule experiments reveal multiple FRET states

Biotinylated W-W-Q^{647}-D^{Cy3}-W-W was immobilized via a streptavidin linkage on a PEG-modified glass coverslip, and smFRET trajectories were recorded using TIRF microscopy. Figure 2A shows a FRET efficiency histogram constructed from individual FRET trajectories in the presence of 1 mM ATP. The histogram was asymmetric, indicating multiple FRET states, and was fit well by a two-Gaussian distribution, consistent with a model in which two main subunit populations exhibit distinct FRET efficiencies. Based on inter-dye distances expected from crystal structures, we assigned the low-FRET population to subunits in the U conformation and the high-FRET population to subunits in the L conformation. Integration of the two Gaussian functions showed ~75% average occupancy of the L conformation. This value is intermediate between the values expected for 4L:2U hexamer (66%) and a 5L:1U hexamer (83%), suggesting that both types of hexamers are populated under the conditions of this experiment. A FRET efficiency histogram from trajectories recorded in the presence of 1 mM ATPγS (Fig. 2B) showed ~83% average occupancy of the L conformation, as

expected for a 5L:1U hexamer. ATPγS is hydrolyzed by ClpX more slowly than ATP, and thus it is possible that the hydrolysis rate influences the relative proportion of 5L:1U and 4L:2U rings.
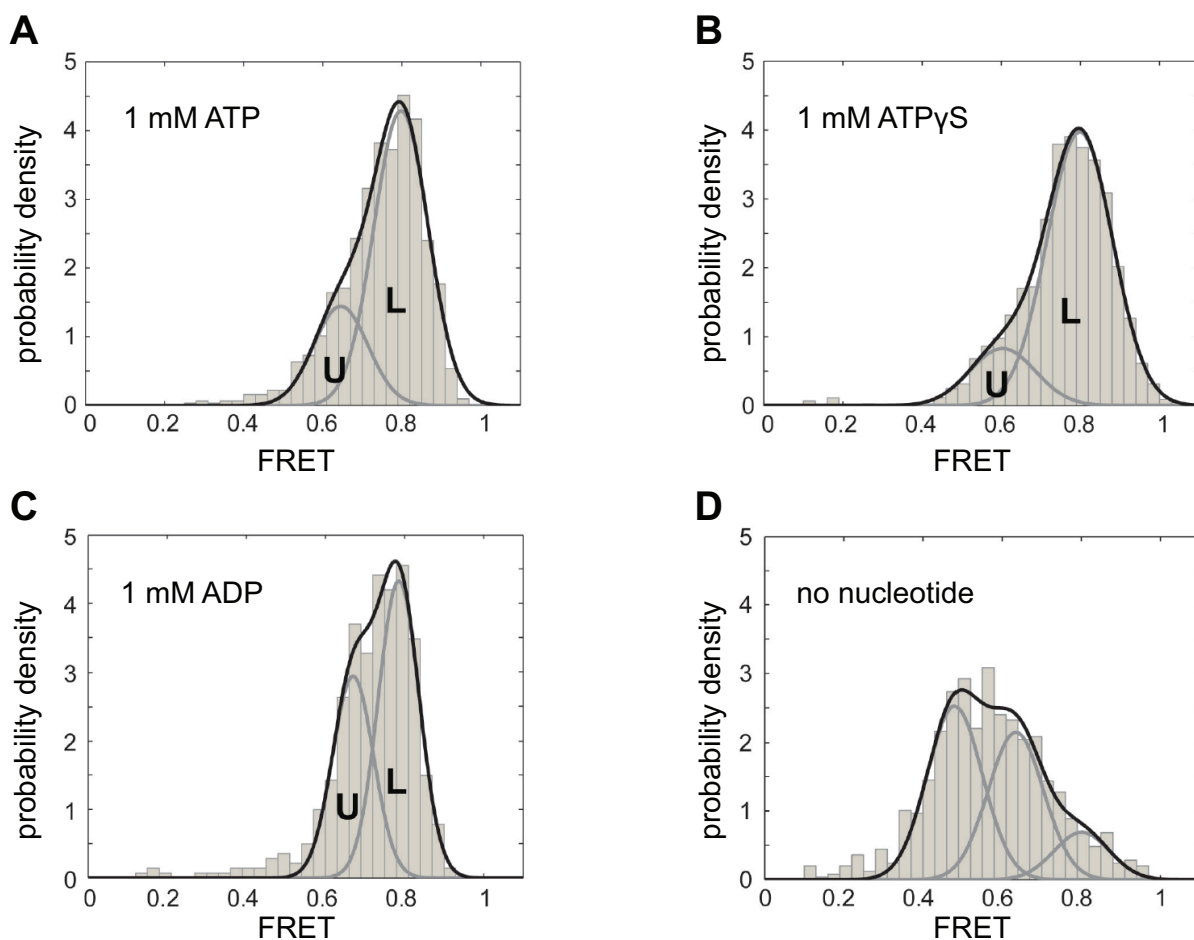
Figure 2. FRET-efficiency histograms from single-molecule experiments using W-W-Q^{647}-D^{Cy3}-W-W in the presence of 1 mM ATP **(A)**, 1 mM ATPγS **(B)**, 1 mM ADP **(C)**, or no nucleotide **(D)**. In panels **A-C**, distributions were fit to a double Gaussian function. In panel (D), the distribution was fit to a triple Gaussian function with a fixed standard deviation (0.07). (A) 1 mM ATP, integration values 75% (L), 25% (U). (B) 1 mM ATPγS, integration values 83% (L), 17% (U). (C) 1 mM ADP, integration values 60% (L), 40% (U). Figure courtesy of Y. Shin.

Multiple FRET states were also observed in the presence of 1 mM ADP (~60% L conformation; Fig. 2B) and in the absence of nucleotide (Fig. 2D). Notably, the no-

nucleotide FRET histogram required a third Gaussian function with a lower FRET efficiency for adequate fitting. These results support a model in which nucleotide binding alters accessible ClpX conformational states and shortens the average distance between labeled residues.

Individual smFRET traces show dynamic conformational switching

Do subunits switch dynamically between L and U conformations? Figures 3A-D shows representative FRET trajectories for each nucleotide condition. The ATP and no nucleotide trajectories contained 5 or more switching events in ~35 s. By contrast, no switching events were observed over 15 s with ADP and only a single event was observed in 30 s with ATPγS. Thus, subunits can switch conformations but with rates that depend on the nucleotide.

We performed auto-correlation analysis on multiple smFRET trajectories in each nucleotide condition to quantify the kinetics of switching between FRET states (Figure 3E). Single exponential fits yielded time constants of 1.36 s and 1.75 s for ATP and ATPγS, respectively, indicating that L⇔U switching occurs slightly more quickly in the presence of ATP. Auto-correlation for the ADP condition decayed immediately to zero, a result characteristic of random noise about a constant mean, providing further evidence that the ADP-loaded hexamer does not undergo significant L⇔U switching within the observation time frames (typically 10-40 s). In the absence of nucleotide, the auto-correlation time constant was 0.58 s, suggesting that the nucleotide-free hexamer samples multiple conformations more rapidly than nucleotide-bound hexamers.
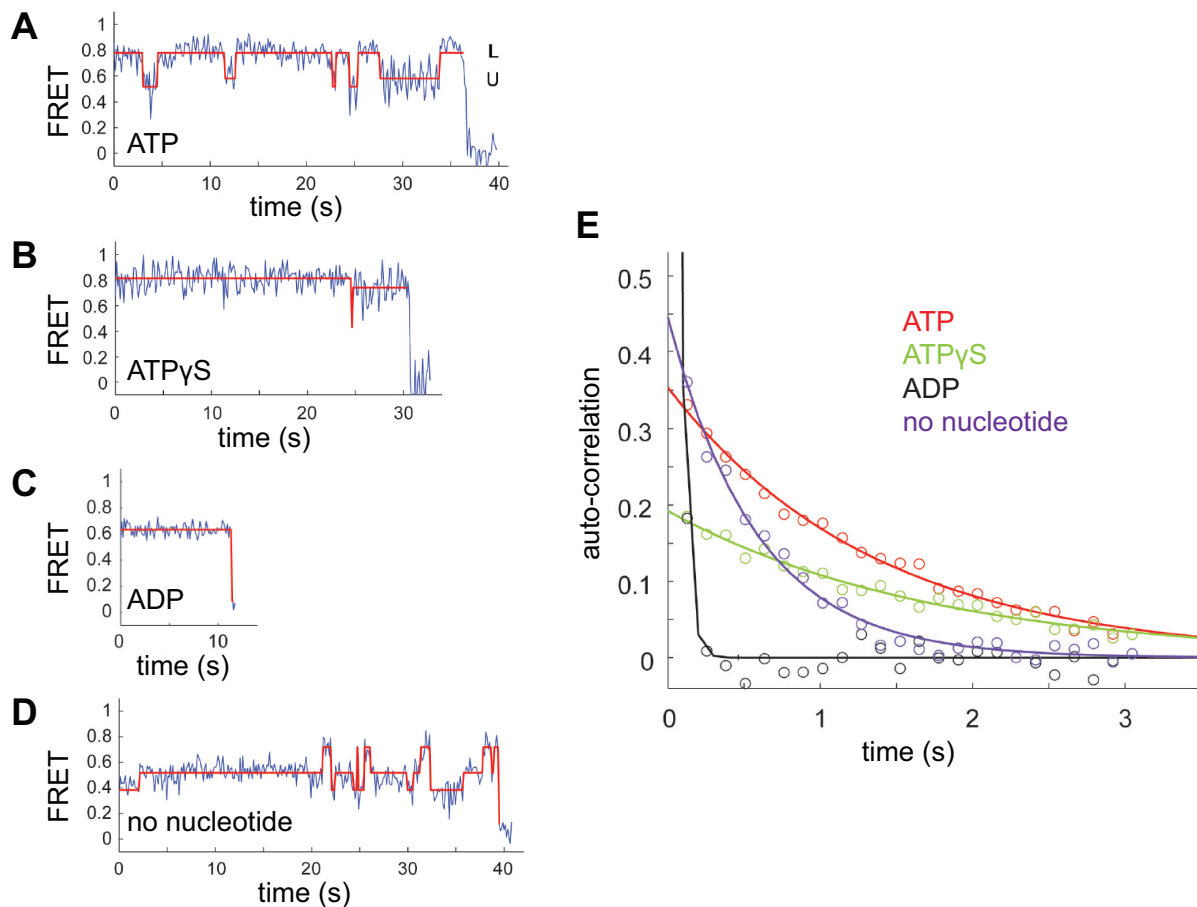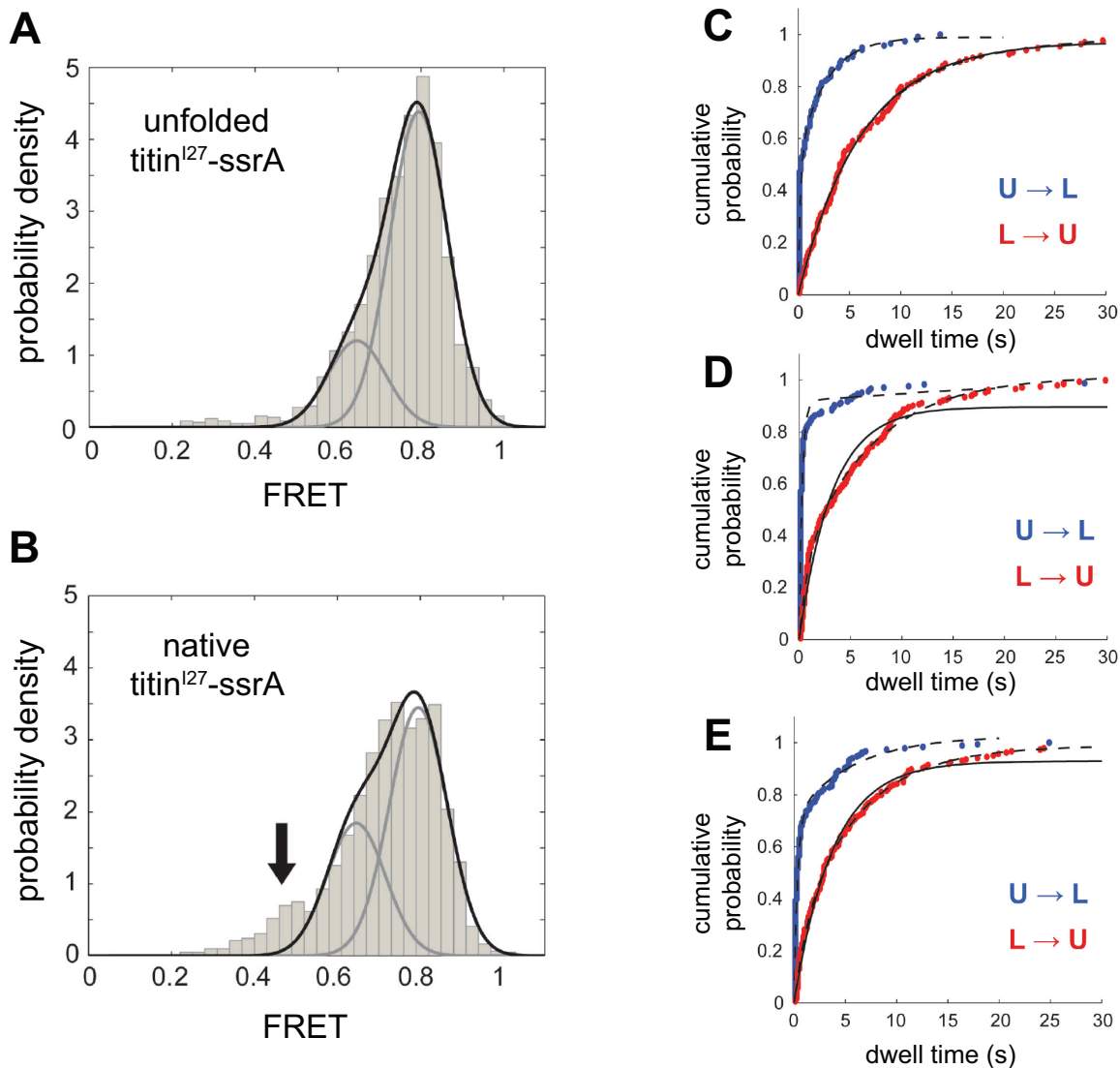
Figure 3. Conformational switching within single-molecule trajectories in the presence of 1 mM ATP (**A**), 1 mM ATPγS (**B**), 1 mM ADP (**C**), or no nucleotide (**D**). Each trace in A-D terminates with a photobleaching event. Panel **E** shows auto-correlation of smFRET signals under different nucleotide conditions. Time constants of single exponential fits were 1.36 s (ATP), 1.75 S (ATPγS), 0.04 s (ADP), and 0.58 s (no nucleotide). Figure courtesy of Y. Shin.

Substrate dependence of conformational switching

We recorded additional smFRET trajectories in the presence of ATP and either a native or unfolded titin[I27]-ssrA protein substrate. Unfolded titin[I27]-ssrA was prepared by carboxymethylation of endogenous buried cysteines with iodoacetic acid (Kenniston et al., 2003). The FRET histogram for the unfolded-substrate condition showed a similar distribution to the ATP condition in the absence of protein substrate, with ~75% of the subunits in the population in the L state (Figure 4A). Figure 4B shows the FRET

histogram obtained with folded substrate. Notably, a new population with very low average FRET was present, suggesting that ClpX hexamers pulling on a stable substrate transit through conformations not populated during normal ATP hydrolysis and polypeptide translocation.

Figure 4. Conformational switching in the presence of different protein substrates and ATP. **(A)** and **(B)** show FRET-efficiency histograms in the presence of unfolded titin[I27]-ssrA (15 μM) and native titin[I27]-ssrA (15 μM), respectively. Distributions were fit to a double-Gaussian function with integration values of 78% (L) and 22% (U) for unfolded titin[I27]-ssrA and 65% (L) and 35% (U) for native titin[I27]-ssrA. **(C)-(E)** show dwell-time distributions without and with protein substrate. Solid lines are single exponential fits and dashed lines are double exponential fits. **(C)** No protein

substrate. The L-dwell single-exponential fit had a time constant of 6.2 s. The L-dwell double-exponential fit had time constants and amplitudes, respectively, of 5.3 s and 76%, and 12.5 s and 24%. The U-dwell double-exponential fit had time constants and amplitudes, respectively, of 0.2 s and 52%, and 2.7 s and 47%. **(D)** Unfolded titin[I27]-ssrA. The L-dwell single-exponential fit had a time constant of 3.2 s. The L-dwell double-exponential fit had time constants and amplitudes, respectively, of 0.8 s and 28%, and 6.8 s and 73%. The U-dwell double-exponential fit had time constants and amplitudes, respectively, of 0.3 s and 92%, and 34.6 s and 11%. **(E)** Native titin[I27]-ssrA. The L-dwell single exponential fit had a time constant of 3.8 s. The L-dwell double exponential fit had time constants and amplitudes, respectively, of 1.2 s and 22%, and 6.0 s and 77%. U dwell double exponential fit had time constants and amplitudes, respectively, of 0.33 s and 71%, and 5.6 s and 31%. Figure courtesy of Y. Shin.

For in ATP trajectories collected with no substrate, unfolded substrate, and native substrate, we employed hidden Markov modeling (HMM) to determine dwell times of L and U FRET states (Figures 4C-E). L→U transitions had longer dwell times than U→L transitions, consistent with the majority of subunits adopting an L conformation. We fit the L→U dwell-time distributions with single exponential (solid line) and double exponential (dashed line) functions. These fits were indistinguishable in the no-substrate condition, but double-exponential fits of the distributions with substrate showed a fast phase accounting for 20-30% of the total amplitude. Double-exponential fits of U→L dwell time distributions showed a corresponding increase in the amplitude of the fast phase in the presence of substrate, consistent with the time-averaged proportions of L and U subunits remaining similar across all substrate conditions. Multiple classes of nucleotide binding sites in the ClpX hexamer have been reported (Hersch et al., 2005; Stinson et al., 2013). The double-exponential kinetics observed for L→U and U→L conformational switching in the presence of protein substrate indicate the presence of multiple subunit conformational classes as well.

DISCUSSION

Our results provide evidence of L/U subunit asymmetry in solution and allow real-time observation of L⇔U switching in individual subunits. This conformational switching is critical for robust machine function (Stinson et al., 2013). Integration of fits to FRET efficiency histograms suggests that ClpX hexamers on average have 4-5 L subunits per hexamer. Most crystal structures show hexamers containing four L subunits, and a bulk fluorescence assay suggests the hexamer contains 4-5 L subunits depending on its nucleotide state (Glynn et al., 2009; Stinson et al., 2013). Furthermore, a hexamer with two subunits locked in the U conformation lacks significant ATP hydrolysis activity, whereas a hexamer with one U-locked subunit hydrolyzes ATP robustly (Chapter 3). Taken together, these results are consistent with a model in which the 5L:1U state is a working conformation and the 4L:2U state is a transiently populated intermediate.

We find that the distribution of accessible conformational states and rates of conformational switching depend on nucleotide conditions. In the absence of nucleotide, subunits appear to have a wider variety of accessible states that interconvert quickly. ATP and ATPγS appear to stabilize a narrower range of states that interconvert more slowly. In the presence of ADP, FRET states corresponding to L and U subunits are apparent in separate trajectories, but almost no switching was observed before sample photobleaching terminated the experiment. Taken together, these results support a model in which the barrier to conformational transitions is low relative to thermal energy in the absence of nucleotide, and this barrier is increased to varying extents depending on the type of nucleotide bound. By this model, nucleotide-binding energy stabilizes a subset of conformations accessible without nucleotide. ATP and ATPγS slow the rate of

switching by increasing the barrier between conformational states, and ADP increases this barrier further, preventing switching within the observation window.

In the absence of protein substrate, the time constant for ATP hydrolysis by a ClpX hexamer is ~1 s (Martin et al., 2007), whereas L$\rightarrow$U switching in a single subunit occurs with a time constant of ~6 s. These values are consistent with a model in which ATP hydrolysis causes one subunit in the ring to switch from L$\rightarrow$U and another subunit to switch from U$\rightarrow$L. However, our results suggest that L$\Leftrightarrow$U switching is not tightly linked to the ATPase cycle. If L$\Leftrightarrow$U switching were tightly linked to the ATPase cycle, there should be minimal switching in the absence of nucleotide and slow switching in the presence of ATPγS, which ClpX hydrolyzes ~10-fold more slowly than ATP (Burton et al., 2003). By contrast, we find that rapid switching can occur in the absence of nucleotide, and the auto-correlation time constant in the presence of ATPγS is increased less than 1.5-fold relative to ATP. Thus, although ATP stabilizes certain conformational states and affects switching kinetics, it does not appear to provide the primary driving force for L$\rightarrow$U and U$\rightarrow$L conformational changes. We prefer a model in which thermal energy drives conformational switching stochastically. Thermally-driven switching may allow the hexamer to escape situations in which hexamer function would be compromised, such as after a failed unfolding attempt or when ADP is improperly bound.

Our results also show that the presence of protein substrate affects accessible conformational states and rates of switching among them. In the presence of native

titin[I27]-ssrA and ATP, we observed a new low-FRET state that was not observed with unfolded titin[I27]-ssrA and ATP or with no substrate and ATP. Native titin[I27]-ssrA is a stable substrate, requiring on average hundreds of ClpX ATP hydrolysis events per molecule degraded (Kenniston et al., 2003). The new low-FRET state, which likely corresponds to a U-like conformation, may represent a strained conformation of the hexamer as it pulls against a stable domain. Furthermore, stable substrates are frequently released from ClpX after unsuccessful unfolding attempts (Kenniston et al., 2003). Thus, the low-FRET state might represent a transient state in which ClpX has released substrate, allowing the hexamer to reset for another unfolding attempt. Interestingly, a similar low-FRET state is also observed for the ClpX ring in the absence of nucleotide. These observations might be reconciled if substrate release and nucleotide release occurred concurrently after failed unfolding.

The proportion of fast-switching L and U subunits increases when ClpX encounters native or unfolded titin[I27]-ssrA. Because ClpXP degrades these substrates at rates differing by ~16-fold (Kenniston et al., 2003), we expect that the observed differences in switching kinetics arise as a consequence of substrate binding rather than mechanical translocation or unfolding. Indeed, the results in Chapter 3 show that limiting conformational switching in one subunit results in weakened substrate binding. Thus, fast conformational switching during substrate binding may be a mechanism to promote efficient engagement of protein substrates.

Future smFRET experiments using W-W-Q[647]-D[Cy3]-W-W ClpX, protein substrates of

varying stability, ATP at different concentrations, and detailed HMM analysis of larger numbers of trajectories should allow better characterization of conformational switching, particularly among sub states within the broader L and U conformational classes.

EXPERIMENTAL PROCEDURES

Proteins

Genes encoding the W-W-Q and D-W-W ClpX trimers were constructed by standard PCR methods and purified and labeled with Alexa 647 C_2 maleimide (Molecular Probes) or Cy3 maleimide (GE Healthcare) as described in Chapter 3 for variants with reactive cysteines. W-W-Q contained a C-terminal LPETG sortase recognition tag, and D-W-W contained an N-terminal poly-glycine motif revealed upon digestion with TEV protease. Sortase-mediated ligation was performed as described in Chapter 3. D-W-W also contained a C-terminal biotin acceptor peptide sequence (GLNDIFEAQKIEWHE) to allow biotinylation *in vivo* or *in vitro* for subsequent immobilization on TIRF coverslips.

smFRET assay (courtesy of Y. Shin)

Single-molecule FRET assays were performed using a custom built objective-side TIRF microscope equipped with a 100X 1.49 NA TIRF objective, an EMCCD camera (Andor) and a 532/640 nm two-color illumination system. Cy3 and Alexa-647 emissions were split by a 640 nm long-pass dichroic mirror (Chroma) and simultaneously focused onto the EMCCD camera.

PEG-modified glass coverslips were prepared based on a published protocol. Briefly, glass coverslips were sonicated sequentially in deionized water, methanol, and 1 M

KOH. The cleaned coverslips were then sonicated with a solution of 1% methoxypolyethyleneglycol-silane (1% mixture of biotin-PEG-silane; mPEG-silane-5000, and biotin-PEG-silane-5000, Laysan Bio) in anhydrous toluene in the presence of 0.8 mM triethylamine. The reacted coverslips were washed with toluene and deionized water, and finally dried under Argon gas. PEG-modified coverslips were stored under vacuum at −20 °C and assembled into flow chambers before use.

Flow cells were made from double-sided sticky-tape gaskets sandwiched between a glass slide and the PEG-modified coverslip. While flow cells were treated with 0.01 mg/mL streptavidin, labeled ClpX (10nM) was incubated with ClpP (0.84 μM), 1 mM ATP, and an ATP-regeneration system in PD buffer (25 mM HEPES pH 7.6, 100 mM KCl, 10 mM MgCl2, 10% glycerol (vol/vol)) to form ClpXP complexes. After unbound streptavidin was washed away, assembled ClpXP (diluted to 0.625 nM) was introduced into the flow cell and incubated for 20 min to allow ClpXP binding to the biotin-PEG surface. Samples were then washed with imaging buffer (PD buffer supplemented with ClpP (0.67 μM), appropriate nucleotides/substrates, and an oxygen-scavenging system (0.8 % D(+)-glucose, 16500 units/mL glucose oxidase, 217000 units/mL catalase, and 2 mM Trolox) and were incubated for 5 min before imaging. Single-molecule traces were recorded with 116 ms time frames.

Single-molecule data were processed using custom-made MATLAB scripts. Briefly, fluorescent peaks in the images were identified and traced throughout the trajectory. Traces that showed a single-donor bleaching event were used for data analysis. The

FRET efficiency was calculated from donor and acceptor intensities (I_D, I_A) by using according to $(1 + \gamma(I_D/I_A))^{-1}$ where γ is the ratio of the change in average acceptor intensity (ΔI_A) to the change in average donor intensity (ΔI_D) upon acceptor photo bleaching. FRET histograms were built using averages of every 3 points up to initial 10 points of each FRET trace. MATLAB embedded functions were used to calculate auto-correlation of signals. Correlations were calculated using individual traces and then weight averaged with lengths of traces. Hidden Markov modeling (HMM) of FRET traces was performed using the HaMMy program (McKinney et al., 2006). To prevent underestimation of rates, only traces last longer than 5 s were used for HMM.

REFERENCES

Baker, T.A., and Sauer, R.T. (2011). ClpXP, an ATP-powered unfolding and protein-degradation machine. Biochimica Et Biophysica Acta (BBA) - Molecular Cell Research.

Burton, R.E., Baker, T.A., and Sauer, R.T. (2003). Energy-dependent degradation: Linkage between ClpX-catalyzed nucleotide hydrolysis and protein-substrate processing. Protein Sci *12*, 893–902.

Glynn, S.E., Martin, A., Nager, A.R., Baker, T.A., and Sauer, R.T. (2009). Structures of asymmetric ClpX hexamers reveal nucleotide-dependent motions in a AAA+ protein-unfolding machine. Cell *139*, 744–756.

Gottesman, S., Roche, E., Zhou, Y., and Sauer, R.T. (1998). The ClpXP and ClpAP proteases degrade proteins with carboxy-terminal peptide tails added by the SsrA-tagging system. Genes Dev *12*, 1338–1347.

Hanson, P.I., and Whiteheart, S.W. (2005). AAA+ proteins: have engine, will work. Nat. Rev. Mol. Cell Biol. *6*, 519–529.

Hersch, G.L., Burton, R.E., Bolon, D.N., Baker, T.A., and Sauer, R.T. (2005). Asymmetric interactions of ATP with the AAA+ ClpX6 unfoldase: allosteric control of a protein machine. Cell *121*, 1017–1027.

Kenniston, J.A., Baker, T.A., Fernandez, J.M., and Sauer, R.T. (2003). Linkage between ATP consumption and mechanical unfolding during the protein processing reactions of an AAA+ degradation machine. Cell *114*, 511–520.

Martin, A., Baker, T.A., and Sauer, R.T. (2005). Rebuilt AAA + motors reveal operating principles for ATP-fuelled machines. Nature *437*, 1115–1120.

Martin, A., Baker, T.A., and Sauer, R.T. (2007). Distinct static and dynamic interactions control ATPase-peptidase communication in a AAA+ protease. Mol Cell *27*, 41–52.

Martin, A., Baker, T.A., and Sauer, R.T. (2008a). Pore loops of the AAA+ ClpX machine grip substrates to drive translocation and unfolding. Nat Struct Mol Biol *15*, 1147–1151.

Martin, A., Baker, T.A., and Sauer, R.T. (2008b). Diverse pore loops of the AAA+ ClpX machine mediate unassisted and adaptor-dependent recognition of ssrA-tagged substrates. Mol Cell *29*, 441–450.

McKinney, S.A., Joo, C., and Ha, T. (2006). Analysis of single-molecule FRET trajectories using hidden Markov modeling. Biophys. J. *91*, 1941–1951.

Stinson, B.M., Nager, A.R., Glynn, S.E., Schmitz, K.R., Baker, T.A., and Sauer, R.T. (2013). Nucleotide Binding and Conformational Switching in the Hexameric Ring of a AAA+ Machine. Cell *153*, 628–639.

Wang, J., Hartling, J.A., and Flanagan, J.M. (1997). The structure of ClpP at 2.3 A resolution suggests a model for ATP-dependent proteolysis. Cell *91*, 447–456.

CHAPTER 5

Single molecule measurements of nucleotide occupancy

and subunit coordination in the ClpX hexamer

INTRODUCTION

AAA+ enzymes harness the energy of ATP binding and hydrolysis to perform mechanical work on macromolecular substrates. Members of this family serve many biological functions, including unwinding of DNA and RNA duplexes and the disaggregation, unfolding, and degradation of proteins (Ogura and Wilkinson, 2001). AAA+ machines are multimeric, and must coordinate ATP binding and hydrolysis among subunits to drive the conformational changes that power mechanical work (Hanson and Whiteheart, 2005). Characterization of nucleotide transactions in individual subunits of these enzymes is central to understanding their detailed molecular mechanisms.

Ring hexamers of the *Escherichia coli* ClpX, a AAA+ protein unfoldase, recognize a peptide tag in protein substrates and employ multiple cycles of ATP binding and hydrolysis to unfold and translocate the substrate polypeptide into the degradation chamber of the barrel-shaped ClpP peptidase (for review, see (Baker and Sauer, 2011)). Nucleotides bind in the cleft between the large and small AAA+ domains of ClpX (Glynn et al., 2009). Although each ClpX subunit has the same amino-acid sequence, individual subunits interact with nucleotide differently. For example, biochemical experiments show that some subunits do not bind nucleotide and other subunits bind with different affinities (Hersch et al., 2005; Stinson et al., 2013). Crystal structures show two basic classes of ClpX subunits, distinguished by a major rotation between the large and small AAA+ domains (Glynn et al., 2009; Stinson et al., 2013). A well-formed nucleotide-binding pocket is present in loadable (L) subunits, whereas this pocket is

sterically occluded in unloadable (U) subunits. Most crystal structures show four L subunits and two U subunits arranged in an L/L/U/L/L/U pattern, although there is substantial structural variability within these L and U classes.

How is nucleotide binding coordinated among six asymmetric subunits to ensure robust machine function? To answer this question, previous studies have relied on subunit-specific mutations that perturb ATP binding and/or hydrolysis (Martin et al., 2005; Stinson et al., 2013). Such mutations are necessary to introduce chemical asymmetry into the hexamer and to probe the functional contributions of individual subunits. Here, we present a single-molecule method to study nucleotide transactions in ClpX hexamers with six functional nucleotide-binding sites. Our method combines an ATP analog that quenches fluorescence when it binds ClpX and total internal reflection fluorescence (TIRF) microscopy to measure communication among individual ClpX subunits that would otherwise be obscured through ensemble averaging.

RESULTS

Experimental logic

We sought to measure nucleotide occupancy of individual ClpX subunits at the single-molecule level. Our approach was to label individual subunits with a fluorophore and measure binding to the labeled subunit with an ATP analog containing a fluorescence-quenching moiety. To fluorescently label specific subunits with a TAMRA-maleimide fluorophore, a unique K330C substitution was introduced into genes encoding three ClpX$^{\Delta N}$ subunits containing the C169S mutation, which removes the only endogenous

reactive cysteine. K330C is located near the nucleotide-binding site of L subunits (Glynn et al., 2009; Stinson et al., 2013). Fully covalent ClpX hexamers were generated by sortase linkage (Chapter 3) and contained one or two fluorophore-labeled subunits and a biotinylation site for immobilization on TIRF coverslips through streptavidin binding.

Synthesis of a fluorescence-quenching ATP analog

We used the method of Hazlett *et al*. to synthesize a ribose-modified ATP analog that would quench fluorescence (Figure 1; see Methods for details)(Hazlett et al., 1993). Briefly, the 2´ and 3´ hydroxyls of ATP were activated by addition of carbonyldiimidazole, forming a cyclic carbonate sepcies, and subsequently reacted with ethylenediamine to yield ethylenediamine-ATP (eda-ATP). The eda-ATP molecule was then reacted with the succinimidyl ester of the DABCYL Plus quencher to form mixed 2´ and 3´ isomers of DABCYL-Plus-eda-ATP, which we will call ATP^Q. Chromatography of the mixed isomers on a DEAE-sepharose column gave two peaks (Figure 2A(i)), which contained molecules that migrated with slightly different mobilities in thin-layer chromatography (Figure 2B-C). The purified isomers were stored at pH 6.0 and –80 °C to minimize isomerization (Oiwa et al., 2000). The two peaks re-isomerized upon extended incubation at room temperature (Figure 2A(ii-iii)). As identification of which peak corresponds to the 2´ isomer and which corresponds to the 3´ isomer was not possible, we refer to them as ATP^Q_1 and ATP^Q_2. In principle, ^{1}H-NMR experiments could identify the isomeric nature of each peak (Oiwa et al., 2000).
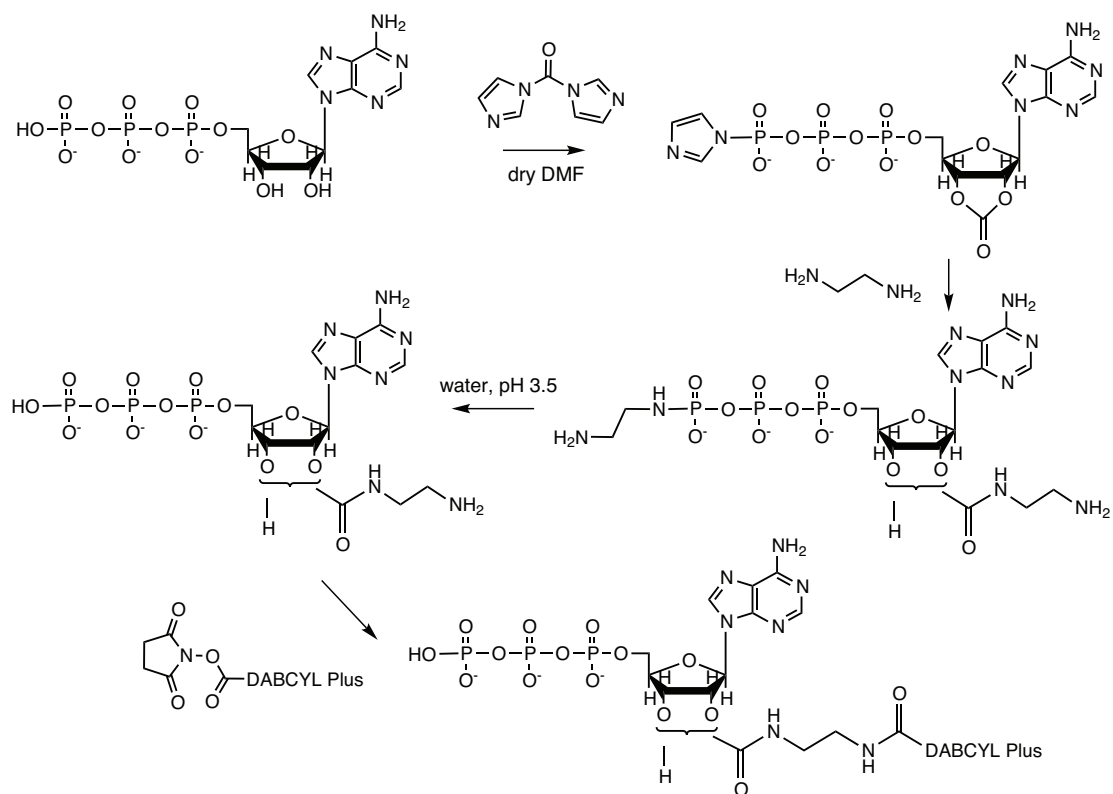
Figure 1. ATP^Q synthesis scheme. See Methods for details.

ATP^Q support of ClpX activity and quenching of fluorescence

ClpX alone catalyzed hydrolysis of both ATP^Q isomers at a rate ~7-fold slower than it hydrolyzed ATP (Figure 3A). However, addition of ClpP and a protein substrate stimulated ClpX hydrolysis of both ATP^Q isomers to rates that were 60-80% as fast as ATP hydrolysis (Figure 3A). ATP$^Q_2$ supported degradation of the protein substrate by ClpXP about half as well as ATP, whereas almost no degradation was observed with ATP$^Q_1$ (Figure 3B). Accordingly, we focused on ATP$^Q_2$ for subsequent experiments.
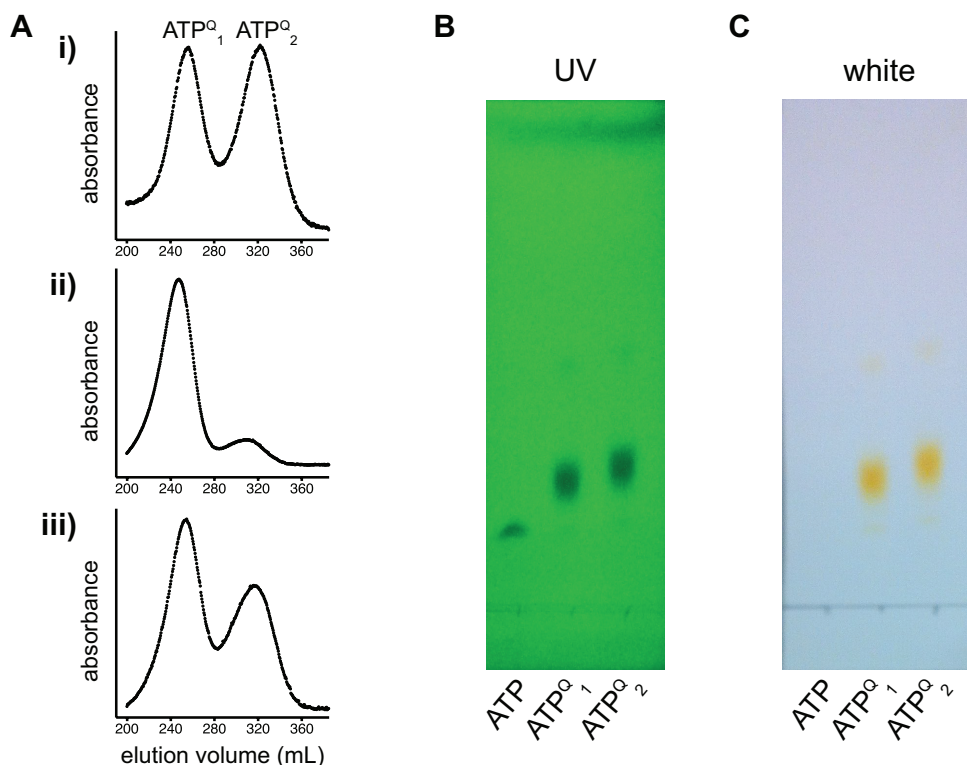
Figure 2. ATP^Q isomers. **(A)** Purification of ATP^Q isomers by chromatography on a DEAE-Sepharose column was monitored by absorbance at 280 nm. **(i)** The initial reaction mixture contained two peaks, corresponding to 2′ and 3′ isomers of ATP^Q. **(ii)** Isolated ATP$^Q_1$, chromatagrpahed immediately after thawing. **(iii)** Isolated ATP$^Q_1$ chromatographed after 5 days at room temperature. **(B)-(C)** ATP and purified ATP^Q isomers were chromatographed on F254 indicator silica gel TLC plates and detected by UV illumination (B) or white light illumination (C).
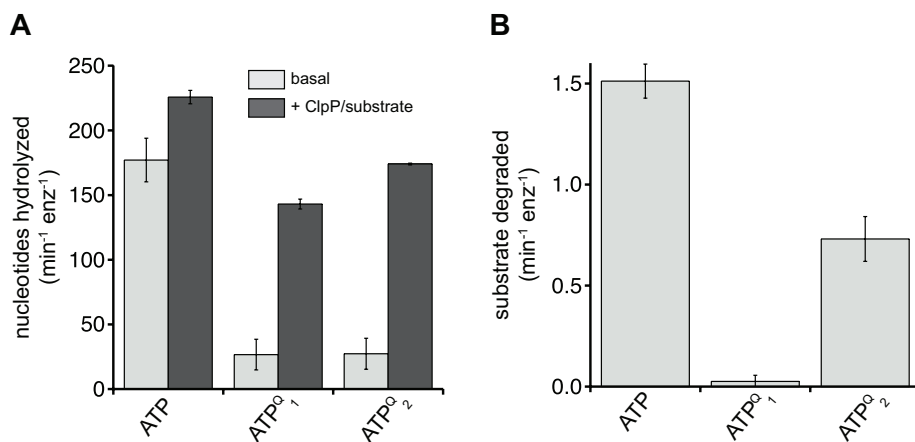
Figure 3. ClpX activity supported by ATP^Q isomers. **(A)** Hydrolysis of ATP and ATP^Q isomers by ClpX (50 nM covalent hexamer) in the absence or presence of ClpP (150 nM) and cp7-GFP-ssrA protein substrate (10 μM). **(B)** Degradation of cp7-GFP-ssrA (10 μM) by ClpX (100 nM covalent hexamer) and ClpP (300 nM) with 2 mM nucleotide. For (A)-(B), values represent means ± SD (N=3).

126

To assay binding, we incubated a fixed concentration of a ClpX hexamer containing one TAMRA-K330C modified subunit with increasing concentrations of ATP^Q_2 and measured changes in fluorescence. The ATP^Q analog bound ClpX with an apparent affinity of ~2 μM and saturating concentrations quenched ~65% of the initial fluorescence (Figure 4A). Importantly, ATP competed for ATP^Q_2 quenching (Figure 4B), suggesting that ATP^Q_2 and ATP bind to the same site. ATP^Q_2 affinity for ClpX is similar to affinities measured for other nucleotides (Chapters 2-3).
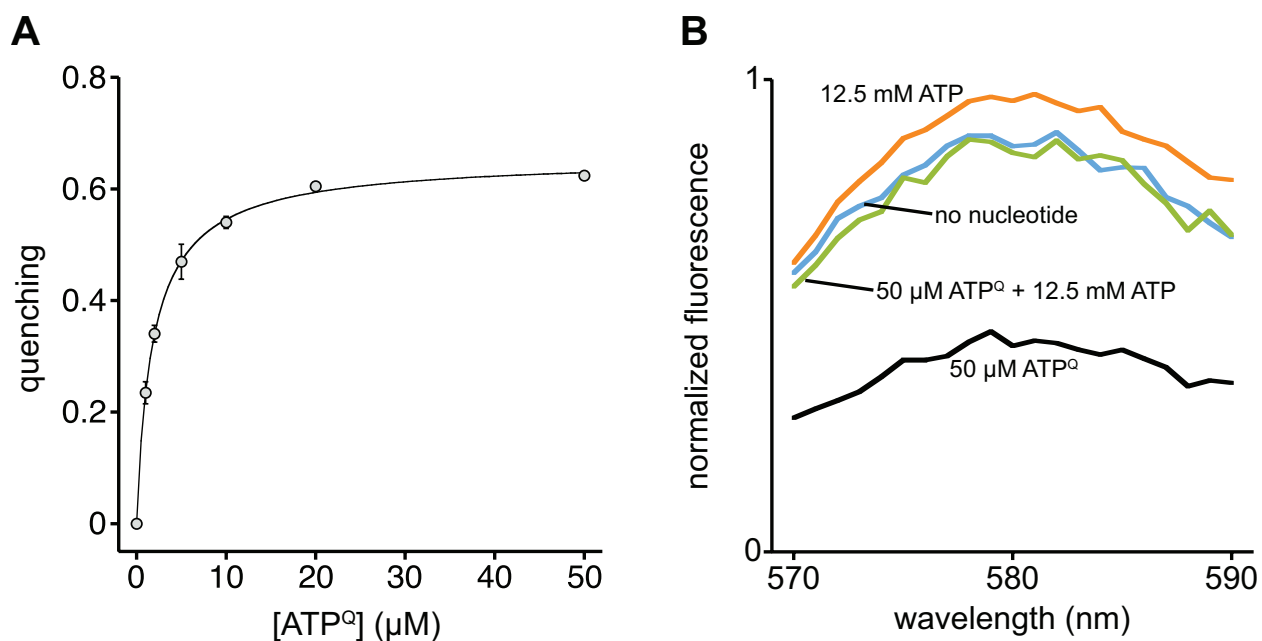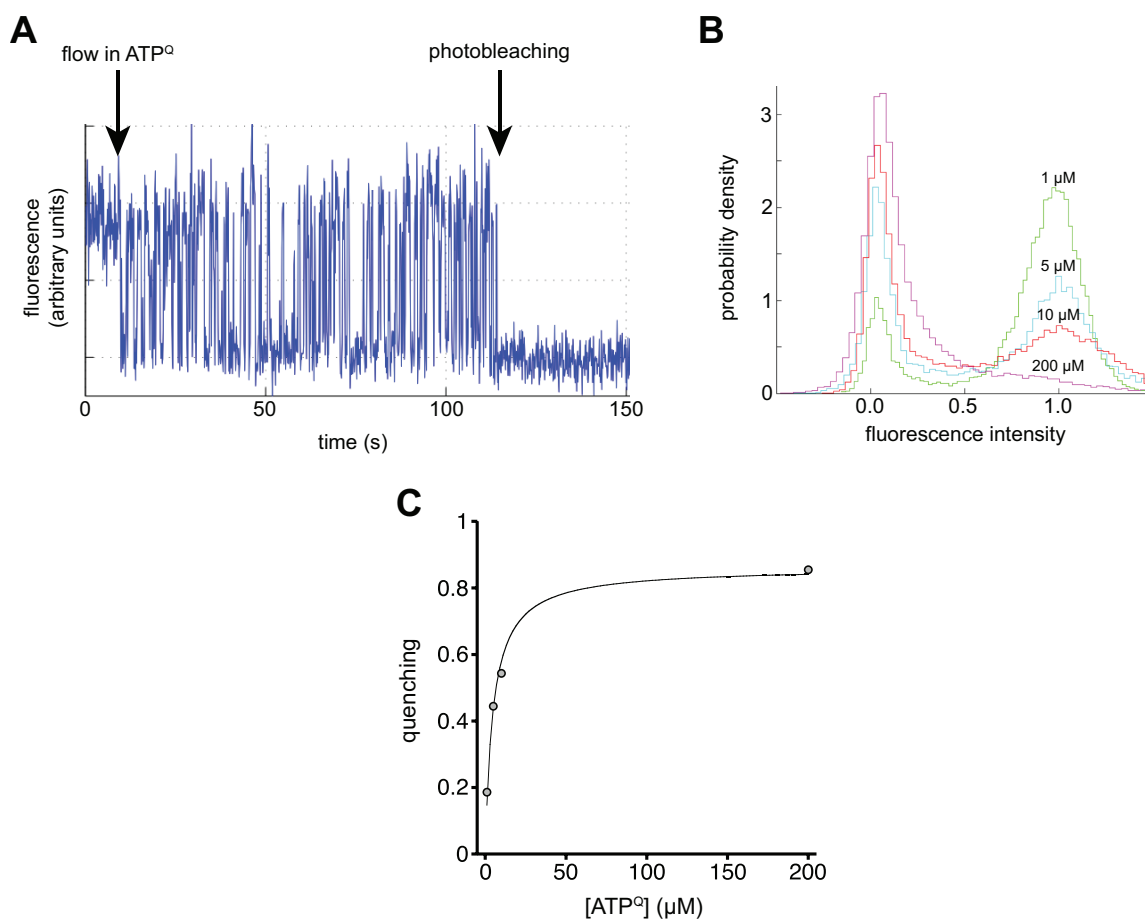

Figure 4. Fluorescence quenching by ATP^Q_2 in bulk experiments. **(A)** A ClpX covalent hexamer (50 nM) containing a single K330C subunit modified with TAMRA was incubated with increasing concentrations of ATP^Q_2, and quenching was fit to a hyperbolic equation (apparent affinity 1.9 ± 0.1 μM; maximal quenching 66 ± 1 %). Values are means ± SD (N=2). **(B)** Fluorescence emission spectra of a ClpX covalent hexamer (50 nM) containing a single K330C subunit modified with TAMRA with no nucleotide (blue), 12.5 mM ATP (orange), 50 μM ATP^Q_2 (black), or 50 μM ATP^Q_2 and 12.5 mM ATP (green).

Single-molecule nucleotide binding

We immobilized singly modified TAMRA-ClpX hexamers on glass coverslips and used

TIRF microscopy to measure fluorescence in the presence of different concentrations of ATP^Q_2. Figure 5A shows a representative trajectory. At the beginning of the experiment, no ATP^Q was present and the fluorescence signal was reasonably stable. Flowing ATP^Q_2 into the observation chamber after 10 s resulted rapid transitions between high and low fluorescent states, which we interpret as nucleotide-unbound and nucleotide-bound, respectively. Eventually, the TAMRA fluorophore photobleached in a single step. We performed experiments at multiple concentrations of ATP^Q_2, collected trajectories that exhibited a stable signal for the first 10 s and single-step photobleaching, and constructed histograms of fluorescence intensity normalized by the average intensity during the first 10 s of each trace (Figure 5B).

Figure 5. Fluorescence quenching by ATP^Q_2 in single-molecule experiments. **(A)** A representative trace of a ClpX covalent hexamer containing a single K330C subunit modified with TAMRA in the presence of 5 μM ATP^Q_2. ATP^Q_2 was added after 10 s. **(B)** Histogram of fluorescence intensities for singly labeled ClpX and different concentrations of ATP^Q_2. Intensities were normalized to the average fluorescence intensity before introduction of ATP^Q_2. **(C)** Areas under the low-fluorescence peak (quenching less than 0.5) in the histograms in panel B were plotted as a function of ATP^Q_2 and fit to a hyperbolic binding equation (apparent affinity 5 ± 1 μM; maximal quenching 86 ± 4 %). Slightly higher maximal quenching for the single molecule experiments may result from lack of correction for the inner filter effect. (A) and (C) courtesy of H. Manning.

The histograms showed two populations, one centered near 0 intensity and the other centered at 1. This result suggests two important points. (1) ATP^Q_2 binding to the labeled subunit results in almost complete quenching. (2) ATP^Q_2 binding in subunits adjacent to the non-labeled subunit does not result in significant quenching, as this would result in intermediate populations between 0 and 1. Importantly, the histograms showed an increase in the quenched population with increasing ATP^Q_2 concentration and a concomitant decrease in the unquenched population, with an apparent ATP^Q_2 affinity of ~5 μM and ~85% maximal quenching (Figure 5C), similar to the corresponding values obtained from the bulk experiment (Figure 4A). The maximal quenching values of 65-85% of initial fluorescence suggest that the ClpX hexamer binds 4-5 nucleotides at saturating concentrations (see Discussion).

ClpX hexamers containing two labeled subunits

We constructed ClpX hexamers with two TAMRA-labeled subunits in "ortho," "meta" and "para" arrangements, performed single-molecule experiments using 0, 10, or 100 μM ATP^Q_2, and constructed histograms of fluorescence intensity (Figure 6). As observed for the singly labeled hexamer, increasing ATP^Q_2 concentration led to a decrease in the high-fluorescence population and an increase in the low-fluorescence population.

Notably, however, the histograms obtained using doubly labeled hexamers consisted of three populations, centered near 0, 0.5 and 1. We interpret these populations as having both, one, or no labeled subunits bound by ATP^Q, respectively.

A

ortho

B

meta

C

para
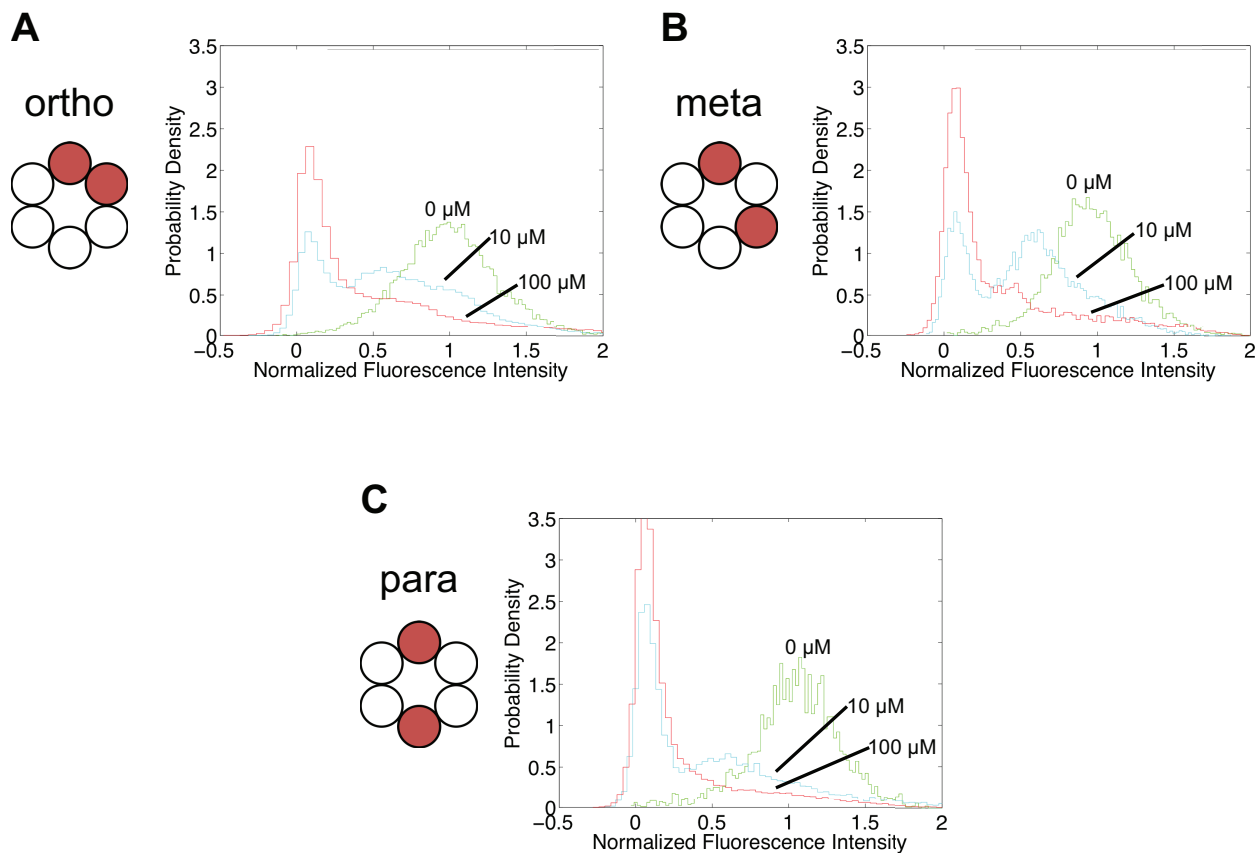
Figure 6. Histograms of single-molecule fluorescence intensities for doubly labeled ClpX variants in the presence of 0, 10, or 100 µM ATP^Q_2. Intensities were normalized to the average fluorescence intensity before introduction of ATP^Q_2. Histograms courtesy of H. Manning.

We focused on experiments conducted at 10 µM ATP^Q_2, as this concentration produced histograms in which all three binding states were substantially populated. Each histogram was fit with a triple Gaussian function, and the integrated areas of each population are shown in Figure 7A-C. Notably, the relative populations of ATP^Q_2 doubly bound, singly bound, and unbound hexamers differed for the three ClpX variants. For

130

example, the fraction of doubly bound subunits was highest for the para variant. As we explain in more detail in the Discussion, these results suggest that nucleotide-binding interactions can be non cooperative or positively cooperative depending on the relative positions of the two subunits in the ClpX ring. Indeed, bulk experiments of ATP^Q_2 binding to doubly labeled variants showed modest positive cooperativity for the ortho and para variants (Hill constants 1.3 ± 0.1 and 1.5 ± 0.2, respectively) and no cooperativity for the meta variant (Hill constant 1.1 ± 0.1).

DISCUSSION

Our results provide a method to study nucleotide transactions in specific subunits of a single ClpX hexamer by TIRF microscopy. The non-fluorescent nature of ATP^Q_2 permits use at high concentrations without contributing to background noise. Furthermore, ATP^Q_2 binds to the same ClpX site as ATP and supports machine function.

Single-molecule experiments show that ATP^Q_2 binding results in complete quenching of the labeled subunit(s). Accordingly, the percentage of ATP^Q_2 quenching relative to initial fluorescence should represent the percentage of labeled subunits bound. At saturating ATP^Q_2 concentrations we observe 65-85% quenching, indicating that the ClpX hexamer binds at most 4-5 nucleotides, an observation consistent with previous experiments (Hersch et al., 2005; Glynn et al., 2009; Stinson et al., 2013). Notably, our results reveal binding stoichiometry in a ClpX hexamer that is actively hydrolyzing nucleotide in solution, whereas previous experiments have relied on hydrolytically inactive ClpX variants, ADP, or ClpX crystals.
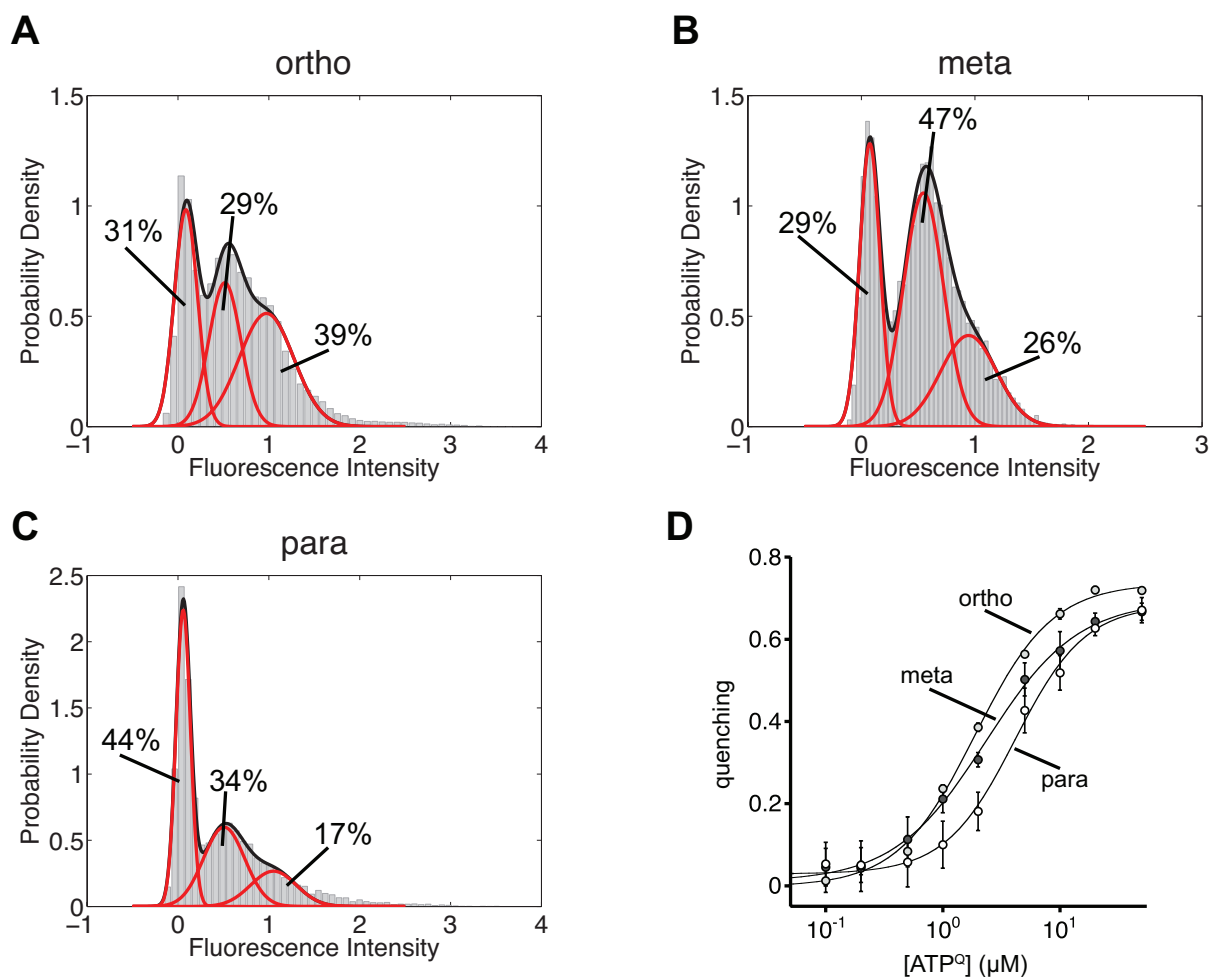
Figure 7. (A)-(C) Histograms of single-molecule fluorescence intensities for doubly labeled ClpX variants in the presence of 10 μM ATP^Q_2 were fit to a triple Gaussian function. Peaks were assigned as doubly bound, singly bound, and unbound from the left to the right. In the triple Gaussian fit, the mean and variance of the doubly-bound and unbound peaks were fixed based on single Gaussian fits in the presence of 100 μM ATP^Q_2 or no ATP^Q_2 as shown in Figure 6. Percentages are integration values of individual Gaussian functions from the triple Gaussian fit. **(D)** Fluorescence quenching by ATP^Q_2 in bulk experiments. ClpX covalent hexamers (25 nM) containing two K330C subunits modified with TAMRA were incubated with increasing concentrations of ATP^Q_2, and quenching was fit to $b + a*[ATP^Q_2]^n/([ATP^Q_2]^n + K_{app}^n)$ (ortho: K_{app} 1.9 ± 0.1 μM, maximal quenching 74 ± 2 %, n 1.3 ± 0.1; meta: K_{app} 2.3 ± 0.2 μM, maximal quenching 68 ± 2 %, n 1.1 ± 0.1; para: K_{app} 4.1 ± 0.4 μM, maximal quenching 66 ± 3 %, n 1.5 ± 0.2). Values are means ± SD (N=2).

A

$$X^0 + A \leftrightharpoons X^1 + A \leftrightharpoons X^2$$

B
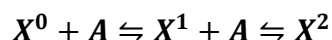
	K_1 (µM)	K_2 (µM)	$K_1 \times 4$ (µM)
ortho	13	9	54
meta	6	16	22
para	5	8	20

Figure 8. Cooperativity between subunits. (A) Reaction model for ATP^Q_2 binding to two labeled ClpX subunits. X^0, X^1 and X^2 correspond to unbound, singly-bound, and doubly-bound ClpX species, respectively, and A corresponds to ATP^Q_2. (B) A table of macroscopic dissociation constants calculated from integration values in Figure 6.

Assays of ClpX hexamers containing two labeled subunits enable measurements of inter-subunit communication. Depending of the relative orientations of the two labeled ClpX subunits, we observe different relative populations of doubly bound, singly bound and unbound hexamers. As shown in Figure 8, macroscopic equilibrium constants for binding to the first labeled subunit (K_1 = [unbound][ATP]/[singly bound]) and second labeled subunit (K_2 = [singly bound][ATP]/[doubly bound]) were calculated from the integration values in figure 7A-C. If the two labeled subunits had the same average binding constants, then K_2 would be expected to be ~$4K_1$ in the absence of cooperativity, <$4K_1$ for positive cooperativity, and >$4K_1$ for negative cooperativity because of statistical factors[1]. By these criteria, ATP^Q_2 binding to meta subunits is essentially non cooperative. Indeed, as expected for independent or non-cooperative binding, the binding histogram for the meta variant shows a near 1:2:1 distribution of unbound, singly bound, and doubly bound subunits at 50% ATP^Q_2 binding, and the Hill constant in a bulk binding assay is 1.1 ± 0.1. For subunits in the ortho and para

---

[1] As the experiment measures binding averaged over all configurations of the ClpX ring, it is reasonable to assume that each labeled subunit has the same microscopic binding constant for nucleotide binding.

orientations, by contrast, modest positive cooperativity is indicated by a K_2 value less than $4K_1$ in single-molecule experiments and by Hill constants of 1.3 ± 0.1 (ortho) and 1.5 ± 0.2 (para) in solution binding experiments.

What is the role of communication between subunits in nucleotide binding and hydrolysis? Previous experiments show that the majority of subunits in the ClpX ring must be occupied before robust hydrolysis and machine activity can occur (Stinson et al., 2013). Cooperative nucleotide binding may allow the ring to assume a specific configuration of nucleotide occupancy conducive to function. Future single-molecule experiments at varying ATP^Q_2 concentrations with ClpX variants containing 3 or more labeled subunits should help determine which arrangements of nucleotide-bound subunits are prevalent. Our method will also enable detailed kinetic analysis of nucleotide occupancy in multiple subunits, and experiments using ClpX labeled in multiple subunits with distinct dyes may allow determination of how nucleotide occupancy in one subunit affects the kinetics of occupancy of the other subunits. Multiple lines of evidence suggest that ClpX is a dynamic and probabilistic machine (Chapter 3, Martin et al., 2005; Cordova et al., 2014), and experiments of this type will provide important constraints on models of ClpX function.

EXPERIMENTAL PROCEDURES

Synthesis of ATP^Q

ATP^Q was synthesized by a variation of published procedures (Maeda et al., 1977; Cremo et al., 1990; Hazlett et al., 1993; Jameson and Eccleston, 1997). DABCYL

Plus^{TM} acid, SE was purchased from Anaspec; other reagents were purchased from Sigma. A solution of ATP disodium salt (275 mg dissolved in 2 mL water) was passed over a column of Dowex 50W X8 (0.77 g; H$^+$ form) to generate the free ATP acid. Ethanol (100 mL) was added and the mixture was evaporated to dryness by rotary evaporation. The residue was dissolved in methanol (8 mL plus 476 µL tributylamine), and the mixture was evaporated to dryness by rotary evaporation. The resulting ATP tributylammonum salt was dissolved in anhydrous DMF (8 mL) stored over 4 Å molecular sieves and dried by repeated rotary evaporation of dry DMF (3x). Dry DMF (8 mL) was added and the solution was placed under an argon atmosphere and cooled to 4 °C. Carbonyldiimidazole (405 mg) was added, the reaction was stirred at 4 °C for 4 h, and unreacted carbonyldiimidazole was destroyed by addition of methanol (144 µL). To this solution, ethylenediamine (167 µL in 5 mL dry DMF) was added drop wise at 4 °C. The resulting white precipitate was recovered by centrifugation and washed 3x with dry DMF. The precipitate was dissolved in water (30 mL), adjusted to pH 2.5 with HCl, and stirred at 4 °C overnight to remove the γ-phophoramidate. The solution was then adjusted to pH 7.0 and chromatographed on a MonoQ column using a gradient of 10 mM to 600 mM triethylammonium bicarbonate buffer (pH 7.8). Fractions containing eda-ATP were identified by TLC, pooled, lyophilized, dissolved in water (2 mL), mixed with DABCYL Plus acid, SE (25 mg dissolved in 1 mL DMSO), and allowed to react at room temperature overnight in the dark. DABCYL Plus-eda-ATP was precipitated by addition of 6 volumes of acetone, collected by centrifugation, and washed 3x with acetone to remove unreacted dye. The resulting red-orange precipitate was dissolved in water (2 mL), loaded onto a 100 mL DEAE Sepharose column, and eluted isocratically with 0.6

M ammonium bicarbonate (pH 7.8). Mass spectrometry verified that the major peaks corresponded to isomers of DABCYL Plus-eda-ATP. These peaks were pooled separately, lyophilized, dissolved at a concentration of 20 mM in 50 mM MES (pH 6.0), and stored frozen at –80 °C.

Aluminum-backed silica gel 60 F254 TLC plates were used to track reaction progress with a water:ammonia:isopropanol:1,4-dioxane (4:3:2:4) solvent system. RF values: ATP, 0.21; ADP, 0.26; eda-ATP, 0.13; ATP^Q_1, 0.34; ATP^Q_2, 0.38; ADP^Q_1, 0.57; ADP^Q_2, 0.58.

Bulk assays

ClpX hexamers were constructed, purified, and labeled as described in Chapter 4. Fluorescence measurements were acquired with a SpectraMax M5e plate reader (Molecular Devices). ATP hydrolysis was measured by the Enz Chek phosphate assay (Molecular Probes) and quantified by comparison to an inorganic-phosphate standard curve. Degradation of the cp7-GFP-ssrA protein substrate by ClpXP variants was monitored by changes in fluorescence (excitation 467 nm; emission 511 nm)(Nager et al., 2011). Fluorescence quenching of K330C-TAMRA labeled ClpX by ATP^Q was monitored by excitation at 540 nm and collecting and averaging the emission spectrum from 570-590 nm. Quenching was defined as $1-F/F_0$, where F_0 is fluorescence intensity in the absence of ATP^Q. Bulk quenching values were corrected for the inner-filter effect by subtracting the quenching observed with unreacted TAMRA-maleimide dye and an equivalent concentration of ATP^Q.

Single molecule TIRF microscopy (courtesy of H. Manning)

ClpX hexamers were constructed, purified, and labeled as described in Chapters 3-4.

Single-molecule fluorescence quenching assays were performed using a custom built objective-side TIRF microscope equipped with a 100X 1.49 NA TIRF objective, an EMCCD camera (Andor) and a 532 nm illumination system. Tetramethylrhodamine (TAMRA) emission was focused onto the EMCCD camera.

PEG-modified glass coverslips were prepared based on a published protocol. Briefly, glass coverslips were sonicated sequentially in deionized water, methanol, and 1 M KOH. The cleaned coverslips were then sonicated with a solution of 1% methoxypolyethyleneglycol-silane (1% mixture of biotin-PEG-silane; mPEG-silane-2000, and biotin-PEG-silane-5000, Laysan Bio) in anhydrous toluene in the presence of 0.8 mM triethylamine. The reacted coverslips were washed with toluene and deionized water, and finally dried under Nitrogen gas. PEG-modified coverslips were stored under vacuum at −20 °C and assembled into flow chambers before use.

Flow cells were made from double-sided sticky-tape gaskets sandwiched between a glass slide and the PEG-modified coverslip. While flow cells were treated with 0.01 mg/mL streptavidin, labeled ClpX (10nM) was incubated with ClpP (0.84 µM), 1 mM ATP, and an ATP-regeneration system in PD buffer (25 mM HEPES pH 7.6, 100 mM KCl, 10 mM MgCl2, 10% glycerol (vol/vol)) to form ClpXP complexes. After unbound streptavidin was washed away, assembled ClpXP (diluted to 0.625 nM) was introduced into the flow cell and incubated for 20 min to allow ClpXP binding to the biotin-PEG

surface. Samples were then washed with imaging buffer (PD buffer supplemented with ClpP (0.67 µM), appropriate nucleotides/substrates, and an oxygen-scavenging system (0.8 % D(+)-glucose, 16500 units/mL glucose oxidase, 217000 units/mL catalase, and 2 mM Trolox) and were incubated for 5 min before imaging. Single-molecule traces were recorded with 116 ms time frames.

Single-molecule data were processed using custom-made MATLAB scripts. Briefly, fluorescent peaks in the images were identified and traced throughout the trajectory. Hidden Markov modeling (HMM) of fluorescence traces was performed using the vbFRET program (Bronson et al, 2009). Only traces lasting longer than 25 s were analyzed to allow sufficient quenching events to occur.

REFERENCES

Baker, T.A., and Sauer, R.T. (2011). ClpXP, an ATP-powered unfolding and protein-degradation machine. Biochimica Et Biophysica Acta (BBA) - Molecular Cell Research.

Bronson, J.E., Fei, J., Hofman, J.M., Gonzalez Jr., R.L., Wiggins, C.H. (2009). Learning rates and states form biophysical time series: a Bayesian approach to model selection and single-molecule FRET data. Biophys. J. *97*, 3196-3205.

Cordova, J.C., Olivares, A.O., Shin, Y., Stinson, B.M., Calmat, S., Schmitz, K.R., Aubin-Tam, M.-E., Baker, T.A., Lang, M.J., and Sauer, R.T. (2014). Stochastic but highly coordinated protein unfolding and translocation by the ClpXP proteolytic machine. Cell *158*, 647–658.

Cremo, C.R., Neuron, J.M., and Yount, R.G. (1990). Interaction of myosin subfragment 1 with fluorescent ribose-modified nucleotides. A comparison of vanadate trapping and SH1-SH2 cross-linking. Biochemistry *29*, 3309–3319.

Glynn, S.E., Martin, A., Nager, A.R., Baker, T.A., and Sauer, R.T. (2009). Structures of asymmetric ClpX hexamers reveal nucleotide-dependent motions in a AAA+ protein-unfolding machine. Cell *139*, 744–756.

Hanson, P.I., and Whiteheart, S.W. (2005). AAA+ proteins: have engine, will work. Nat. Rev. Mol. Cell Biol. *6*, 519–529.

Hazlett, T.L., Moore, K.J., Lowe, P.N., Jameson, D.M., and Eccleston, J.F. (1993). Solution dynamics of p21ras proteins bound with fluorescent nucleotides: a time-resolved fluorescence study. Biochemistry *32*, 13575–13583.

Hersch, G.L., Burton, R.E., Bolon, D.N., Baker, T.A., and Sauer, R.T. (2005). Asymmetric interactions of ATP with the AAA+ ClpX6 unfoldase: allosteric control of a protein machine. Cell *121*, 1017–1027.

Jameson, D.M., and Eccleston, J.F. (1997). Fluorescent nucleotide analogs: synthesis and applications. Meth. Enzymol. *278*, 363–390.

Maeda, M., Patel, A.D., and Hampton, A. (1977). Formation of ribonucleotide 2',3'-cyclic carbonates during conversion of ribonucleoside 5'-phosphates to diphosphates and triphosphates by the phosphorimidazolidate procedure. Nucleic Acids Res. *4*, 2843–2853.

Martin, A., Baker, T.A., and Sauer, R.T. (2005). Rebuilt AAA + motors reveal operating principles for ATP-fuelled machines. Nature *437*, 1115–1120.

Nager, A.R., Baker, T.A., and Sauer, R.T. (2011). Stepwise unfolding of a β barrel protein by the AAA+ ClpXP protease. J Mol Biol *413*, 4–16.

Ogura, T., and Wilkinson, A.J. (2001). AAA+ superfamily ATPases: common structure--

diverse function. Genes Cells *6*, 575–597.

Oiwa, K., Eccleston, J.F., Anson, M., Kikumoto, M., Davis, C.T., Reid, G.P., Ferenczi, M.A., Corrie, J.E., Yamada, A., Nakayama, H., et al. (2000). Comparative single-molecule and ensemble myosin enzymology: sulfoindocyanine ATP and ADP derivatives. Biophys. J. *78*, 3048–3071.

Stinson, B.M., Nager, A.R., Glynn, S.E., Schmitz, K.R., Baker, T.A., and Sauer, R.T. (2013). Nucleotide Binding and Conformational Switching in the Hexameric Ring of a AAA+ Machine. Cell *153*, 628–639.